EFFECTS OF POWDER COHESION AND SEGREGATION ON PHARMACEUTICAL MIXING AND GRANULATION

by

SARANG OKA

A dissertation submitted to the

Graduate School – New Brunswick

Rutgers, The State University of New Jersey

In partial fulfillment of the requirements

For the degree of

Doctor of Philosophy

Graduate Program in Chemical and Biochemical Engineering

Written under the direction of

Fernando J. Muzzio and Rohit Ramachandran

And approved by

_____

_____

_____

_____

New Brunswick, New Jersey

May 2016

ABSTRACT OF THE DISSERTATION

Effects of Powder Cohesion and Segregation on Pharmaceutical Mixing and Granulation

By SARANG OKA

Dissertation Directors:

Fernando J. Muzzio and Rohit Ramachandran

This work is a collection of three distinct powder mixing problems, generally applicable to the manufacturing of pharmaceutical solid oral dose products. The first problem investigates scaling up of dispersive transport of poorly flowing powders in a rotating cylinder setup. The rate of self-dispersion of a material along the axis of a rotating cylinder is quantified by tracking the rate of axial transport of a dyed tracer. The dispersion is found to follow Fick's second law and the rate constant term of the equation, called the axial dispersion coefficient, provides a measure of the rate of the axial dispersion. The effects of flow properties of the material, the scale of the system and rotation speed of the cylinder on the axial dispersion coefficient were investigated. It was observed that the rate of axial dispersion increases with increasing powder cohesion. Poorly flowing materials tend to form aggregates during operation, which break when they collide with the free surface of the powder bed, leading to enhanced dispersion. The dispersion coefficient was also found to increase with the scale of the system. The powder experiences a greater consolidation stress at larger scales leading to formation of

bigger aggregates which contribute to greater dispersion. Lastly, the dispersion coefficient also depends on the rotation speed of the cylinder, and in conjunction, the regime of operation. The dispersion coefficient was observed to increase with increasing rotation speed, as the material transitioned from the cascading to the cataracting regime, but decreased as the material began to centrifuge at even higher speeds.

The possibility of efficiently mixing highly segregating ingredients using continuous blenders was examined. It was found that continuous blenders are superior compared to batch blenders in their ability to mix disparate ingredients. Five mixtures with variable segregation tendencies were tested. Continuous blenders operate by forced convection where mixing occurs due to the action of the rotating blades. The dependence of mixing performance on the properties of the material was thus found to be minimal, facilitating mixing of disparate materials. This is in contrast to traditional batch blenders, in which powder ingredients are blended by the virtue of their tumbling motion. In such systems, the particles are allowed to tread their independent paths and accumulate in separate regions. They were thus found to separate, since unlike particles traversed different paths. The finding that continuous mixers prevent segregation opens the door to manufacture by direct compaction formulations that are currently granulated or reformulated due to segregation concerns. Relationships were found between the bulk properties of the ingredients, namely their median particle size and bulk density, and the segregation index of their mixtures. Relationships between the segregation index of mixtures and their mixing performance in batch systems were also obtained.

The roles of powder mixing and ingredient wetting properties on the content uniformity of granules made by a high shear wet granulation process were investigated. Content non-

uniformity in granulated product manifests itself as non-uniform distribution of the active ingredient across granule size classes. It was observed that a non-uniform initial mixture and a large difference in wettability of the ingredients can both contribute towards the content non-uniformity in the granules. Furthermore, a soluble ingredient can also dissolve in the binder fluid during granulation. The active ingredient recrystallizes during drying and appears as fines leading to further non-uniformity. The impact of process parameters on granule properties and granules microstructure was examined. Furthermore, the role of granule microstructure on performance attributes, such as the rate of release of the active ingredient in various dissolution media, was investigated. It was found that the rate of release is dictated by the internal pore structure – higher porosity facilitates dissolution. Rate of release was also found to be proportional to the square of the granule diameter. Content non-uniformity across granule size classes, however, undermines the ability to model and predict such performance attributes. Relationships between process parameters and the resulting product microstructure on the one hand, and between the product microstructure and its end-use properties such as dissolution on the other hand, were established.

Acknowledgements

The work has been a culmination of several years of effort, and is a result of the contribution of many individuals. I would like to thank each one of them. I would like to thank my advisers Fernando Muzzio and Rohit Ramachandran for their guidance, support and mentorship. Fernando has been a source of tremendous inspiration throughout my Rutgers years. I cannot thank him enough for his role in my life and career. In him, I have someone who I look upto and aspire to be. I would thank Rohit for involving me in his fruitful collaboration with Dr.Frantisek Stepanek, and providing me with several local and international travel opportunities. My visits to Prague count as the some of my best academic and life experiences. I would like to thank my committee members, Dr.Glasser and Dr.Eric Jayjock for providing valuable input to the dissertation. A special mention to Eric Jayjock, a former colleague at Rutgers, who has provided valuable input to my publications, and from whom, I learn something new about continuous processing with each conversation.

The endeavor would be impossible without the support of my fellow graduate students, from whom I have learnt a great deal about science, beer and world cultures. I would like to thank former and current Muzzio group member, Dr. Aditya Vanarase, Dr. Alisa Vasilenko, Dr. William Engisch, Dr. Juan Osorio, Dr. Athanas and Dr. Sara Koynov, Abhishek Sahay, Pallavi Pawar, Dr. Krizia Karry, Yifan Wang, Wei Meng, Jin Maeda, Dr. James Scicolone, Dr.Kellie Anderson, Dr. Gerardo Callegari, Dr. Sejal Shah, Thamer Omar, Hao Chen and Zhanjie Liu. I would specially like to thank Chinmay Pathak and Peyton Randolph, who have been an integral part of the axial dispersion work and have helped me with several experiments. A special thanks to Dr. Heather Emady, for reading

through my publication and dissertation drafts, and for all the fun adventures. I would also like to acknowledge past and current members of the Ramachandran group Dr. Anwesha Chaudhury, Dr. Maitraye Sen, Dr. Dana Barrasso, Ashu Tamrakar, Anik Chaturbedi, Chandrakanth Bandi, Franklin Bettencourt and Anuj Varghese; and members of the Ierapetritou group Dr. Fani Boukouvala, Dr. Amanda Rogers and Sebastian Escotet. Thank you for the good times, and being my family away from home. I would also like to acknowledge my collaborators at ICT Prague, Prof. Frantisek Stepanek, Dr. Ondrej Kaspar, Dr. Viola Tokarova and David Smrcka, from whom I have learnt a great about analytical methods, imaging techniques and distance running.

The financial support of from the NSF Engineering Research Center for Structured Organic Particulate Systems (ERC-SOPS) and the Department of Chemical and Biochemical Engineering at Rutgers cannot be discounted. My experiences in the ERC-SOPS have played a big role in shaping my personality and career. I would like to thank them for providing me with wonderful public speaking, networking, teaching, leadership and mentoring opportunities; a special mention to the ERC-SOPS staff Charanjeet Kaur, Dr. Doug Hausner and Dr.Eric Erenrich. I could not have asked for a better graduate student experience.

This endeavor would not have been possible without the support of family and friends. My best friends', Neel Kulkarni and Siddhesh Jaiswal have a huge role in shaping my ideals, career and sense of humor. Thank you for the laughs. My family's role is, perhaps, greater than anyone else's. My parents gave up a part of their lives so I could have the one I wanted. My parent's and my grandmother's belief in me is the single greatest

source of motivation. Thank you for the right upbringing, support and love. And to the great power that watches over us. Thank you.

Table of Contents

List of Tables

List of Figures

Chapter 1 : Introduction

The process of making therapeutic solid oral dose products is largely an exercise in powder technology. These products, namely, tablets and capsules, account for 80% of all marketed therapeutics in the United States [1]. The process involves creating uniform mixtures of two or more powder ingredients, and compressing them into tablets (or filling them into capsules). The ingredients in these mixtures can be divided into two classes, namely, active pharmaceutical ingredients (API) and excipients. The APIs deliver the therapeutic effect while the excipients serve a variety of other functions. They provide volume to the dosage form. They can act as disintegrants, binders, lubricants, taste masking agents, and surfactants. All processes prior to tableting, from the point the ingredients are available in powder form, are focused on creating uniform mixtures of the API and the excipients.

1.1 Need for creating homogeneous mixtures

Each tablet, like every therapeutic product, is designed to contain a highly specific amount of the active ingredient. Active ingredients are chemically toxic compounds and their over-administration can result in undesirable side effects. Under-administration results in the product not having the desired therapeutic effect. It is thus critical that each tablet consistently contains the exact, pre-specified amount of the active ingredient. It is imperative that a highly uniform mixture of the active ingredient and the excipients is sent to the tableting process.

A process flow diagram of the unit operations involved in manufacturing a tablet is shown in Figure 1-1. It can be observed that there are three possible routes to making a tablet. The simplest route is direct compaction which involves dry mixing the API and

the excipients and compressing them into tablets. The two other routes, classified as granulation routes, involve increasing the particle size and density of API-excipient mixtures, followed by lubricant blending and tablet compaction. Thus, granulation routes are pursued when the physical properties of the mixtures are desired to be modified while in direct compaction, the properties of the powder mixture are deemed satisfactory to directly compress a tablet, which will have the desired therapeutic effect.

There is an exclusive unit operation in all three routes that is specifically designed to mix powder ingredients. The process, in the traditional batch based operation, involves adding the excipients and active ingredients in a vessel followed by tumbling the vessel for a few hundred revolutions, in an attempt to create a uniform mixture of the ingredients. The mixing devices are called tumble blenders. Besides the blending unit operation, there is also inter-mingling, mixing and demixing of powder ingredients in other unit operations that deal with one or more powder ingredients. That is mixing and demixing is prevalent even in unit operations that are not specifically designed to perform mixing. Despite this, achieving a uniform mixture of the API and excipients remains a substantial challenge.

1.2 Theoretical considerations

The uniformity of the blend at the end of the blending process is tested to ensure that a non-homogeneous mixture of the API and the excipient is not sent to the tableting process. This is done by extracting samples from different locations in the blender and analyzing the content of the samples [2, 3]. The mean concentration of the active ingredient across all extracted samples is computed and is divided by its standard deviation. The resultant quantity is referred to as the relative standard deviation.

$$\%\ Relative\ Standard\ Deviation\ (RSD) = \frac{Standard\ Deviation}{Mean} * 100$$

The blending is deemed satisfactory if the value of the RSD is less than 5%.

1.3 Mechanisms of Mixing

The mechanisms of powder mixing, in any mixing device, including tumble blenders, can be classified in to two distinct classes – based on the driving force for mixing or based on scale at which mixing takes place. Depending on the scale at which mixing takes place, mixing can be classified as micromixing or macromixing. Macromixing occurs at the scale of several particles while mircomixing is typified by mixing at the single particle level. Micromixing is also often associated with changes to the properties of individual particles.

Particulate mixing, both micromixing and macromixing, based on the driving force can be classified into convective mixing, shear and dispersive mixing [4-6]. They can occur individually or simultaneously. Dispersive mixing is caused by small scale random motion of particles, typically when high particle mobility exists. It is also found to follow mass action law. Velocity gradients between individual particles or particle planes results in shear based mixing. There is often, transfer of material across the shearing planes. Convective mixing occurs at the scale of several particles and involves moving large portions of material from one location to another.

Mixing in typical batch tumble blenders is a result of a combination of all three aforementioned mixing mechanisms. Majority of the homogenization is caused by the convective mixing component. Convective mixing occurs in the direction orthogonal to the direction of the axis of rotation. Dispersive mixing on the other hand occurs in the

direction parallel to the axis of the rotation. Dispersive mixing is generally very slow and its contribution is small compared to the convective mixing component. However, dispersive mixing leads to a more complete mixing since it's a random process. Although the dispersive mixing of free flowing materials has been investigated [7-9], the dispersion of cohesive materials remains largely investigated.

1.4 Scale up of Dispersive Mixing for Cohesive Materials

A large majority of pharmaceutical ingredients exhibit a discernible degree of cohesion. Cohesion is more prevalent in powders with small primary particles. This is because the inter-particle cohesive forces become comparable to the weight of the particle with decreasing particle size. In larger particles, the cohesive forces are negligible compared to their weight – the gravity forces. The presence of cohesive forces between fine powder particles makes them travel in lumps [10]. Unless the lumps are destroyed, the system behaves as if it has an effective particle size much larger than the size of the primary particles. Moreover, cohesive powders, unlike free flowing powders are compressible, meaning the bulk powder can exhibit a range of densities [11, 12] depending on the normal consolidation stresses. This makes the behavior of poorly flowing powders scale dependent. Several such attributes make poorly flowing materials very intriguing and complex to study. Certain physical rules applied to free flowing powders cannot be applied to the poorly flowing materials.

Several studies have investigated the mixing of cohesive or weakly cohesive particles in batch systems. These studies have focused mainly on two things – convective mixing to achieve macro uniformity [13-16] and shear based mixing to achieve micro-uniformity

[17-19]. The dispersive mixing of poorly flowing powders, especially the effects of scale, remains largely uninvestigated. This is the focus of Chapter 3.

A rotating cylinder setup is used to study the dispersion of poorly flowing powders within themselves. The effect of powder cohesion, speed of rotation and scale of the system on the rate of dispersive transport is investigated. Fick's second law is used to model dispersion profiles. The dispersion constant is used to quantify the rate of dispersion. The dispersion constant is correlated to the scale of the system, rotation speed and powder properties with the help of dimensionless numbers, specifically the Bond and the Froude number.

1.5 Continuous Mixing of Highly Segregating Ingredients

Another long standing challenge in batch based tumble mixing is demixing of ingredients during processing. Demixing or segregation is caused by disparity in convective transport due to disparity in the properties of the ingredients. Different ingredients traverse different paths within the blender during the tumbling action, leading to their separation [20-22]. Non-homogeneity of the blend leads to content non-uniformity in the final product, which is undesirable. This is circumvented either by reformulating the recipe – choosing ingredients whose properties are similar, or by granulating the dry mixture. Both strategies involve additional steps, consume additional time and energy. The strategies are undesirable but inevitable.

An alternative solution is to mix the ingredients *continuously* in forced convective mixers. Transport and consequently mixing of ingredients in these blenders is forced by rotating blades. This makes the process generally independent of properties of the materials. However, the possibility of continuously mixing segregating ingredients has

been largely untested in pharmaceutical manufacturing [23]. This is because the overwhelming majority of solid oral products marketed today are manufacturing in batch based systems. Continuous manufacturing of tablets and capsules is a novel technology. There are only handful products, marketed today, which are manufactured by continuous process. However, the technology is gaining popularity due to realization of its tremendous potential advantages [24] and a conducive regulatory environment [25, 26]. It is thus, worthwhile to investigate the continuous mixing of segregating ingredients. A positive result could lead to the possibility of the directly compacting those formulations, which would otherwise be manufactured via granulation, due to segregation concerns. This is the focus of Chapter 4.

Five mixtures with variable segregation tendencies have been studied and have been attempted to be homogenized by mixing them continuously. This mixing performance is compared to the degree of homogenization achieved from a traditional batch mixing process.

1.6 Content Non-Uniformity in High Shear Wet Granulation

As previously mentioned, content non-uniformity in dry powder mixtures is often circumvented by granulating them. The process involves spraying the mixture with a granulating liquid and physically fusing the active ingredient and the excipient in a macro-assembly, called a granule. The granule is expected to contain the active ingredient and the excipients in the same ratio as the original bulk mixture. Tablets compressed from these granules will consistently have the same composition.

Ironically, in some cases, the active ingredient may be preferentially found in the fine or the coarse granules [27, 28], undermining the objective of the process. Segregation of

granules further downstream may translate into content non-uniformity in tablets. Chapter 5 investigates potential sources of content non -uniformity in granule made by high shear wet granulation processes. Specifically, granule content non-uniformity caused by disparity in the wettability of the active ingredient and the excipient, poor mixing during granulation and partial solubilization of the active ingredient in the binder fluid has been studied. Chapter 6 focuses on the impact of this content non-uniformity on certain performance attributes of the granules, such as the rate of release of the active ingredient from the granule. It also focuses on the understanding the effect of process parameters in a high shear wet granulation process on other quality attributes of the granules, such as morphology, particle size and size distribution, and porosity. Lastly, the effect of these quality attributes on performance metrics, such as the rate of release of the active ingredient, is examined.

1.7 Overview of the Thesis

The thesis is a collection of three distinct powder mixing problems, generally applicable to pharmaceutical solid oral dose manufacturing. The introduction chapter sets the stage and puts into perspective the applicability of the problems in the manufacturing process train. Chapter 2 elucidates the most common experimental and analytical and methods used throughout the work. Methods specific to an individual problem have been explained as and when the problem is discussed. Chapter 3, Chapter 4, Chapter 5, and Chapter 6discuss the technical work introduced above. These chapters begin with an introduction to the problem. The introduction encompasses the background of the problem, the motivation and discusses relevant findings from published literature. This is followed by specifying the materials and methods used in that work. The key findings are

then presented and discussed, followed by concluding comments. Chapter 7 presents the overall conclusions from the thesis and suggests possible future directions.

1.8 Figures for Chapter 1

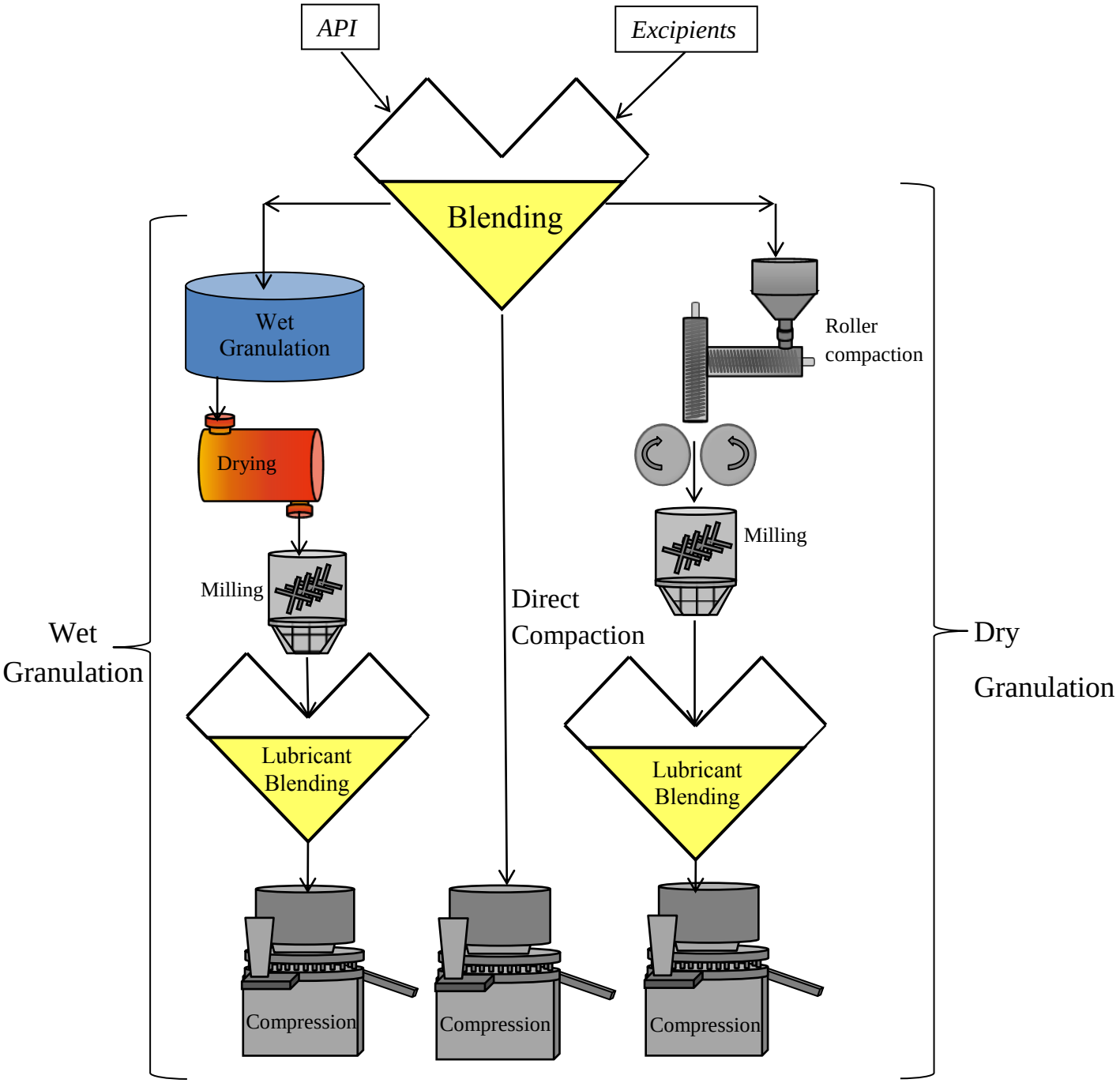

Figure 1-1: Three manufacturing routes, namely, direct compaction, wet granulation and dry granulation for making therapeutic solid oral dosage forms. Direct compaction is the simplest and the most economical of the three routes. All three routes have an exclusive blending step.

Chapter 2 : Experimental Methods

2.1Introduction

The most common material characterization and analytical techniques, which were used in this work, have been presented in this chapter. Analytical and primary material characterization methods which were specific and unique to a small part of the work have been presented in the individual chapters.

The particle size distribution of the starting material was measured for all materials. The particle size distribution of a powder material is one of its most important characteristic that dictates a host of properties. Powders with a small particle size, typically less than 300 μm, tend to be more complex. The inter-particle force between individual particles is comparable to the weight of the particles. Such materials thus tend to exhibit discernible cohesion, can be affected by electrostatic charging and tend to be loosely packed. The properties of larger particles on the other hand tend to be dictated by gravity forces. Such materials tend to be freely flowing, exhibit little inter-particle attraction and tend to pack optimally. The particle size distribution of the starting material, which typically was a fine powder, was measured using a laser diffraction method. The size distribution of granules was measured by sieving them in size classes.

Similar to particle size distribution, the bulk density of the starting material and the granules was always measured. The standard technique of pouring a known mass of material in graduated cylinder and recording the occupied volume was employed.

As previously mentioned, one of the objectives of the work was to investigate the causes of content non-uniformity of the active ingredient across granule size classes. It was thus imperative that content of the granules was accurately investigated. Granule content was

determined by a UV-VIS spectroscopy method. The method measures the absorbance of UV light that is shined on the sample. The absorbance values can be used to determine the amount of the ingredient of interest, using a previously developed calibration curve.

The difference in color of two powder ingredients was used to determine the content of one ingredient in its mixture with the other. A dry colorimetry method was used for this purpose. The colorimeter shines visible light on a sample and measures the reflectance value. This value can be used to determine the amount of colored material in a sample using a pre-developed calibration curve.

Each characterization methods mentioned above is now discussed in detail.

2.2 Particle Size Distribution

2.2.1 Laser Light Diffraction

The primary particle size of ingredients was measured using a laser diffraction particle size analyzer (Beckman Coulter, LS 13 320) shown in Figure 2-1. This device like others in this class, works on the principle of scattering of visible light. It correlates the pattern of scattered light, as measured by the intensity at different angles, to the particle size distribution of the sample. The measurement results in a volume percent as a function of the particle size, a data series from which the particle distribution parameters such as d10, d50 and d90 can be computed. In this case, the associated software of the equipment readily computes the particle size distribution parameters. Each measurement was performed in triplicate, whenever this technique was used. The average value of the three measurements has been reported, unless stated otherwise. As an example, the size distribution profile of 150-250 μm glass beads is shown in Figure 2-2. Also shown in

Figure 2-2 are the particle size distribution parameters of the sample which are readily computed by the software.

2.2.2 Sieve Analysis

The particle size distribution of all granules produced by the high shear wet granulation process was measured by sieve analysis. This method, unlike laser light scattering is non-destructive, enabling further analysis of the sieved samples. The method also helps to classify a granulation batch into size classes. This enables the analysis of granule properties, namely, content uniformity, dissolution performance and porosity across size classes.

A vibrational sieve shaker, 'Endcotts Octagon 2000', shown in Figure 2-3, was used for sieving. The sieves were cleaned and dried. No more 100-200g of materials was sieved in each run. The material was loaded on the top sieve and the sieve stack was secured with clamps. The shaker was run in 'continuious' mode at an amplitude of 6, for 12 minutes. The number of sieves and the sizes were selected such that no more than 20% of the total weight of the starting material is retained on one sieve. Standard 8'' sieves were used. After sieving, the mass of the powder on individual sieves was weighed and plotted as bar chart for visualization (Figure 2-4a). Particle size distribution parameters (d10, d50, or d90) were read from the cumulative particle size distribution graph using linear interpolation (Figure 2-4b).

2.3 Bulk Density

Bulk density of granules and primary materials was measured by gently pouring a known mass of material in a graduated 200 ml cylinder. The volume occupied by the mass was

noted, ensuring that the cylinder is not disturbed throughout the operation. Each measurement was repeated thrice and the average value has been reported.

2.4 Content Uniformity and Release Kinetics of Granules

The content uniformity of the granules was measured by a UV-VIS spectroscopy (Specord 205 BU, Analytik Jena, Germany) method. Under ambient conditions, the solubility of acetaminophen, which was used as the active ingredient in the study, in absolute ethanol is approximately an order of magnitude larger than in water. Ethanol was thus used as a dissolution medium to measure the API content of the granules. To measure the concentration of the API in the granules, a pre-weighed amount of granules (approximately 400 mg) were incubated in 10 ml of ethanol overnight on a shaking platform without access to light (acetaminophen is UV sensitive). 10 µL of the extract was added to 3 ml of pure ethanol in a cuvette and the absorbance was measured at a wavelength of 250 nm. Measurements were performed in duplicates. The extinction coefficients of acetaminophen in ethanol was previously measured by calibration experiments and was found to be $\lambda_{250,EOH} = 12896$ mol.L^{-1}.cm^{-1}.

The release kinetics of different size classes were measured using a similar technique. Approximately 400 mg of granules from each sieve fraction were incubated in 10 ml of ethanol on a shaking platform for a period of 24 hours. The API release profile was developed by periodically extracting 10 µl of the sample and analyzing it for its APAP content by measuring its absorbance at 250 nm. Ethanol was used as a dissolution medium rather than a traditional aqueous buffer in order to assess the contribution of the granule pore structure to the release process [29]. While APAP is well soluble in ethanol, the excipient is not, and therefore the granule as a whole does not dissolve. This method

makes it possible to separate the effect of granule internal microstructure from the contributions of granule break-up and intrinsic dissolution kinetics of the drug.

In addition to measuring the release of APAP in ethanol, the release kinetics of APAP in water was also investigated is some cases. The general procedure was similar. 150 mg of granules were incubated in 10 mL of water on shaking platform (120 rpm) and 10 μL of the extract was periodically removed and added to 3 mL of water in a cuvette and measured at 244 nm. The extinction coefficients for APAP water was determined by calibration measurements and was found to be $\lambda_{244,H2O} = 5800$ mol.L.$^{-1}$cm^{-1}.

2.5 Powder Colorimetry

The amount of colored powder material in its mixture with white powder was measured using a dry colorimetry method. A color spectrophotometer, X-rite VS-450 (Figure 2-5), was used to measure the reflectance of visible light from a sample containing unknown quantities of colored and white material. A sampling spoon was used for presenting the powder sample to the light source. The spoon has a fill volume of 21.5 mL. However, since the sample size was much smaller than the spoon capacity, the spoon was fitted with a solid cutout, reducing the fill volume of the spoon to approximately 5 mL of powder. The powder sample was distributed in the spoon and its surface was made smooth using a plastic scraper. Figure 2-6a shows the empty sampling spoon. Figure 2-6b shows the sampling spoon with the solid cut-out loaded with a mixture of sugar and $CuSO_4$, ready to be scanned by the colorimeter. A 6 mm aperture was used to scan the sample. Each sample was scanned in triplicate, with the process of loading then unloading a sample repeated between scans. Calibration samples were scanned five times. The wavelength at which the calibration curve was developed was chosen based on

the visual characterization of the spectrum at all wavelengths. The wavelengths at which the distinction between the individual reflectance values was maximum, was chosen. The reflectance measured at this wavelength from an unknown sample was used to evaluate the concentration of colored material with the help of a calibration curve. Further details on the colorimeter can be found in the work of Emady et al. [30].

2.6 Figures for Chapter 2

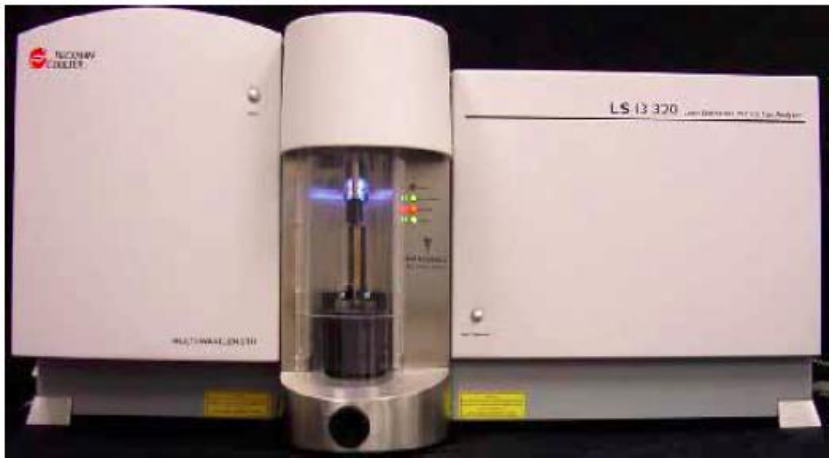

Figure 2-1: Beckman Coulter LS 13 320 laser diffraction based particle size analyzer. The tornado system fluidizes particles to measure the size of individual grains

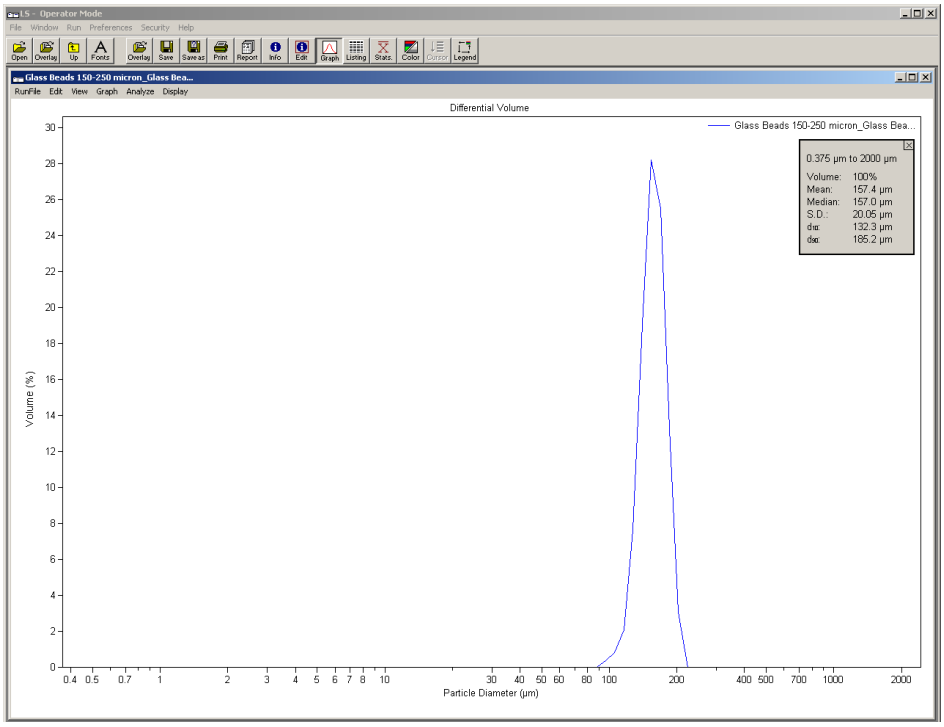

Figure 2-2: A sample particle distribution profile obtained from the Beckam Coulter LS 13 320 laser diffraction instrument. Note the particle size distribution parameters presented at the right top corner.

Figure 2-3: Endocotts sieve shaker. The shaking ensures percolation of the grains through the sieves until they encounter perforations smaller than, typically, their second largest dimension.

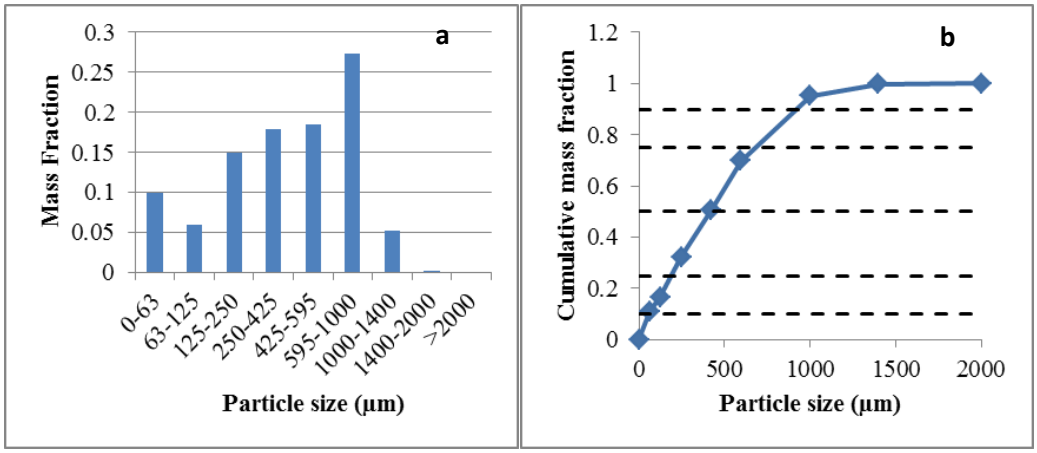

Figure 2-4(a): An example of a particle size distribution profile expressed as a bar chart. (b) The cumulative distribution is used to compute the particle size distribution parameters.

Figure 2-5: X-Rite VS-450 colorimeter. The colorimeter shines visible light on the sample and measures the consequent reflectance

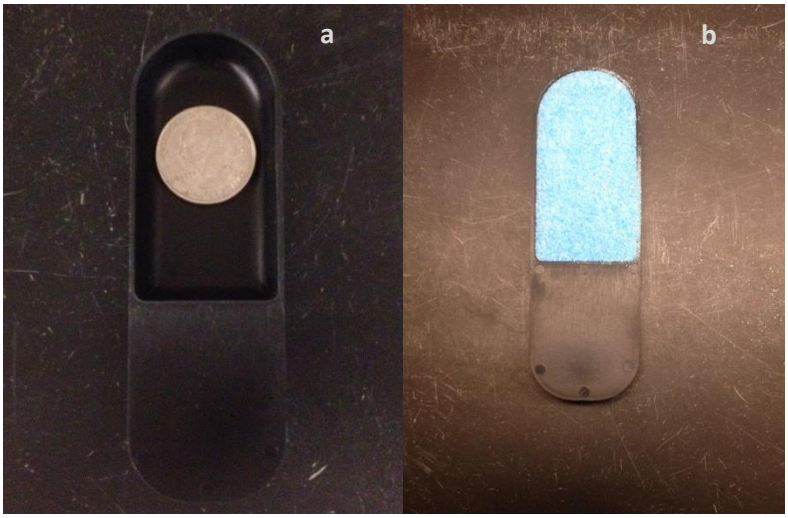

Figure 2-6: Sample spoon of the dry powder colorimeter. The empty spoon has a fill volume of 21.5 mL. To accommodate smaller samples, the empty cavity was filled with a solid cut-out reducing its fill volume to 5 mL. (b). A sample of CuSO4 and sugar ready to be scanned.

Chapter 3 : Axial Mixing of Poorly Flowing Powders in Rotating Cylinders

3.1 Introduction

The rotating cylinder has been a popular apparatus to study granular dispersion. The setup involves horizontally filling an appropriately sized cylinder with a single ingredient or a mixture of ingredients, and rotating the cylinder along the horizontal axis. The transport of the material along the axial direction (and the radial) is monitored and quantified.

It is now generally accepted that the axial dispersion of granular materials in rotating cylinders obeys Fick's second law [31].

$$\frac{\partial C(z,t)}{\partial t} = D_{ax}\frac{\partial^2 C(z,t)}{\partial z^2}$$

z is the position along the axial length of the drum, t is the time and D_{ax} is the axial dispersion coefficient, a constant. The axial dispersion coefficient is computed by loading the cylinder with a tracer, as a single particle, narrow pulse or a wide band, followed by measuring the dispersion of the tracer. The dispersion is measured as concentration *C* of the tracer, as a function of time and axial position. Sherritt and coworkers [32] reviewed various methods for loading the tracer particles in the cylinder and consequent mathematical solutions for computing D_{ax}.

Interestingly, majority of the research on understanding the axial dispersion of granular materials in rotating cylinders has dealt with free-flowing granular materials [33-35]. Early work on understanding self-dispersion in rotating cylinders was performed by Hogg and co-workers [36]. Parker *et al.* [37] used positron imaging particle tracking to

evaluate the axial dispersion of glass beads ranging from 1.5 mm to 3 mm, in cylinders ranging from 10 cm to 14.4 cm in size, and showed a dependence of the dispersion coefficient on the particle size of the beads. McLaren *et al*. [38] experimentally determined the axial dispersion coefficient of glass beads ranging from 1.14 mm to 3.15 mm and found that the dispersion coefficient was dependent on the rotation speed of the cylinder and the particle size of the glass beads. The dispersion coefficient increased proportionally to rotation speed as $\omega^{0.8}$ and proportional to the particle diameter as $d_p^{1.84}$. These experimental results were found to be in agreement with their discrete element model (DEM) based simulations [39, 40]. The simulations also revealed that the axial dispersion coefficient is found to be independent of the diameter of the drum, for large *D,* simultaneously making the dispersion coefficient non-scalable by the Froude number.

The Froude number is a dimensionless number and is defined as the ratio of the centripetal force to the force of gravity. In case of rotating cylinder like systems, it is given as $Fr = \frac{D\omega^2}{g}$. For free flowing systems, researchers have been able to identify relationships between the Froude number and regime of operation, that is, the flow pattern the material assumes as the cylinder rotates. A summary of this relationship can be found in Sherritt *et al*. [32]. However, finding scaling relationships between the axial dispersion coefficient and dimensionless numbers has proven to be more challenging, even for free flowing materials. Ding *et al*. [41] were able to combine several process parameters such as the particle-to-drum diameter ratio, drum fill percentage, and particle restitution coefficient together with the Froude number to give a single dimensionless number for operations in the rolling regime and for Froude numbers greater than 0.003.

Developing scaling relationships for poorly flowing materials is naturally considered more challenging. The use of largely free flowing materials has allowed researchers to model the axial dispersion independent of the bulk properties of the material. The inter-particle force in well-flowing materials, with large particle sizes, is usually negligible. Dispersion is thus dependent only on process parameters and properties of the particles that constitute the material. On the contrary, the inter-particle forces in cohesive materials are comparable to the gravity forces. The bulk properties of the material are thus not a trivial sum of the properties of the individual particles that constitute the material. These materials exhibit change in their bulk properties upon the application of a constant normal stress [42] or periodic vibrations. Poorly flowing materials are also characterized by the presence of a tensile stress, a minimum force required to induce slip between material planes. Although, the behavior of cohesive materials in the rotating cylinders has been studied [10-12, 43-45] to a certain extent, the axial dispersion of such materials remains largely uninvestigated. The effect of bulk cohesive properties on the axial dispersion behavior of poorly flowing materials was studied in the recent work of Koynov *et al.* [46]. They observed that the axial dispersion coefficient increases with increase in particle cohesion. This was attributed to an increase in the effective particle size with increase in cohesion, which led to increase in axial dispersion.

This work builds on the work of Koynov and coworkers [46] and focuses on the effect of rotation speed and cylinder diameter on the axial dispersion coefficient for poorly flowing materials. Three materials with varying flowing properties have been investigated for their axial dispersion behavior, at three scales and three rotation speeds. An attempt has been made to scale the process using dimensionless numbers, specifically,

the Froude number which captures process parameters and the Bond number, which incorporates material cohesion. The Bond number used in this case considers the increase in cohesive forces in the presence of an external consolidation stress. Empirical relationships between D_{ax} and the aforementioned dimensionless numbers have been computed and presented.

3.2 Materials

Lactose Monohydrate was purchased from Foremost Farms (Beloit, WI). Microcrystalline Cellulose (Avicel PH-101) was provided by FMC Biopolymer (Philadelphia, PA) and Compap L acetaminophen (90% Anhydrous) was purchased from Mallinckrodt (Hazelwood MO). Acetone (ACS reagent, > 99.5%) for dyeing was purchased from Sigma Aldrich. Permeant markers (Sharpie, Fine Point, Black,) were purchased from OfficeMax.

3.3 Experimental Design

The axial dispersion coefficient was computed by measuring the concentration of the dyed tracer as a function of axial position and time. Three cylinder sizes, namely, 4 inches, 8 inches and 16 inches were investigated. Three speeds for each material were studied. These speeds varied depending on the size of the cylinder and the material in consideration. The objective was to ensure that a similar set of flow profiles are obtained for each material at each speed level. The first speed level resulted in cascading behavior. The two higher levels resulted in cataracting behavior. Table 3-1 lists all the speeds at which the experiments were performed. All runs were performed in triplicate.

In addition to the experiments listed above, two additional experimental points were investigated. The axial dispersion behavior of Avicel PH-101 and Lactose were studied in

the centrifuging regime in the 4 inch cylinder. The regime could not be achieved for Compap L in the 4 inch cylinder even at the highest speed setting of the rollers.

3.4 Methods

The particle size distribution of the starting material was measured using a laser diffraction method described in Section 2.2.1. Each measurement was performed thrice and the average value is reported in Table 3-2.

3.4.1 Compressibility and Conditioned Bulk Density

The FT4 Powder Rheometer was used to obtain the compressibility and bulk density of the investigated materials. The test measures cohesion of powders by correlating the change in the volume of the powder bed upon the application of a normal force. The sample was placed in a cylindrical cup and pre-conditioned by a pass-through of a helical blade. The mass and the volume of the bed were recorded and a value of the conditioned density was computed. The sample was then consolidated slowly with a vented piston by applying a normal force between 0.5 and 15 kPa, in small increments. The change in volume of the bed upon compression was measured. The compressibility index (CI) was calculated as the ratio of density under compression (density measured at 15 kPa) to the conditioned bulk density at no consolidation. Each measurement was performed in triplicate and the average value has been reported in Table 3-2

3.4.2 Dyeing Procedure

Material was dyed in a twin-axis blender by mixing dye-infused acetone with the material. Ink cartridges from Sharpies were removed from their casing, split into two and allowed to leach in acetone overnight. The number of cartridges and acetone needed for dyeing each material is presented in Table 3-3. The cartridges were removed from the acetone post leaching. The dye-infused acetone was added to the material previously

loaded in the blender. The blender was rotated at 15 rpm for 20 minutes after which the wet, dyed material was discharged. The material was air-dried overnight. Several such batches were made for each material based on its requirement. All the dried batches were combined by dry mixing them together in the twin-axis blender at 15 rpm for 20 minutes. The final combined batch of dyed material was used to develop the calibration curve and perform all experiments.

Concentration of dyed powder in a sample, containing an unknown quantity of dyed powder in undyed powder, was evaluated using a visible light spectroscopy method described in Section 2.5. Reflectance values at 600 nm were used. The calibration curves obtained for each material are presented in

Table 3-4. As an example, the calibration curve of Lactose is shown in Figure 3-1.

3.4.3 Axial Dispersion Experiment

As previously mentioned, the axial dispersion coefficient was computed by measuring the concentration of the dyed tracer as a function of axial position and time. The tracer was loaded as a wide band in the center of the cylinder (Figure 3-2), surrounded by undyed material on either side.

The length of the band was 1/3rd the total cylinder length. A fill volume of 35% was kept constant for all materials. The cylinder was placed on a set of rollers and rotated at a speed based on the design point. At appropriate time intervals, the process was stopped

and the surface of the powder bed was sampled, along ten evenly distributed positions along the axis of the cylinder. The 4 inch and 8 inch cylinders were 30 cm in length while the 16 inch cylinder was 60 cm in length. Approximately, 2-5 g of material was extracted per sample. The cylinder was closed shut and rotated until the next time point. Sampling intervals were such that the tracer distribution profile exhibited a gradual change until the tracer was completely dispersed in the powder bed. The bed was sampled at six time points. In case of the 4 inch cylinder, due to the possibility of a substantial loss in mass of the powder bed due to sample extraction, the experiment was performed using two loaded cylinders. The first cylinder was run and sampled until the 3rd time point, after which, the second cylinder was run and only first sampled at the 4th time point. Combination of the results from the two cylinders provided a full profile consisting of data at six time points. Each experiment was performed in triplicate, except the trials at 16 inch scale. These experiments were only performed once due to high material requirements.

3.4.4 Numerical Methods

The dispersion in Fick's second law was solved numerically in gPROMS using the software's built parameter estimation algorithm. An initial condition was applied such that the concentration of colored powder was zero at all points except for an interval in the middle of the domain, where the concentration was one. Because this colored section of powder could not be placed precisely during experiments, the midpoint and width of this interval were also estimated using parameter estimation. Boundary conditions were applied such that the flux at each end was zero. The model was solved in gPROMS ModelBuilder using a centered finite difference method with 300 grid points.

3.4.5 Theoretical Considerations

Two dimensionless numbers were used to understand relationships between the axial dispersion behavior of the material and the forces acting on the system and on individual particles that drive the axial dispersion. As previously defined, the Froude number in rotating systems is a ratio of the centripetal force to the force of gravity and is given by

$$Fr = \frac{D\omega^2}{g}$$

Where D is the diameter of the drum, ω is the rotation speed and g is the acceleration due to gravity.

The Bond number is a ratio of the cohesive force between individual particles and its weight measured as the force of gravity acting on the particles. Several relationships can be used to determine the force of attraction between two particles. In the presence of an external consolidation stress, the inter-particle attraction can be given by Rumpf's expression [47], shown below.

$$F = \frac{\Pi d_p^2}{\Phi k}\sigma$$

Where d_p is the particle diameter, σ is the consolidation stress, Φ is the solid volume fraction and k is the co-ordination number. The co-ordination can be estimated by the following expression [48].

$$k = 1.25(1 - \Phi)^{3/2}$$

Powder at the bottom of a cylinder is consolidated by the weight of the powder above it. Since a 35% fill level was kept constant in all runs, σ was computed as

$$\sigma = 0.35 D \rho_b g$$

where ρ_b is the bulk density of the material. The Bond number computed in this study was thus, not only a function of material but also accounted for the external consolidation stress. The final expression is given as

$$Bo = \frac{F}{W_g}$$

3.5 Results

The axial dispersion profile was also found to folllow Ficks second law for the poorly flowing materials investigated in this study, similar to the finding of Koynov et al. [46]. Figure 3-3 shows the axial dispersion profile for Avicel PH-101 in the 4-inch cylinder at the first speed level at various times. The series of dots represents the experimental data points while the smooth curve is the model prediction. It can be observed that model fits the data fairly well. Fick's second law is able to model the axial dispersion behavior of the material. The axial dispersion coefficient can thus be used as a representative parameter to quantify the rate of axial dispersion.

The individual values of axial dispersion obtained for 27 experiments performed in this study with their standard deviations are presented in Table 3-5.

By now, it is generally accepted that the axial dispersion in rotating cylinder is driven by random collisions on the free surface. Higher the number of these collisons, higher is axial dispersion. The axial dispersion thus increases with increasing speeds, as the collision freqeuncy increases at higher speeds. As previously mentioned, majority of the research on this topic has dealt with free flowing materials. Consequently, these theories also largely apply to free flowing materials, whose bulk properties are independent of any

external stress. The number of collisions is only depedent on the collision frequency, dictated by rotation speed, and the number of particles in the system. The bulk properties of poorly flowing materials, on the other hand, are the function of their consolidation state. Poorly flowing materials densify in the presence of a normal consolidation stress. This densification can result in the formation of macro-assemblies, commonly knows as aggregates or chuncks. These chunks can be modeled as a single particle, ableit with a larger particle size.

A poorly flowing powder situated at the bottom of the powder bed in a cylinder experiences the weight of the powder above it. This normal force is hypothesized to consolidate the powder at the base of the cylinder. This may result in the formation of chunks. The chunks rise to the free surface when the cylinder rotates, and traverse down the free surface as the material cascades or cataracts. These loose powder assemblies break due to collisions with the free surface, other agglomerates or primary particles, leading to the enahcned dispersion.

Figure 3-4 illustrates the the axial dispersion coefficient as a function of the compressibility of the investigated materials. Compressibility of the material, as previosly mentioned, is defined as the change in the volume of the powder upon the application of a normal consolidation stress. Higher is the compressibility of the material, poorer is the flow and larger is its tendency to form chunks. It can be observed that the axial dispersion coefficient increases with increasing compressibility. A more compressible material leads to the formation of larger chunks, which leads to enhanced axial dispersion as the larger chunk disperses more material in the axial direction when it breaks. A similar result was observed by Koynov et al. [46] for five materials spanning a range of flow properties.

Their work showed that under the same experiemental conditions, the bulk properties of the material have a statiscally significant effect on the axial dispersion coefficient. Moreover, the cohesivity of the material characterized by its median particle size, flow function coefficient or compressibility exhibited identical relationships with the axial dispersion coefficient; an increase in cohesion leads to higher axial disperson.

What is also observed in Figure 3-4, for the same material, is the increase in the axial dispersion coefficient with increasing scale of the system (except for Lactose with CI = 1.25 between the 8 inch and 16 inch cylinder). The height of the powder bed in a larger cylinder, at the same fill volume, is higher than in the smaller cylinder. The magnitude of the normal stress that material at the bottom experiences due to the material above is also conseqeuntly, higher. This increase in the normal stress results in the formation of larger chunks. A larger chunk, containing more material, leads to higher axial dispersion when it breaks on the free surface. The axial dispersion is thus found to be dependent on the scale of the system for poorly flowing materials since poorly flowing materials exhbit a change in their bulk properties upon the application of a consolidation stress, unlike free flowing materials.

Relationship between particle cohesion and the axial dispersion coefficient is further highlighted in Figure 3-5. Figure 3-5 illustrares the axial dispersion coefficient as a function of the Bond number. As described in Section 3.4.5, the Bond number, in this case, not only quantifies the inter-particle attraction but also the attraction due to the presence of an external consolidation stress, which is higher at larger scales. The possibility of forming large chunks is thus higher at higher Bond numbers. It can be observed that axial dispersion exhibits a linear increase with increasing Bond number.

Figure 3-4 and Figure 3-5 represent data in the cascading regime, achieved at the smallest speed level across all scales. Similar relationships were observed at the higher speed levels.

In addition to the properties of the material, it is well known the axial dispersion coefficient is a function of rotation speed of the system and in conjunction, the regime of operation. Shown in Figure 3-6 is the axial dispersion coefficient of Lactose and Avicel PH-101 in the 4-inch cylinder, as a function of the flow regime. The x-axis, traversing right, represents increasing speeds. It can be observed that the dispersion coefficient increases as the flow transitions from the cascading to the cataracting regime but decreases significantly as the material begins to centrifuge. As previously mentioned, the axial dispersion in poorly flowing materials occur as chunks of materials break upon collisions with other chunks, the free surface and other primary particles. In the cascading regime, the powder assemblies are gently impacted against the free surface or roll down the free surface. At higher speeds, as the material begins to cataract, these chunks are slammed against the free surface which leads to enahnced dispersion. Moreover, since the speed of the process is higher, the material recirculates faster which increases the overall rate of collisons. Thus, not only does each collison lead to enhanced dispersion but the overall rate of collisons is higher which results in a significant increase in the axial dispersion coefficient.

With further increase in speeds, the material begins to centrifuge. The centripetal force equates the force of gravity and the material adhreses to the walls of the cylinder as it spins. The are little or no collisons which significantly decreases axial movement of the

material. This is reflected in the D_{ax} value. The axial dispersion coefficient of the material is significantly lower in the centrifuging regime compared to the cataracting regime.

The quantitative effect of rotation speed on axial dispersion of each material is illustrated in Figure 3-7. The first data point at each scale is obtained in the cascading regime while the next two data points were obtained when the material was cataracting. As expected, the axial dispersion coefficient increases with increasing speeds. Interestingly, it is also observed that the relationship between the axial dispersion coefficient and rotation speed is different at different scales for all three materials. The rate of change of axial dispersion as function of the rotation speed is thus *scale* dependent. This is an important finding since it contrary to the finding for free flowing materials, where for large D, the axial dispersion coefficient is independent of the scale of the system.

The axial dispersion coefficient exhibits a liner relationships with the rotation speed for Avicel PH-101 (Figure 3-7 (a)) and Lactose (Figure 3-7 (b)), that is $D_{ax} \propto \omega^{\sim 1}$. This is again, in contrast to finding to findings for free flowing materials, where $D_{ax} \propto \omega^{<1}$ [38]. Furthermore, in case of Compap L (Figure 3-7 (c)), the axial dispersion coefficient has an exponential relationships with the rotation speed or could also be modeled as $D_{ax} \propto \omega^{>1}$. A potential explanation for the higher exponentials of speed in the case of poorly flowing materials has been previously mentioned. At higher speeds, not is the rate of collison of the chunk higher, but each collison results in more material being dispersed as chunks collide with greater impact at higher speeds dispersing more material.

In case of Figure 3-7(a) and Figure 3-7(b), the absolute values of axial dispersion coefficient obtained at the 16 inch scale for Lactose and Avicel PH-101 are smaller than

those obtained at the 8 inch scale. This is because of the operating regime in 16-inch cylinders. It was observed that even at comparable flow behavior on the free surface, that is, even if the free surface was cascading or cataracting, a large fraction of the powder bed was slumping. This was attributed to the difference in coefficient of friction between the 4 and 8 inch cylinders and the 16 inch cylinder. The recirulation freqeuncy of the material was much lower leading to slower rates of axial dispersion in the 16 inch cylinder.

To further elucidate the effect of properties of the material on the system, the same of set data can be replotted at each scale (Figure 3-8). It can be observed that at comparable scales and rotation speeds, the rate of change of the axial dispersion coefficient is different for different materials. Avicel PH-101 and Lactose have linear relationships with rotation speeds while Compap L shows an exponential relationship (or could be modeled with a speed exponent greater than 1). The relationship between the axial dispersion coefficient and rotation speed is thus *scale* and *material* dependent.

The effect of speed and scale can be simultaneously investigated by plotting the axial dispersion coefficient as a function of dimensionless Froude number. The Froude number is ratio of centripetal force to the force of gravity and thus for materials with similar coefficient of frictions with the wall of the cylinder, comparable Froude numbers should lead to comprable operating regimes. A summary of the various operating regimes as a function of the rotation speed and percent fill can be found in the work of Sherrit *et al*. [32], as a regime map. The rate of axial dispersion can thus be hypothesized to scale with the Froude number. The axial dispersion coefficient did not scale with the Froude number in the work of Third *et al.* [40], for free flowing materials. Shown in Figure 3-9 is the

axial dispersion coefficient as a function of the Froude number for each material investigated at various scales.

As expected, the axial dispersion coefficient did not scale with the Froude number, in this work, since it became clear that the axial dispersion coefficient is a function of the properties of the material, and not merely the process parameters. To develop a scaling relation, the relation must incorporate a quantity that captures the bulk properties of the material, and their change with changing scales.

Since a linear relationship was observed between the axial dispersion coefficient, and the Bond and the Froude number (except in the case of Compap L), a linear regression model was developed using *Minitab 17* (Minitab, State College, PA). The regression model and corresponding ANOVA results are presented in Table 3-6 and Table 3-7. Shown in Figure 3-10 is the normality plot of the residuals which shows a fairly normal distirbution of the residuals. The constant term, in the model, was set to zero since no axial dispersion is expected to occur if the cylinder is at rest. The model excluded certain outliers, specifically, dispersion values at the 8-inch scale obtained in the cataracting regimes for Lactose and Avicel PH-101. The final model is constructed using 20 values of the axial dispersion, out of a possible 27, over three scales and three speed levels. It can be observed that the Froude number is significant and while the interaction of Bond and Froude number is also significant. It is important to note that the model is statistical in nature, with the inclusion of the Froude and the Bond number being mechanistic contributions. The model is developed for the values across the cascading the cataracting regimes but does not incoporate the nature of the regime in the equation. Any purely mechanistic model that developed for axial dispersion of the poolr flowing materials,

must not ony incorporate the formation of the agglometates but also their breakage upon rolling or impact with the bed surafce, which is the driver for axial dispersion.

$$D_{ax} = 15.62 * Fr + 0.001413 * Bo * Fr$$

In order to provide a visual represpresentation of the model, a contour plot of the axial dispersion coefficient as a function of the Froude and the Bond number is shown in Figure 3-11. As expected, an increase in both dimensionless numbers results in increase in the dispersion coefficient.

The increase in the dispersion coefficient with increasing Froude number results from the increasing recicurlation rates of the material or change in flow regimes with increasing speeds. The change in material cohesion with changing scales is quantified by the Bond number. The Bond number used in this study not only incorporates cohesive forces between particles but also incorporates the presence of increasing consolidates stresses in larger cylinders. This leads to the formation of larger powder macro assemblies, which disperse more material when they break. The axial dispersion coefficient is thus dependent on the scale of the system, the rotation speed and the bulk material properties.

3.6 Conclusions

The axial dispersion coefficient of poorly flowing materials in rotating cylinders was investigated for three materials at the three speeds and three scales of operation. It was observed that the dispersion coefficient is dependent on the regime of operation. The axial dispersion increases as the material transitions from the cascading to the cataracting regime but decreases when the material begins to centrifuge at high speeds. The dispersion coefficient was found to be proportional to $\boldsymbol{\omega^{\geq 1}}$. The dispersion coefficient

was also observed to increase with increasing powder cohesion. Cohesive materials form aggregates during operation, the size of the aggregates increasing with increasing cohesion. These chunks breaks during operation leading to dispersion. Consequently, a larger chunk disperses a greater quantity of material. The dispersion coefficient was thus found to be scale depedent since larger chunks are formed at bigger scales, due to the presence of higher consolidation stresses.

3.7 Figures for Chapter 3

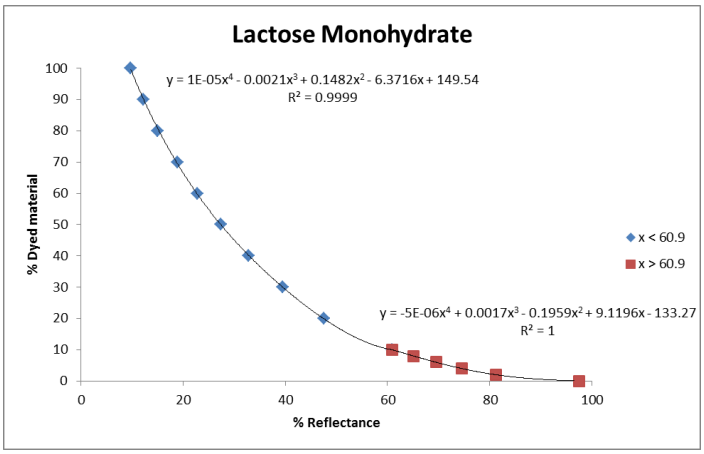

Figure 3-1: Calibration curve of Lactose Monohydrate. The curve determines the percent of dyed lactose in a mixture of pure and dyed lactose based on the reflectance value of a colorimeter

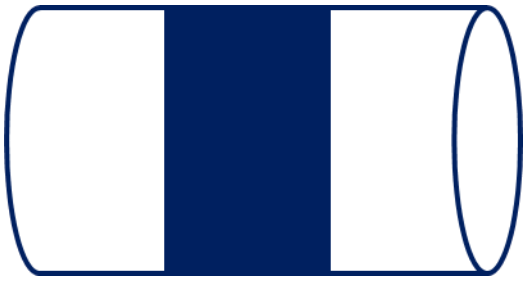

Figure 3-2: Initial loading condition of the cylinder. The middle 1/3rd of the cylinder is loaded with dyed material. 1/3rd sections on the two ends are loaded with undyed material. A fill volume of 35% was kept constant for all materials.

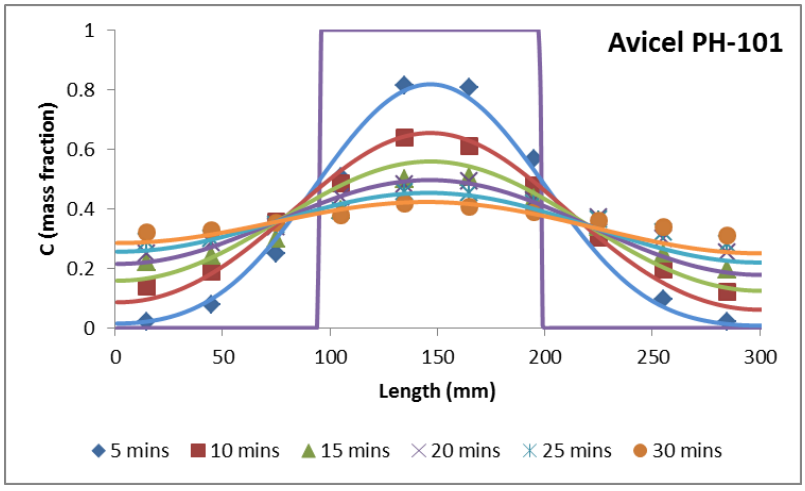

Figure 3-3: Axial dispersion profile of Avicel PH-101 at the first speed level. The dots are experimental measurements while the smooth lines represent the model fit.

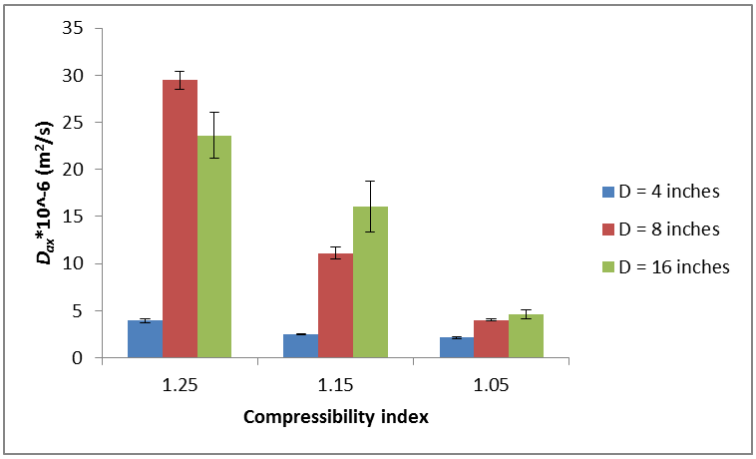

Figure 3-4: Axial Dispersion coefficient as a function of material compressibility. Increasing compressibility index (increasing cohesion) results in enhanced axial dispersion. The data represents D_{ax} values in the cascasding regime for all materials. A compressibility of 1.25 represents Lactose Monohydrate, 1.15 represents Avicel PH-101 and 1.05 represents Compap L.

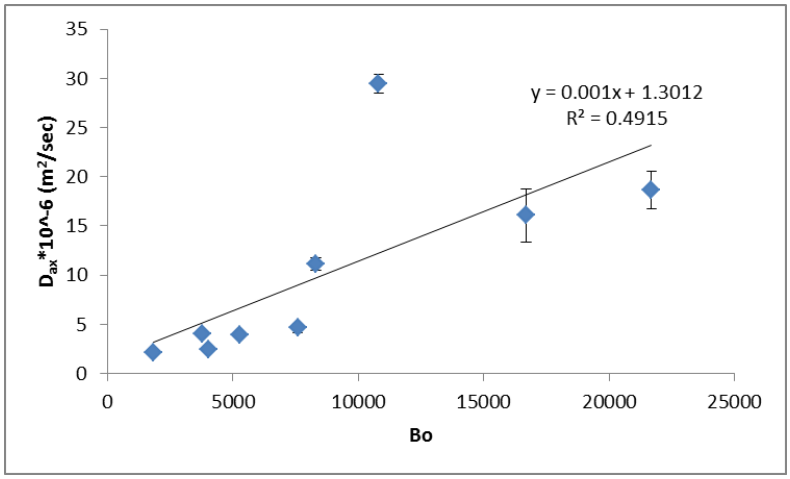

Figure 3-5: Relationship between the axial dispersion coefficient and the Bond number. A higher Bond number indicates higher inter-particle cohesion which results in the formation of larger chunks. The breakage of a larger chunk results in higher axial dispersion.

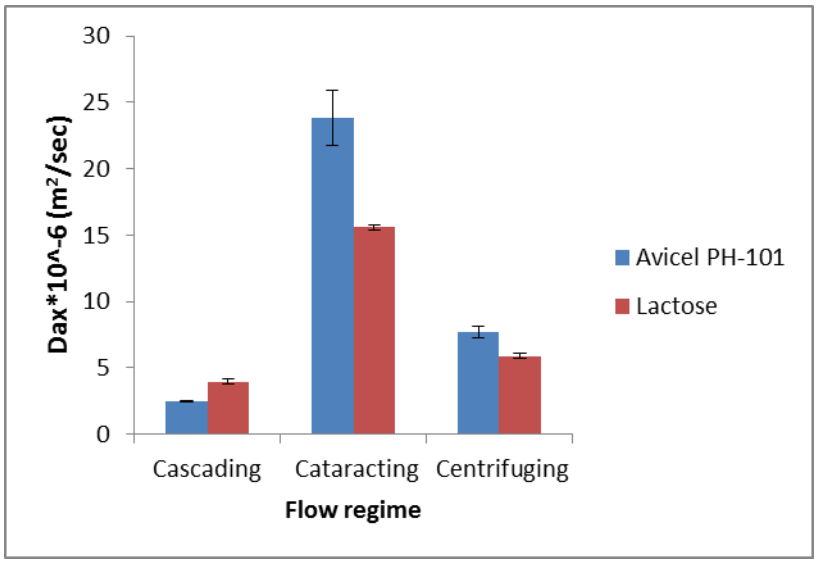

Figure 3-6: Dependence of the axial dispersion on the flow regime in the 4 inch cylinder. The value of D_{ax} increases as the material transitions from the cascading to the cataracting regime, but decreases when the material begins to centrifuge.

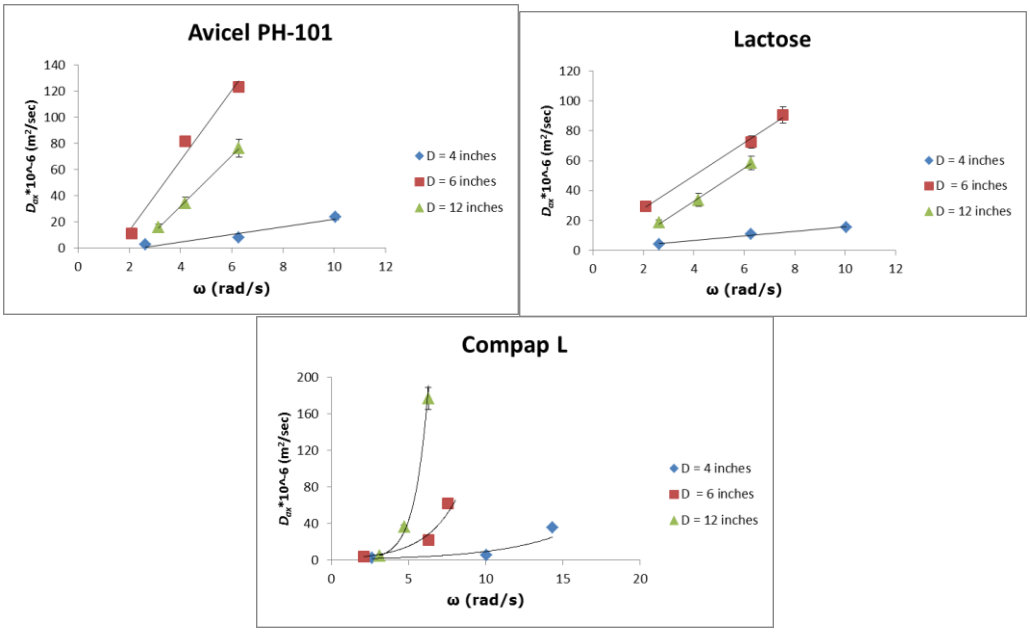

Figure 3-7: Correlation between the axial dispersion coefficient and the rotation speed in radians/s. Relationship for a) Avicel PH-101, b) Lactose and c) Compap L. The relationships are scale dependent.

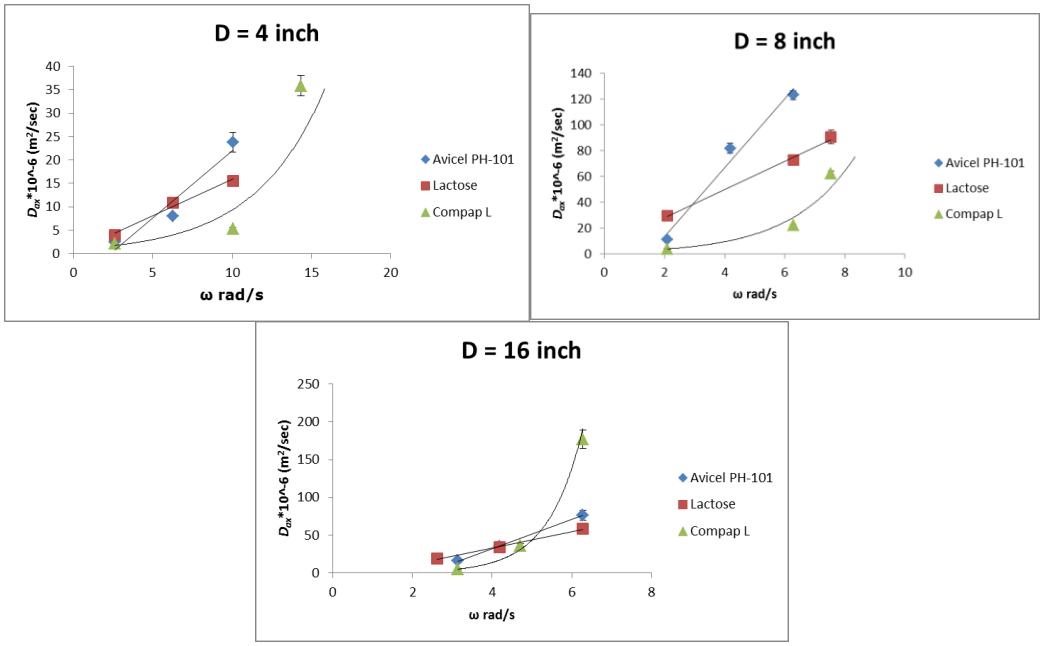

Figure 3-8: Correlation between the axial dispersion coefficient and the rotation speed in radians/s. Relationship for a) 4 inch, b) 8 inch and c) 16 inch cylinders. The relationships are material dependent.

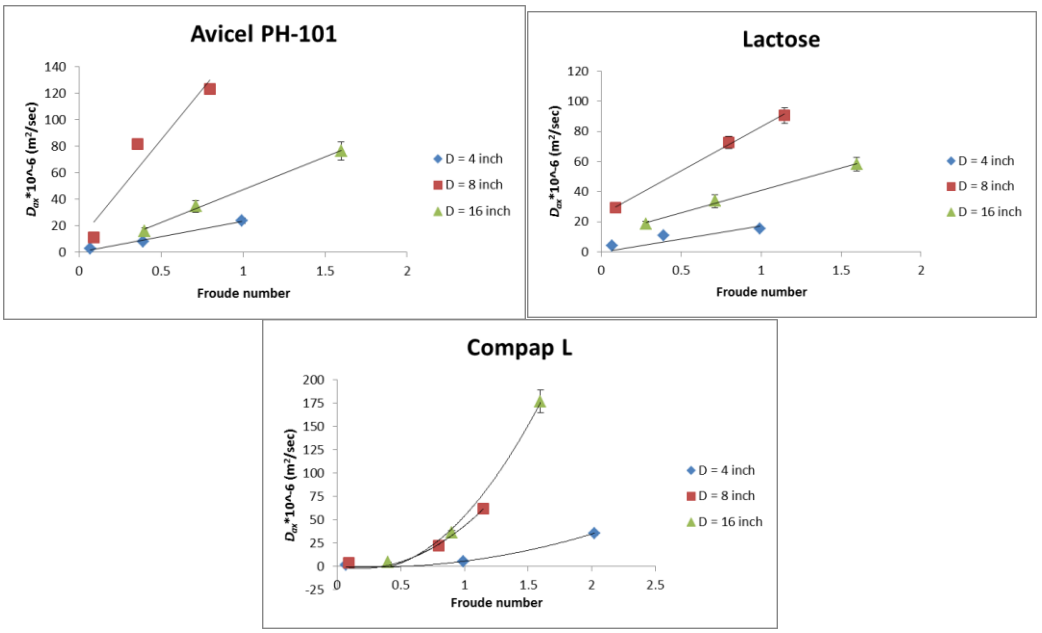

Figure 3-9: Correlation between the axial dispersion coefficient and the Froude number. Relationships for a) Avicel PH-101 b) Lactose and c) Compap L. The materials do not scale with the Froude number since the materials exhibit a change in their properties with changing scales.

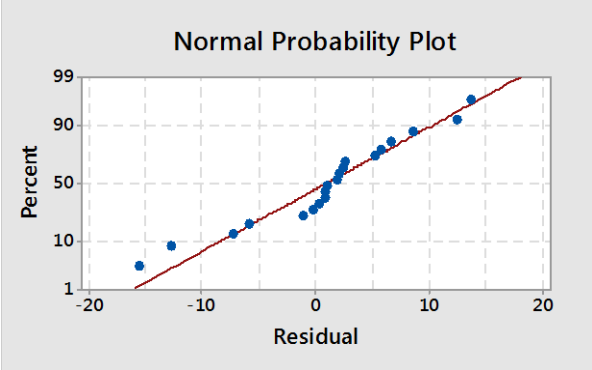

Figure 3-10: Distribution of the residuals obtained from the regression model developed to correlate the axial dispersion coefficient to the Froude and the Bond number

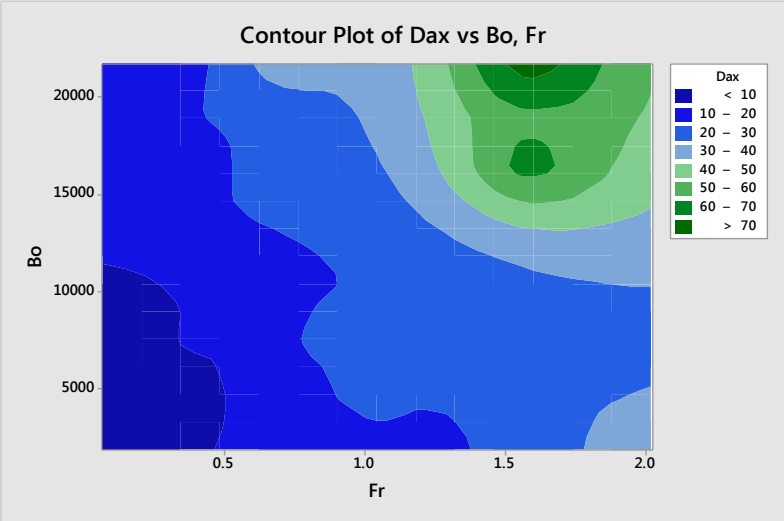

Figure 3-11: Contour plot of the axial dispersion coefficient vs the Froude and Bond number. Units of the dispersion coefficient are D_{ax}*10^{-6} m^2/s.

3.8 Tables for Chapter 3

Table 3-1: Speed in rpm at which the tests were performed for the materials and the cylinder sizes listed. The selection of speed levels for each material is such that comparable flow profiles are achieved between materials at equivalent speed levels.

	Cylinder Diameter (inches)		
	4	8	16
Avicel PH-101	25	20	30
	60	40	40
	96	60	60
Lactose	25	20	25
	60	60	40
	96	72	60
Compap L	25	20	30
	96	60	45
	137	72	60

Table 3-2: Particle size distribution parameters, conditioned bulk density and compressibility index of materials investigated in the study. The figure in brackets is the standard deviation over three measurements.

Material	d10 µm	d50 µm	d90 µm	CBD (g/cc)	CI at 15 kPa
Avicel PH-101	24.77 (0.18)	74.56 (0.45)	159.63 (2.49)	0.34 (0.0)	1.15 (0.005)
Lactose Monohydrate	14.06 (1.16)	60.32 (4.78)	102.21 (11.08)	0.65 (0.01)	1.25 (0.03)
Compap L	82.33 (2.24)	182.83 (1.85)	337.8 (10.94)	0.49 (0.00)	1.05 (0.00)

Table 3-3: Size of a batch in a dyeing experiment is shown. The corresponding number of ink cartridges and acetone used to distribute the ink is also shown.

Material	Batch size (kg)	Acetone (liters)	Sharpie cartridges
Avicel PH-101	15	8	360
Lactose	18	4	200
Compap L	15	6	270

Table 3-4: Calibration curves for Avicel PH-101, Lactose and Compap L; *x* is the reflectance of the scanned sample, while *y* is the predicted concentration.

Mixture	Calibration Curve	Condition	R^2
Avicel PH-101	$y = -0.0016x^3 + 0.1727x^2 - 7.4876x + 141.78$	x <42.15	0.99
	$y = -0.0001x^3 + 0.0277x^2 - 2.5985x + 83.84$	x>42.15	0.92
Lactose	$y = 1E\text{-}05x^4 - 0.0021x^3 + 0.1482x^2 - 6.3716x + 149.54$	x<60.9	0.99
	$y = -5E\text{-}06x^4 + 0.0017x^3 - 0.1959x^2 + 9.1196x - 133.27$	x>60.9	1
Compap L	$y = -1E\text{-}05x^4 + 0.0006x^3 + 0.0353x^2 - 4.255x + 130.17$	x<48.4	0.99
	$y = 7E\text{-}06x^3 + 0.0047x^2 - 1.1777x + 63.485$	x>48.4	0.99

Table 3-5: Axial dispersion coefficient of three materials at all investigated conditions. The units are in 10^{-6} m^2/s. The standard deviation denoted as SD has the same units.

	D = 4 inch			D = 8 inch			D = 16 inch		
	Speed (rpm)	D_{ax}	SD	Speed (rpm)	D_{ax}	SD	Speed (rpm)	D_{ax}	SD
Avicel PH-101	25	2.49	0.04	20	11.12	0.61	30	16.05	2.66
	60	8.06	0.19	40	81.78	4.04	40	34.54	4.54
	96	23.82	2.07	60	123.0	3.62	60	76.35	6.69
Lactose	25	3.95	0.18	20	29.47	0.97	25	18.64	1.93
	60	10.85	0.91	60	72.51	4.04	40	33.69	4.38
	96	15.58	0.92	72	90.56	5.33	60	58.46	4.51
Compap L	25	2.13	0.10	20	4.00	0.11	30	4.63	0.47
	96	5.35	0.23	60	22.00	0.79	45	36.21	2.66
	137	35.84	2.15	72	62.27	2.18	60	176.64	12.12

Table 3-6: Analysis of variance parameters for the regression equation correlating the axial dispersion coefficient to the Froude and the Bond number

Analysis of Variance

Source	DF	Adj SS	Adj MS	F-Value	P-Value
Regression	2	15431	7715.25	133.12	0.000
Fr	1	1504	1503.89	25.95	0.000
Fr*Bo	1	2011	2011.21	34.70	0.000
Error	18	1043	57.96		
Total	20	16474			

Table 3-7: Model summary of the regression equation correlating the axial dispersion coefficient to the Bond and the Froude number

Model Summary

S	R-sq	R-sq (adj)	R-sq(pred)
7.61289	93.67%	92.96%	87.12%

Chapter 4 : Continuous Mixing of Highly Segregating Ingredients

4.1Introduction

In addition to understanding and scaling mixing processes of cohesive materials, mixing of ingredients with disparate properties has been a long standing challenge. It is well established that a granular mixture with a large disparity in the properties of its ingredients exhibits a natural tendency to separate or de-mix. That is, if the difference in the properties, such as, particle size density and shape is large, a granular mixture segregates upon the application of even a small stimulus, such as vibration, tumbling, discharge through a hopper or a pipe, etc. Creating homogenous mixtures from such ingredients, and sustaining this homogeneity through the process is a challenge.

This scenario is encountered in manufacturing of pharmaceutical solid oral dose products, that is, tablets and capsules. Often, the difference in the properties of the excipients and the active ingredients is large, posing a mixing challenge. While perfect homogeneity is usually an idealization, i.e., some degree of inhomogeneity is always present, poorly homogenized mixtures create a product that can be excessively non-uniform. Regulation, in the interest of patient safety, dictates a high level of blend homogeneity to ensure uniformity in the content of active ingredients in the final product. Non-homogenous product fails this quality criterion, which leads to the entire batch of material being discarded.

The challenge is further amplified since these mixing processes are batch based operations – the most common stimuli which cause segregation transpire in a batch process. In a batch mixing process, ingredients are loaded in a vessel and tumbled for a few hundred revolutions to achieve homogeneity before being discharged into an

intermediate storage vessel or the tablet press. It is well documented that ingredients with large disparities in their properties are near impossible to mix in batch systems; in fact, they can segregate MAXIMALLY in such situations. Alexander and co-workers [20, 21] showed that when glass beads of different particle sizes were mixed in V-blenders, a clear segregation pattern was observed. The nature of the pattern was dependent on the rotation rate and fill level. The de-mixing was attributed to a phenomenon called 'trajectory segregation' where the larger particles with greater inertia exhibited a poor ability to traverse the sharp bends in their path lines. Similar observations were made for mixing in double cone [22] and tote blenders [49]. Simulations of granular mixing and segregation in batch blenders confirmed the experimental findings [9, 49, 50]. Similar to the particle size induced segregation discussed above, density induced segregation is a well-known phenomenon in rotating cylinders [51, 52]. Moreover, when a large mass of powder is then discharged into a large empty container, a third mode of segregation is often observed, where the granular material flows along inclined surfaces and where small particles fall through the gaps between large particles [53-56]. This phenomenon, known as "sifting segregation," compounds the problem.

Finally, a fourth mode of segregation is often observed for such systems – fluidization segregation: As the granular material fills a vessel, typically a chute, displacing air, the counter flow of air and granular materials creates a dragging effect on the smaller particles, lifting them. As a result, when a granular material is discharged into a pipe of a chute, it is common to observe that the bottom of the pipe is largely depleted of fine particles [57, 58]. This often causes further heterogeneity.

A common approach to prevent or minimize segregation in pharmaceutical formulations is to avoid large particles and to attempt to match properties of different ingredients. This can often involve reformulating the original recipe. A second approach is granulation [59-61]. Wet granulation is the most common approach and it involves spraying a liquid binder on the mixture and mixing the wet mass to create a homogeneous powder assembly (granule) that is then dried and compressed into tablets or filled into capsules. For moisture-sensitive ingredients, the so called "dry granulation" process can involve compaction of the dry powder mixture to create ribbons or slugs, which are then milled to create granules, followed by compaction or capsule filling. However, wet or dry granulation involves several additional processing steps, may involve additional ingredients, and is thus lengthier, energy intensive, and more expensive. Avoiding granulation and enabling direct compaction, that is, directly compressing a mixture of active ingredients and excipients is of significant value to the industry. However, despite the well-documented advantages of direct compaction, granulation is used in a majority of products, due to real or perceived risks of segregation (as well as other factors).

However, as previously mentioned segregation is a more serious concern since the mode of manufacturing is batch. The alternative to batch processing is *continuous processing* of ingredients. In a continuous process, at steady state, ingredients are fed to a unit operation at a certain mass rate and the processed blend exits the unit operation at the same rate. The material then continues to the next unit operation in the process. The material typically spends a small amount of time (a fraction compared to the time it spends in a batch-based unit operation) in a single unit operation and continues to the next operation,

usually in a highly dense state. The material is not presented with any time or space to dissociate itself from unlike particles.

Continuous processing is widely prevalent in solids manufacturing, especially for processing large volumes, such as minerals, food, detergents, and construction materials. Despite their prevalence in other industries, these processes, particularly continuous mixing, have received relatively little attention by the scientific community compared to research on batch processing. Studies on continuous solid mixing have been few and far between [62-65]. Moreover, there are few categorical studies that compare batch and continuous mixing processes or that which study continuous blending of unlike ingredients.

In recent years, with increased interest in continuous pharmaceutical solid oral dose manufacturing, continuous powder mixing has begun to receive a significantly higher level of attention. A thorough summary of the state of continuous powder mixing can be found in Pernenkil and Cooney [23]. Research thus far has focused on effect of process parameters [66-68] and material properties [69, 70] on process performance. Attention also has been given to understanding the residence time distribution of the material in continuous mixers [71]. Additionally, Sarkar and others have examined powder behavior inside the continuous blender on a micro-scale using discrete element method simulations [72-75]. However, despite the recent surge in interest, very little is known about continuously mixing ingredients with a high tendency to segregate.

This chapter examines the ability of continuous blenders to mix materials with substantial differences in particle size and density, and consequently with a discernible tendency to

segregate. The performance of continuous blenders was compared to batch blenders for the same materials. Surprisingly, a simple linear relationship was found between the ratio of material properties and the blend's segregation potential. Relationships were also found between the segregation potential of mixtures and their mixing performance in batch systems. No such relationships were found in the case of continuous systems, largely due to the fact that segregation was largely arrested in continuous systems.

Five binary mixture pairs resulting from four materials were studied. Mixtures were ranked by their potential to de-mix by evaluating their segregation index in a segregation tester. Each pair was blended in both batch and continuous blenders at five different concentrations and their performance was compared. Details about the materials employed in the study, and the experimental and analytical methods are provided in Section 4.2 and 4.4, respectively. The results obtained have been discussed in Section 4.5 followed by concluding comments.

4.2 Materials

A total of four materials were used in the mixing studies. These materials spanned a range of particles sizes and densities such that the binary combination of these ingredients will result in a mixture with significant segregation tendency. Mustard seeds were purchased from Subzi Mandi (Edison, NJ). Avicel PH-101, which is microcrystalline cellulose, was provided by FMC Biopolymer (Newark, DE). Granulated sugar was purchased from Target Corporation (Minneapolis, MN), while copper sulphate ($CuSO_4$) was obtained from Alpha Chemicals (Cape Girardeau, Missouri). The additional material, poppy seeds, for segregation testing, was purchased from Superior Nut Company (Cambridge, MA).

4.3Experimental Design

A total of 5 mixtures, at 5 different concentrations each, were blended in batch and continuous blenders. The mixtures and their compositions have been detailed in Table 4-1.

The segregation index of eight mixtures was evaluated, namely, the five mixtures listed in the Table 4-1, and additional mixtures of poppy seeds with Avicel PH-101, $CuSO_4$ and sugar. Details on the mixing procedures, segregation index tests and analytical methods used to evaluate binary samples are discussed in Section 4.4.

4.4 Methods

4.4.1Particle Size Distribution

Particle size distribution of the ingredients was measured using a laser diffraction method (Beckman Coulter LS 13 320) details of which can be found in Section 2.2.1. Each measurement was performed in triplicate and the average value has been reported in Table 4-2.

4.4.2 Bulk Density

Bulk density of the ingredients was measured by a gently pouring a known mass of material in a graduated cylinder. Details of the method can be found in Section 2.3. Each measurement was performed in triplicate and the average value has been reported in Table 4-2.

4.4.3 Segregation index

Segregation potential of a powder mixture was measured by quantifying the extent of de-mixing of a powder mixture when subjected to repeated mass flow in a "Jenike segregation tester," originally developed at Rutgers University [76] and commercialized by Jenike and Johansson. A 500 g 50% (w/w) mixture was prepared by blending the

ingredients in a 4-qt V-blender at 15 rpm for 20 minutes. The mixture was then loaded in a hopper B of the Jenike segregation tester. The hopper was mounted on an identical hopper. Hopper B of the tester has a cone angle of 75 degrees and allows the material to discharge in mass flow. The discharge valve of the hopper was released and the material was allowed to empty into the hopper below. The positions of the hoppers were reversed and the procedure was repeated as material returned to the original hopper. This constituted one cycle of the test. The exchange of material between hoppers was repeated for 10 such cycles. At the end of the 10 cycles, the material from the hopper was discharged a final time and the discharge stream was periodically sampled into scintillation vials. Ten samples, evenly distributed across the discharged mass, were obtained and analyzed. The segregation index (SI) of the mixture is calculated by computing the relative standard deviation (coefficient of variability) of the composition across the 10 samples. The test was repeated in triplicate for each mixture pair and the average value is presented in Table 4-3. Figure 4-1(a) shows the two hoppers mounted on top of each other, as they would be during testing. Figure 4-1(b) shows a mixture of mustard seeds and sugar before starting the test while Figure 4-1(c) exhibits the same mixture after 10 hopper cycles, ready to be discharged for analysis. A distinct separation of the ingredients can be clearly observed in Figure 4-1(c). This extent of separation is quantified as the segregation index.

4.4.4 Continuous blending and sampling

Ingredients were blended in a continuous blender. The blender exit was sampled and evaluated for its content. The entire process consisted of feeding the material through loss-in-weight feeders into a comil, where they were de-lumped and fed into the continuous blender. The setup is a part of a continuous direct compaction line situated at

Rutgers University in Piscataway, NJ. The setup of the line used in this study, which is illustrated in Figure 4-2, is described below.

For the current study, two K-Tron twin-screw, loss-in-weight feeders were employed; a KT-35 and a KT-20. The numbers 35 and 20 indicate the diameter of a screw in millimeters. A larger diameter results in larger feeding capacity. Thus, the minor ingredient of the mixture was always loaded in the KT-20 while the major ingredient was loaded in the KT-35. The total mass-rate was 15 kg/hr for all mixtures. The comil (Quadro 197-S) was fitted with a round impeller, a 6350 μm screen, and operated at 3045 rpm. There was no spacer attached to the impeller shaft of the comil. This resulted in the maximum permissible distance between the impeller blade and the screen, minimizing any comminution upon attrition. The blender (Glatt GCG-70) was operated at 200 rpm. The impeller was fitted with 24 evenly spaced blades. Eight blades ($1/3^{rd}$) on both ends of the impeller were angled forward, while the middle $1/3^{rd}$ were alternated forward and backward. Figure 4-3(a) shows the blender tube while Figure 4-3b illustrates the different blade types the impeller can be fitted with. In this study, type III blades were used. Type VI blades are larger in diameter resulting in a small clearance between the blender tube and edge of the blade. This caused breakage of the larger mustard, sugar and copper sulphate particles. Type V blades were found to be inferior to Type III blades in previous studies and thus the smaller type III blades were used during the course of this entire study.

The feeders, which were previously tared, were calibrated with the actual material before the start of each run. The objective of each run was to perform mixing experiments for all compositions of the ingredient pair. The run was started with the smallest loading of the

minor ingredient. The system was allowed to reach steady state by allowing the process to run unperturbed for 5 minutes. The mean residence time of the material in the entire process is in the order of 1 to 1.5 minutes. A waiting time of 5 minutes ensures about 3 to 5 wash-throughs of the material through the process, which were deemed sufficient to ensure steady state. Once steady state was achieved, the exit stream of the blender was sampled at 30 second intervals until 10 samples were extracted for each condition. A wide-mouth funnel was used to extract samples from the exit stream. The wide mouth of the funnel ensures that the entire process stream is sampled. The funnel was discharged into scintillation vials. The size of each sample was between 1 g – 5 g.

Once sampling was complete, the feeders were adjusted to feed the next composition and the process was repeated. This was continued until all compositions were processed for that material pair, following which, the line was disassembled, cleaned, reassembled and loaded with the next material pair.

4.4.5 Batch blending and sampling

To compare the performance of a continuous blending process to a batch process, mixtures using the same ingredients and in the same ratios were prepared in an 8-qt V-blender and the quality of mixing was assessed. Ingredients were loaded top to bottom, with the minor ingredient sandwiched between two layers of the major ingredient. The batch size was 3 kg for all mixtures, except mixtures of Avicel PH-101 and mustard. A 3 kg loading generally resulted in approximately 50% volume of fill. To achieve the same fill volume for mixtures of Avicel PH-101 and mustard, the loading weight was 2.5 kg. The blender was rotated for 20 minutes at 15 rpm. At the end of the blending process, the blender was opened and five samples were extracted using a Globe-Pharma sampling

thief from distinct locations in the blender. The blender was then closed and rotated for a single revolution. Five additional samples were extracted from the blender from the same locations as the previous five samples' locations. A total of 10 samples were thus extracted from each batch, and analyzed for their contents.

The quality of mixing was quantified by computing the relative standard deviation (RSD) over 10 samples, for samples obtained from both batch and continuous processes. The RSD is the ratio of the standard deviation of the samples to their mean.

4.4.6 Sample analysis

The objective of each analytical method was to accurately evaluate the content of the samples. Techniques to evaluate the composition of each of the five mixtures were developed. These techniques could be classified into two categories, colorimetry and sieve analysis. Mixtures of $CuSO_4$ and Avicel PH-101, and $CuSO_4$ and sugar, were analyzed by colorimetry, while all other samples were analyzed by sieve analysis.

4.4.6.1 Colorimetry

The intense blue color of the copper sulphate powder was used to evaluate its concentration in its mixtures with sugar and Avicel PH-101, both of which are white in color. A color spectrophotometer (X-rite VS-450) was used to measure the reflectance of a sample containing unknown quantities of copper sulphate and sugar/Avicel PH-101. Details of the method can be found in Section 2.5. Reflectance values at 720 nm were used. The measured reflectance was used to evaluate the concentration of copper sulphate with the help of a previously developed calibration curve. It was observed that the ability of the method to accurately determine the concentration of copper sulphate diminished at low concentrations of copper sulphate. Thus, only mixtures with a target concentration of

copper sulphate of more than 60% (w/w) were studied. The calibration curves developed for mixtures of copper sulphate in Avicel PH-101 and copper sulphate in sugar are provided in Table 4-4. The calibration curve for sugar and copper sulphate is illustrated in Figure 4-4, as an example.

4.4.6.2 Sieve analysis

Samples containing mustard seeds or poppy seeds were analyzed for their composition by using the difference in particle size between the large seeds and the sub-millimeter sized ingredients, namely, Avicel PH-101, sugar and $CuSO_4$.

The total weight of a sample was measured and the sample was then loaded on an appropriately sized sieve. A 500 μm sized was used for mixtures containing poppy seeds while a 710 μm sieve was used for mixtures containing mustard seeds. The smaller ingredient was sieved off and the weight of the retained mustard/poppy was measured.

4.5 Results

For the sake of lucid narrative, this section has been divided in three parts. The first part describes relationships between segregation indices of material pairs and their bulk material properties. The second part compares mixing performance between batch and continuous processes, while the third part presents relationships between the degree of homogeneity of mixtures obtained from batch and continuous systems and their segregation indices.

4.5.1 Correlation of segregation index to bulk material properties

A relationship was observed between the segregation index of a mixture (Table 4-3) and the ratio $\frac{(d_{50}*\rho)_1}{(d_{50}*\rho)_2}$, where d_{50} is the median particle size of the material, while ρ is its bulk density. Suffix 1 in the ratio denotes material with the larger particle size and, while

suffix 2 denotes material with the smaller particle size of the two. It was interesting to observe that the relationships were different for free flowing materials, which readily flowed out of the hopper during segregation testing, and poorly flowing mixtures.

The relationship for free flowing mixtures is illustrated in Figure 4-5. Mixtures 1, 2, 4, 5 and 8 in Table 4-3 were free flowing. In order to confirm that the relationship is indeed valid for a larger set of materials, two additional free flowing mixtures, namely poppy seeds with CuSO4 and poppy seeds with sugar, were examined. The poppy seed mixtures were not part of the blending study. These mixtures were retrospectively examined for their segregation tendency after it became evident that there exists a relationship between segregation index of mixtures and their material properties. The final relationship constructed in Figure 4-5 thus consists of five experimental data points. The data point (1,0) on the graph in Figure 4-5 was explicitly added to the data series, since it would be fair to assume that ingredients with identical particle sizes and densities will not segregate.

Poorly flowing mixtures were found to rat-hole as they emptied the hopper during the segregation testing. Thus, these mixtures cannot be considered to have been subjected to sustained mass flow during testing, unlike the free-flowing mixtures. Nevertheless, such poorly flowing mixtures also show a linear relationship between the segregation index and the ratio of particle sizes and densities, illustrated in Figure 4-6. As mentioned before, the presence of this simple relationship is surprising and needs further examination. Mixtures 3, 6 and 7 from Table 4-3 constitute the data points in Figure 4-6.

4.5.2 Comparison between batch and continuous blending

Figure 4-7 compares the homogeneity of the mixtures obtained from batch and continuous systems. The homogeneity of the mixture is quantified as the relative standard deviation (RSD) as previously mentioned.

It can be observed that for four of the mixtures (all five, except $CuSO_4$ + Avicel), at all concentrations, the performance of the continuous blender is markedly superior to the batch blender. Mixtures exiting the continuous blender are more homogeneous compared to state of homogeneity achieved at the end of a batch blending process.

It is well known that for non-ideal mixtures, the measure of homogeneity of a blend is a function of the scale of the scrutiny of the analysis [77]. For the same state of overall homogeneity, a larger scale of scrutiny, that is, using larger samples, would result in a measurement of lower variability between samples (i.e., the measurement would suggests greater homogeneity). Conversely, if smaller samples are used, more variability between samples is typically observed, indicating a less homogeneous mixture. Also known, and related, is the fact that mixtures with a smaller proportion of a given ingredient would show an increased variability of that ingredient. Both facts are related – as the amount of a given ingredient in the samples decreases, whether because the samples are smaller or because the proportion of that ingredient decreases, any source of variation in concentration of the ingredient is amplified. Consider a random mixture of two identically sized ingredients. Samples of such a mixture would follow a binomial distribution. The RSD is given by the series of equations below.

$$RSD_{binomial} = \frac{Standard\ deviation}{Mean}$$

…(1)

$$RSD_{binomial} = \frac{\sqrt{np(1-p)}}{np}$$

…(2)

$$RSD_{binomial} = \sqrt{\frac{(1-p)}{np}}$$

…(3)

Where p is the number fraction of the component on which the RSD is being measured and n is the total number of particles in the sample. The main fact exemplified in these equations is that for random mixtures, the RSD is inversely proportional to the square root of the sample size n. Figure 4-8 shows the RSD as a function of the scale of the scrutiny n, and the fraction of the component on which the RSD is being measured, p. It can be observed that with increasing n, the $RSD_{binomial}$ decreases, while the RSD decreases with increasing p. To ensure that the effects of sample size and loading fractions do not confound the results, the experimental RSD was normalized by the theoretical RSD calculated by assuming the ingredients in the mixture follow a binomial distribution.

However, this analysis could only be performed for mixtures containing mustard seeds. The mustard seeds are large and discrete, and can thus be individually counted. A calibration curve (Figure 4-9) was created correlating the weight of the mustard seeds to the number of mustard seeds.

During sample analysis, the weight of each sample was measured and the average of 10 samples constituting a run or a batch was computed. The number of mustard seeds that constitute a sample of that weight was calculated assuming the entire sample only

contains mustard. This number was used as *n* in equation 3, while the mean concentration of the 10 samples was used as *p*. The theoretical RSD assuming a binomial distribution of the ingredients was then computed using equation 3. The actual RSD was normalized by $RSD_{binomial}$ and results have been presented in Figure 4-10. A value of 1, for the ratio $\frac{RSD}{RSD_{binomial}}$ indicates the highest possible state of mixedness (i.e., that of a random mixture), while a higher value of the ratio is indicative of poor mixing.

Analysis performed for mixtures containing mustard cannot be easily extended for mixtures of $CuSO_4$ and Avicel PH-101, and sugar and $CuSO_4$. This is because these mixtures contain fine powders with a wide distribution of sizes, which make them non-discrete, making their modeling as binomial distributions impractical. Distinct particles cannot be identified and hence cannot be counted to compute *n* in equation 3. Moreover, samples obtained from both batch and continuous processing for these mixtures were analyzed by exposing an identical area of material to the color probe. The scale of scrutiny for samples of these mixtures is thus identical, eliminating the need for them to be normalized by their sample size.

It is clear from Figure 4-7 and Figure 4-10 that the samples obtained from the continuous process indicate that the blend is much more homogeneous than that obtained from the batch process for four of the five mixtures, irrespective of the loading of the minor ingredient. As previously discussed, it is well known that in batch blending devices, when tumbling unlike ingredients, the difference in properties of the ingredients causes them to separate into patterns. Particles with similar densities but different particle size have different inertia. The larger particles with the greater inertia are unable to traverse the bend in the pathlines during tumbling. This causes them follow a path different from the

fines, leading to their separation. Particles with similar inertia but varying in density will de-mix with a mechanism similar to that in rotating cylinders with the heavier particles continuing to sink to the bottom. A constant direction reversal may even result in the formation of a central core in such cases. What is inevitable is a degree of separation of materials depending on their properties.

On the other hand, in a continuous blender, operating at steady state, the rate of input equals the rate of output. Moreover, in a properly designed system, there is no place where particles of a given type can accumulate. The materials enter the blender as an unmixed stream. They powder stream is lifted by the rotating blades of the impeller, folded, stretched and pushed backward or forward. The material itself has very little freedom to traverse its own path. Its path is dictated by the processing condition. Thus, except for minor fluctuations, the ratio in which the ingredients enter the system is equal to the ratio in which they exit. This is largely responsible for the arrested segregation.

The challenge, as the material traverses the blender tube, is to ensure sufficient dispersion of the ingredients while the material is within the blender. Dispersion of materials is brought about by the rotating blades. The total amount of dispersion is proportional to the total number of blade passes that the material experiences within the blender. The total number of blade passes is a function of the residence time and the impeller speed. In most tubular blenders, including the Glatt GCG-70, the orientation of the blades can also be adjusted. A forward oriented blade pushes the material forward, while a blade oriented backward will push the material opposite to the direction of the overall material flow, thereby increasing the holdup and residence time of the material in the blender. Thus, the number of blades, their orientation, impeller speed and the mass flow-rate all have a

significant effect on the mixing performance. The choice of the blade configuration and the impeller speed for this study was decided based on previous experience with the Glatt GCG-70. The blender has 24 blades in total, of which, the middle 1/3rd were alternated backward and forward. The blade configuration provides sufficient dispersion under the set conditions of the impeller speed and mass-flow rate to ensure homogeneity of the exiting material. The blender configuration (impeller and blade arrangement) is perhaps, not optimum for all material pairs but it can be observed that even with a non-optimized configuration, the continuous blender significantly outperforms the batch device. There is sufficient dispersion to ensure mixedness of the exiting material.

In the case of the mixture of $CuSO_4$ and Avicel PH-101 (Figure 4-7d), the performance of the two systems can be considered comparable. The segregation index of this mixture (SI = 19.34) is second lowest among the mixtures considered for blending studies. This suggests that there may exist a threshold for the segregation index, a value of the segregation index, below which mixing processes in batch systems become effective. This becomes more evident when one observes the batch blending performance of the mixture of sugar with $CuSO_4$ (Figure 4-7e, SI = 5.25) In this case, although the continuous blender moderately outperforms the batch system, the absolute RSD of the mixtures obtained from the batch process is fairly low. This is indicative of a threshold value of the segregation index; a value below which batch systems become effective for producing satisfactorily homogeneous mixtures.

It should also be pointed out that the mean of the mixtures that were obtained from both batch and continuous processes were comparable to the expected theoretical means, expect for the case of $CuSO_4$ and sugar mixtures obtained from the continuous process.

Extensive breakage due to shearing of the material by the blades of the impeller against the wall of the blender tube was observed. As a result, properties of the samples (mainly, the particle size distribution) obtained from the process were different from the properties of the calibration samples. This manifested itself as a shift in the expected mean concentration.

4.5.3 Relationship between segregation index and mixing performance

The relationship between RSD of 50:50 mixtures from batch and continuous processes and their segregation indices is illustrated in Figure 4-11. A clear linear relationship can be observed between the two variables for batch systems, but no such relation is observed for mixtures extracted from a continuous process. The existence of such a relationship for batch systems indicates that the conditions to which material is subjected to in segregation tests may be similar to those that the material experiences during batch blending. As discussed earlier, this could involve percolation of fines through gaps created by larger particles during tumbling, similar to percolation during segregation testing. The pathlines traversed by the material within the blender are a function of the material itself. Materials with disparate properties tend to traverse highly diverse pathlines, leading to poor mixing; the heterogeneity of the blend increases with the increasing difference in the properties of the ingredients being mixed. This is further highlighted by Figure 4-12, as the relationship is distilled for free flowing materials. The RSD of equipotent mixtures at the end of the batch blending process bears a linear relationship to $\frac{(d_{50}*\rho)_1}{(d_{50}*\rho)_2}$. This is to be expected, since a linear correlation was observed between $\frac{(d_{50}*\rho)_1}{(d_{50}*\rho)_2}$ and the segregation index (Figure 4-5). The presence of direct and fairly

simple correlations, similar to those in Figures 5 and 11, could be useful for process and particle design for batch blending systems.

The smaller slope of the trendline in Figure 4-12 indicates that the pathlines traversed by the materials in a continuous blender are a weaker function of the material properties than a batch process. The motion of the particles within the continuous blender is more random and less dependent on their properties, which leads to disorder, superior homogeneity and consequently arrested segregation.

The study highlights the superior ability of continuous blenders over batch blenders to homogenize highly diverse ingredients. It increases confidence in processing largely dissimilar ingredients, without modifying their properties, for example, enabling continuous direct compaction (dry mixing of ingredients as is, followed by compaction) of pharmaceutical formulations that are currently granulated due to segregation concerns in batch processing.

4.6 Conclusions

Ingredients with a substantial tendency to segregate were attempted to be homogenized by batch and continuous blending processes. It was observed that mixtures obtained from a continuous process exhibited a much higher degree of homogeneity compared to those obtained from batch-based operations.

It was also observed that the ratio of the product of median particle size and the bulk density of one ingredient to the other in a binary mixture bears a liner correlation to their segregation index. This correlation, however, is restricted to freely flowing materials, which readily flow out of the mass-flow hopper of a Jenike segregation test.

Moreover, it was observed that the final state of homogeneity achieved by the mixture in a batch blending process bears a linear relation with the segregation index, and thus to the ratio $\frac{(d_{50}*\rho)_1}{(d_{50}*\rho)_2}$. The correlation was not observed for continuous processes. This suggests that mixing processes in batch devices are a stronger function of the properties of ingredients being mixed than in continuous processes. The final state of mixedness of the blend is controlled by the process and less so by the properties of the ingredients, in a continuous process. These results provide a strong incentive to investigate further the relationships observed here between material properties, segregation index, and resulting blend homogeneity, and also to examine in more detail how to use continuous processes to improve process outcomes and product quality. The work also paves the way for those formulations, which would be granulated or reformulated due to segregation concerns, to be manufactured by continuous direct compaction.

4.7Figures for Chapter 4

Figure 4-1: (a) Jenike segregation hoppers mounted as they would be during testing; (b) mixture of sugar and mustard seeds after they are loaded in the hopper, ready for testing; (c) mixture of sugar and mustard seeds after 10 hopper cycles

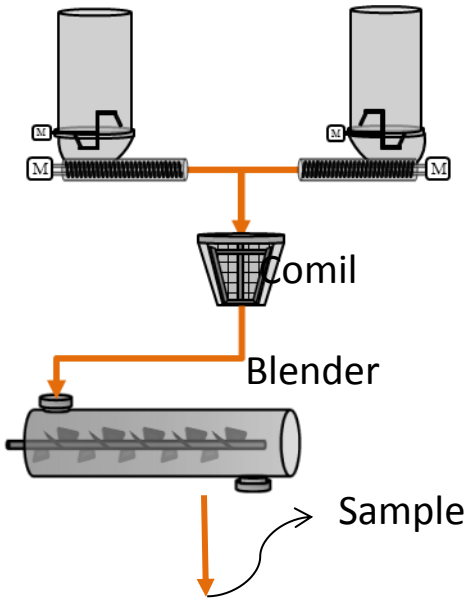

Figure 4-2: Schematic of the continuous blending setup. The loss-in-weight feeders feed the powder material to the comil, which delumps the materials and feeds it to the continuous blender. The continuous blender is sampled at periodic intervals after it has reached steady state.

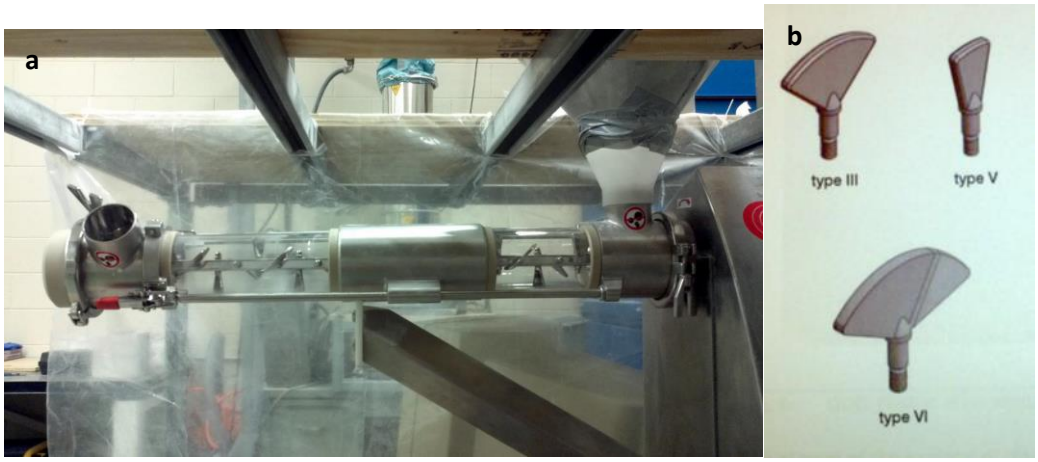

Figure 4-3: (a) Glatt GCG-70 continuous tubular blender with its (b) blade types. Type III blades were used during the course of the entire study.

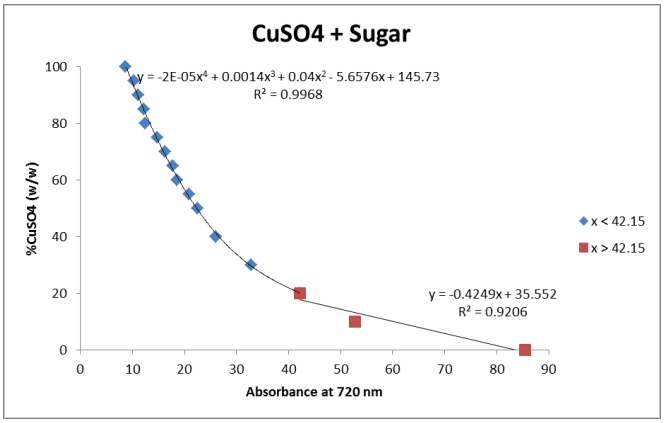

Figure 4-4: Reflectance measurements for varying mixtures of sugar and copper sulphate. The calibration curve is used to determine quantity of copper sulphate in its unknown mixtures with sugar.

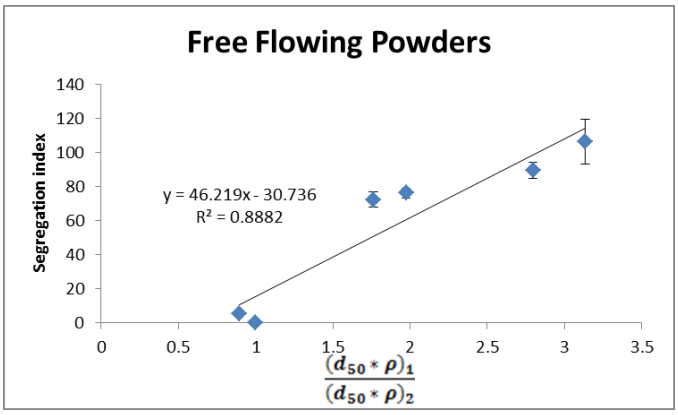

Figure 4-5: Correlation between segregation index of mixtures and their bulk material properties for free flowing materials. Surprisingly, a simple linear correlation is obtained.

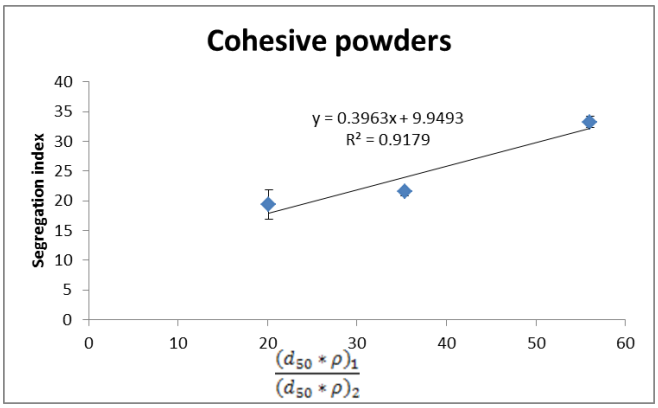

Figure 4-6: Relationship between segregation index and bulk material properties for poorly flowing materials. The relationship is different than that obtained for free flowing materials.

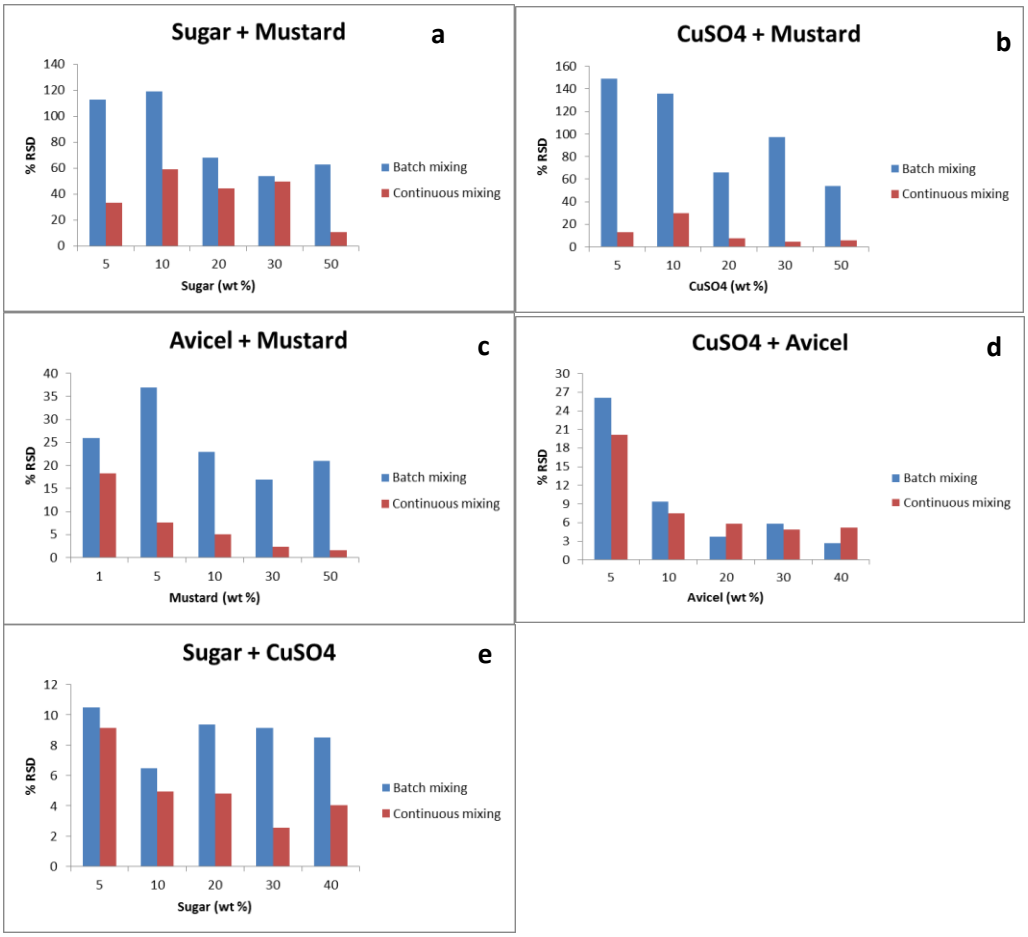

Figure 4-7: RSD of mixtures as a function of the weight percent of the minor ingredient obtained from batch and continuous blenders for mixtures of a) sugar and mustard, b) $CuSO_4$ and mustard, c) Avicel PH-101 and mustard d) $CuSO_4$ and Avicel PH-101 and e) sugar and $CuSO_4$. It can be observed that for four of five mixtures, the at all concentrations, the performance of the continuous blender is distinctly superior to the batch blender.

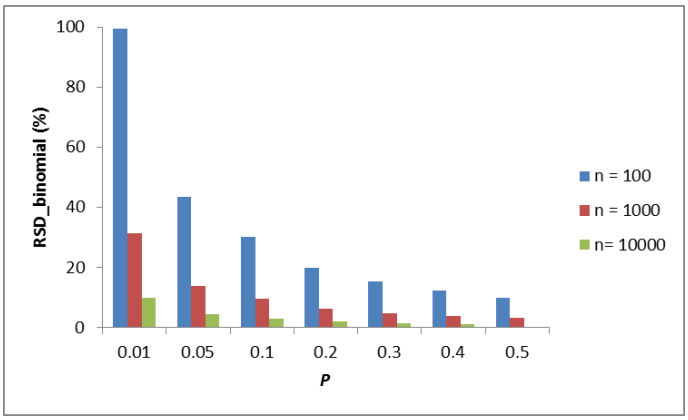

Figure 4-8: The RSD of a binomial mixture as a function of the sample size, *n* and fraction of the minor ingredient, *p*. A decrease in sample size or a decrease in fraction of the ingredient on which the RSD is being measured results in an increase in the theoretical RSD value.

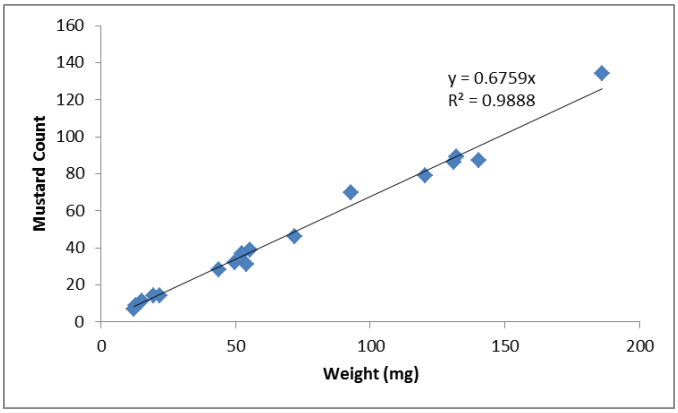

Figure 4-9: Number of mustard seeds as a function of its weight. The calibration curve was used to determine the number of mustard seeds in each sample assuming the entire sample contains mustard. This value was used as *n* in Equation 3.

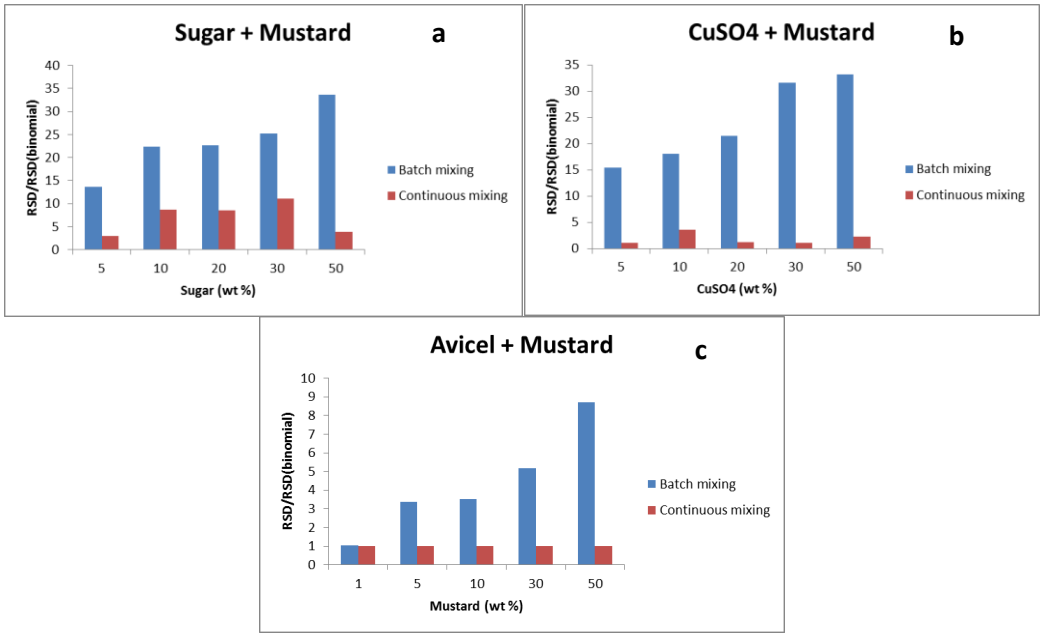

Figure 4-10: The RSD of the samples normalized by the RSD of a binomial mixture as a function of the weight percent of the minor ingredient for blends obtained from batch and continuous systems for mixtures of a) sugar and mustard, b) $CuSO_4$ and mustard and c) Avicel PH-101 and mustard. The normalized RSD of the samples obtained from a continuous process are markedly lower than those obtained from the batch process suggesting superior mixing in the continuous process.

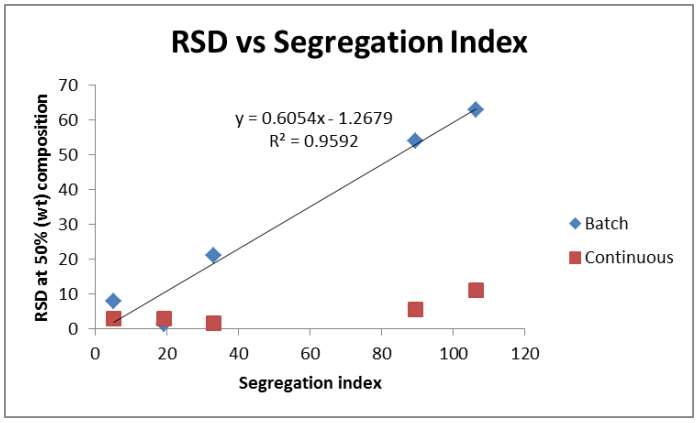

Figure 4-11: Relationship between the homogeneity of equipotent mixtures obtained from batch and continuous blenders and their segregation index. A strong correlation is observed for the batch system unlike mixtures from the continuous process.

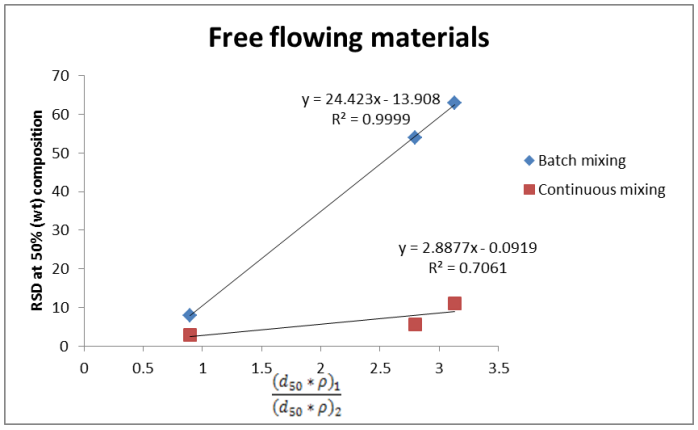

Figure 4-12: Relationship between homogeneity of equipotent mixtures and bulk properties of their ingredients. The smaller slope indicating mixing performance of the continuous blender indicates a smaller dependence on bulk properties unlike the batch process.

4.8 Tables for Chapter 4

Table 4-1: Mixtures and concentrations examined to compare performance of batch and continuous blenders. The first ingredient listed in the table, in bold text, was present in quantities bearing a check mark across the weight percent value. For example, for the ingredient pairing of sugar and CuSO4, five mixtures contacting 5, 10, 20, 30 and 40 percent by weight of sugar were studied.

	Percent (w/w)						
Mixture	1	5	10	20	30	40	50
Mustard + Avicel PH101	✓	✓	✓		✓		✓
CuSO4 + Mustard		✓	✓	✓	✓		✓
Sugar + Mustard		✓	✓	✓	✓		✓
Sugar + CuSO4		✓	✓	✓	✓	✓	
Avicel PH-101 +CuSO4		✓	✓	✓	✓	✓	

Table 4-2: Median particle size and bulk density of ingredients. Each measurement is performed in triplicate and the average value has been reported.

Material	d10 (µm)	d50 (µm)	d90 (µm)	Bulk density (g/cc)
Avicel PH-101	16.4	57.5	132.4	0.33
Copper Sulphate	97.3	287.7	605.3	1.15
Sugar	182.5	355.7	597.8	0.83
Poppy seeds	778.7	1023	1279	0.57
Mustard seeds	1079	1302.5	1502.5	0.71

Table 4-3: Segregation indices of mixtures examined as a part of this work. The quantity in the bracket is the standard deviation of the mean RSD value obtained from repeating the test three times.

Number	Mixture	Segregation index (SD)
1	Mustard + Sugar	106.4 (12.93)
2	Mustard + $CuSO_4$	89.5 (4.94)
3	Mustard + Avicel	33.2 (0.94)
4	Poppy + Sugar	76.19 (2.85)
5	Poppy + $CuSO_4$	72.4 (4.64)
6	Poppy + Avicel	21.49 (0.61)
7	CuSO4 + Avicel	19.34 (2.52)

Table 4-4: Calibration curves for mixtures of Copper Sulphate with Sugar and Avicel PH-101; x is the reflectance of the scanned sample, while y is the predicted concentration of CuSO4.

Mixture	Calibration Curve	Condition	R^2
Sugar + $CuSO_4$	$y = -2E\text{-}05x^4 + 0.0014x^3 + 0.04x^2 - 5.6576x + 145.73$	x <42.15	0.99
	$y = -0.4249x + 35.55$	x>42.15	0.92
Avicel + $CuSO_4$	$y = -0.0087x^2 - 0.5639x + 105.53$	x<53.02	0.99
	$y = 0.0137x^2 - 3.3216x + 190.87$	x>53.02	0.98

Chapter 5 : Role of Mixing and Preferential Wetting in High Shear Granulation

5.1 Introduction

High shear wet granulation is a particle size enlargement process in which a powder assembly is vigorously mixed with a liquid binder to induce particle growth [78, 79]. Typically, size enlargement is accompanied by increased bulk density and superior flow, making the powders amenable to today's high speed tableting processes[80]. Granulation is thus an integral step in the manufacture of a large volume of pharmaceutical solid oral dosage forms (tablets and capsules). In addition to the aforementioned extrinsic changes, granulation also causes change in the microstructure of the particles, namely, porosity and morphology, thus enabling a degree of control over dissolution characteristics of the final product [29, 81].

However, one of the most important necessities for granulation is to ensure homogeneity of the formulation ingredients, especially in the case of low dosage products. Wet massing of the ingredients should result in granules which are homogeneous in content. They are expected to contain the active pharmaceutical ingredient (API) and the excipient in the same proportion as the original bulk mixture. Thus, despite the ability of some formulations to be directly compacted (despite good compaction characteristics and flow properties), they are granulated to improve confidence in content uniformity.

Ironically, that may not always be the case. It has often been observed that granules exhibit a non-uniform distribution of the API across size classes [27, 28, 82-84]. The active ingredient may show a preferential tendency to accumulate in the coarse or the fine granules.

Several mechanisms have been proposed to explain the cause of an uneven distribution of ingredients during high shear wet granulation [27, 28, 82-85]. The solubility of the active ingredient and particle size have been identified as key properties that play an active role in uniform distribution of the drug across granule size fractions.

Egermann and Reiss [82] observed that the ingredient with the smaller primary particles was accumulated in the coarse granules. The results were corroborated by Vromans et al. [28] and Van Dries and Vromans [27], who both showed that the finer primary particles produced stronger granules and had sufficient strength to resist shear forces. This led to the accumulation of the finer ingredient in the coarse granule fraction. Thus, if the primary particle size of the active ingredient was smaller than the filler material, the coarse granules were found to be super-potent and vice versa.

The solubility of the ingredients in the binder fluid was also found to play a part in their distribution across size fractions. Ojile et al. [83] observed that a soluble drug dissolves in the binder liquid and consequently the distribution of the drug depends on the distribution of the binder within the granulated mass. Over-wetted regions were thus found to be super-potent, while under-wetted regions were starved of the drug. Another intriguing effect of drug solubility is the non-homogeneity it can cause due to migration of the binder, and consequently the drug, during drying of the wet mass. It was found that the drug-rich solute is leached to the surface of the granules during drying [84, 85]. The fluid evaporates, leaving deposits of the drug on the crust. These deposits are loosely attached and thus fall off during subsequent powder handling operations, leading to a high concentration of the drug in the fines.

Inhomogeneity in high shear granulation is therefore a complex phenomenon, the cause of which depends on at least two properties of the ingredients. However, all of the above work assumes that the powder bed being wetted is well-mixed. The state of the mixture being wetted is completely random and thus, the probability of a binder-drop being surrounded by API/excipient particles is proportional to the original weight fractions in the bulk mixture. The subsequent formation of a nucleus will be dependent on the properties of the powder ingredients and the binder fluid, but both ingredients will have a proportional chance to be wetted and get incorporated in the nucleus.

It is thus of interest to investigate scenarios where the powder bed being wetted is poorly mixed. If the properties of powder ingredients being granulated are very different from each other they can pose a mixing (dry mixing) challenge. As previously discussed in Chapter 4, a difference in particle size, density or particle shape of granular ingredients can cause granular materials to easily demix [86]. Moreover, creating homogeneous mixtures of these ingredients in batch based blending devices, like the bladed mixer in this case, is very challenging. Granular mixing and de-mixing in bladed mixers (geometry of interest) has been well studied [87, 88]. Researchers have reported various segregation patterns depending on shear levels within the mixer and disparities in the particle sizes of the ingredients being mixed. Thus, if the powder mixture being wetted is poorly mixed, then a drop of binder that falls on the powder bed can be disproportionately surrounded by one of the ingredients, leading to disproportional incorporation of the ingredient within the nucleus and consequently, perhaps, the granules.

Coupled with the above phenomenon, a significant difference in the wettability of the components amplifies the challenge of achieving homogeneous granules. It is well known

that the presence of hydrophobic components in the formulation can lead to poor wetting of the powder bed by the binder, resulting in a non-uniform distribution of the formulation ingredients. Fundamental work on the wetting behavior of powder mixtures was carried out by Lerk et al. [89] and Aulton and coworkers [90]. The work was extended by Nguyen et al. [91], who systematically varied the proportion of the hydrophobic component to quantify its effect on granule uniformity. It was found that achieving content uniformity in granules becomes more difficult with increasing proportions of the hydrophobic component due to granulation competition that arises between the hydrophobic and hydrophilic components. Cavinato et al. [92] reported a similar finding and stated that for those drug compounds that exhibited poor wettability, the liquid distribution within the powder bed was poorer, leading to selective agglomeration and non-uniform drug distribution.

This chapter investigates the role of powder mixing in high shear wet granulation. Specifically, it focuses on the relationship between the states of initial mixedness of the powder to final content uniformity in the granules. Coupled with the role of mixing, the study quantifies the nature of poor drug distribution that arises due to a significant difference in the wettability of the powder ingredients. The active load, impeller speed and wet massing time have been employed as design variables to assist in the comprehension of the above mentioned causative agents.

Materials used in this study and their characterization have been discussed in Section 5.2 and Section 5.3, respectively. The high shear wet granulation procedure and characterizing the homogeneity of initial dry mixture is discussed in Section 5.5. Granule characterization methods have been briefly discussed followed by results and discussions.

5.2 Materials

Micronized acetaminophen (Mallinckrodt Inc, Raleigh, NC) was used as the active pharmaceutical ingredient (API) and microcrystalline cellulose (Avicel PH-101, FMC BioPolymer, Philadelphia, PA) was the excipient. Water was used as a binder. Ethyl alcohol for UV/VIS spectroscopy (>99.8%) was purchased from Lachner. Water for the UV/VIS spectroscopy was purified by a demineralized water generator (Aqual 25) to a conductivity of ~ 1 $\mu S.cm^{-1}$. All experiments were performed at room temperature.

5.3 Primary Material Characterization Methods

The particle size distribution of the primary materials and their contact angle with water was computed. The primary particle size of the ingredients was measured using a laser light diffraction technique as described in Section 2.2.1. Each measurement was repeated thrice and the average value has been reported in Table 5-3.

5.3.1 Contact Angle

The contact angles for acetaminophen (APAP) and microcrystalline cellulose (MCC) with water were determined using the Washburn capillary rise method, where the rate of liquid rise through a powder bed due to capillary action is measured. The Washburn equation in terms of mass of liquid that penetrates a column of powder is given by the following equation:

$$t = \frac{\eta}{C\rho^2\gamma cos\theta}\, m^2$$

Where m is the mass of the liquid that penetrates the column with time t, η is the liquid viscosity, γ is the liquid surface tension, θ is the contact angle and C is the capillary constant.

The apparatus consisted of a glass cylinder fitted with a ceramic membrane at the bottom, and is shown in Figure 5-1. The column was first cleaned by washing it with water followed by hexane and lastly by rinsing it with acetone. It was then dried at 100° C for 15 minutes in a hot air convection oven and packed with the material whose capillary rise was being measured. The column was then subjected to 2000 taps at a frequency of 250 taps per minute on a Quantachrome Autotap (Quantachrome Instruments, Boynton Beach, Florida; Model Number: 2106-60-01). The tapping ensures a uniform packing architecture for each measurement for a given material. The column was attached to a stand which was kept on a measuring scale and dipped in the liquid such that the liquid meniscus and the boundary of the membrane and the material are level. The scale was tared as soon as the liquid rose through the membrane and the scale readings were recorded by Ohaus Balance Talk software Version 4.0.

The capillary constant, *C*, of the column is a material factor dependent on the packing architecture of the powder bed. To solve for the capillary constant of a material, the test was performed using n-hexane, which is a fully wetting liquid (zero contact angle). The time of liquid rise was plotted against the mass squared and the slope of the line was calculated. The capillary constant can be computed from this slope since all other constants are known.

To compute the contact angle for the aqueous binder, the test was repeated by dipping the column in an aqueous solution saturated with the material whose contact angle was being measured (to avoid dissolution of the powder in the column). The solution was prepared by dissolving excess material in deionized water by slightly heating the solution. The solution was then allowed to stand overnight at room temperature. As the solution cools,

the excess material crystallizes out (the solution is filtered to remove recrystallized solids) and the saturated nature of the solution is thus ensured. A graph of time against the mass squared of the water rise in the column was plotted and the slope of the line was computed. Given the slope of the line, the contact angle can be solved for since the capillary constant is now available in addition to the other commonly available parameters. All measurements were repeated thrice. The contact angles with water are 89.0 ± 0.03° for APAP and 36.0 ± 5.6° for MCC.

5.4 Experimental Design

The experimental design was a full factorial 2x2x2 with drug load, impeller speed and the wet massing time employed as design variables. Details of the experimental design have been illustrated in Table 5-1 and the batch nomenclature is given in Table 5-2.

5.5 High Shear Wet Granulation Process

Granulation was performed in a laboratory scale high shear granulator (KG 5 - KEY International Inc., New Jersey, Figure 5-2) fitted with a 3.9 L stainless steel bowl. The vessel was equipped with a chopper to aid in the disintegration of larger agglomerates. The fill weight for all batches was kept constant at 250 g which resulted in ~40% volume fill. The MCC was filled at the bottom of the vessel followed by layering of APAP on the top. The ingredients were dry mixed for 2 minutes followed by a period of water addition which lasted for 2 minutes and 40 seconds for all batches. The impeller speed during premixing was equal to the impeller speed to be used for the design point. Water was added using a pre-calibrated pump (Masterflex LS, Model 7518-12). The L/S ratio (w/w) was kept constant for all batches at 0.8. Following the addition of the water, the system was run for a specified wet massing time based on the design point. The material was

discharged from the granulation vessel and dried in a hot air convection oven at 60 ˚C to a loss on drying (LOD) value of 2%.

5.5.1 Dry Mixing

In order to investigate the state of the mixedness of the dry powder blend at the end of the dry mixing process, a similar procedure to the one described above is followed until the dry mixing stage of the process. Batch weight was 250 g, with MCC loaded at the bottom and the APAP layered on the top. The ingredients were mixed for 2 minutes at an impeller speed based on the design point and a chopper speed of 6500 rpm. At the end of the mixing time, the powder mixture was sampled at 8 locations from two different regions as shown in Figure 5-3 and stored in vials. The sampling region at the center of vessel was labelled as region 1 and that at the outer edge of the vessel was labelled region 2. Samples were carefully extracted only from the surface of the powder bed (up to approx.3-4 mm) since the top of the powder bed is the area of interest. A total of four batches were analyzed (2 speeds and 2 APAP concentrations). Compositions of the extracted samples have been reported in Section 5.7.1. The results provide insight on the nature of the composition of the top surface of the bed, where the initial nucleation takes place.

5.6 Granule characterization

The dried granules were thoroughly characterized by measuring their size distribution and analysing the distribution of content across size classes.

The particle size distribution (PSD) of the granules was measured by sieve analysis as described in Section 2.2.2. A total of 100g of material was sieved at a time. The order of

sieves was different for different batches. The objective was to ensure that more than 20% by weight of the batch is in one sieve.

The content uniformity of the granules was analyzed by an UV-VIS spectroscopy based method described in Section 2.4.

The inhomogeneity of the APAP across size fractions was quantified as the de-mixing potential originally proposed by Thiel and Nyugen [93] .

$$DP\ (\%) = \frac{100}{\bar{p}} \sqrt{\sum \frac{w(p - \overline{p})^2}{100}}$$

Where $\bar{p}$ is the average concentration of the active ingredient and p is is the actual concentration in a particular sieve class with weight percent *w*. The quantity is similar to relative standard deviation, which was previously used in quantifying non-uniformity in mixing. The demixing potential assumes a probability of *w* associated with concentration *p*. This assigns appropriate weights to a sieve class, based on its fraction in the total batch. Like the RSD, the larger the de-mixing potential, the larger is the extent of deviation from the mean of the active ingredient across the size classes.

5.7 Results and Discussion

For the sake a lucid narrative, this section is divided into three parts. Section 5.7.1, describes the obtained results – the coarse granules were found to be sub-potent, and the fine granules were found to contain excess API. Section 5.7.1.1 describes the contribution of poor dry mixing to this content uniformity while Section 5.7.1.2 elucidates the role of the preferential wetting.

5.7.1 Content Non-Uniformity

The primary particle size of the raw ingredients is given in Table 5-3. It can be observed that the median particle size of microcrystalline cellulose is approximately 6 times that of acetaminophen. Microcrystalline cellulose is also insoluble in water while the solubility of acetaminophen in water is 12.78 g/l [94].

Figure 5-4 and Figure 5-5 show the distribution of the active ingredient across size classes for 3% and 7% API, respectively. The percentage of the active ingredient compared to the mean across all size classes is defined as the percentage drug claim and is plotted against the mesh size. A clear trend is observed for all batches. In general, the fine granules are super-potent with respect to the acetaminophen, while the coarse granules are sub-potent.

The calculated de-mixing potential as a function of the process parameters and drug load is summarized in Figure 5-6. To fully discern the observations in Figure 5-4, Figure 5-5, and Figure 5-6 it is necessary to understand the nature of powder mixing in bladed mixers. It is also equally important to understand the relationships between material properties of the granulation ingredients, their interactions with each other and the binder fluid, and their effects on granulation mechanisms (e.g., nucleation and growth). Dry mixing experiments complemented with comparative data on the wettability of the ingredients shed some light on the above.

5.7.1.1 Powder segregation during dry mixing

Figure 5-7 shows the composition of the top layer of the powder bed post dry mixing with samples extracted from two distinct regions, as described in Section 5.5.1. The powder bed is wetted from the top, and this layer is thus the region of interest. It can be

observed that all samples contain substantially less API than the theoretical composition. This indicates that the top layer of the powder bed is sub-potent with respect to the acetaminophen. Thus, a drop of binder that falls on the bed is disproportionately more probable to be surrounded by a MCC particle than by an APAP particle.

The RSD of the samples obtained post the dry mixing is given in Table 5-4. The low value of the RSD is indicative of low between-location variance. Thus, the extent of de-mixing is uniform through the surface of the powder bed independent of proximity to center or walls of the vessel.

As previously mentioned, to quantify homogeneity of the powder bed in the granulator, powder mixing phenomenon in bladed mixers should be well understood. Granular flow patterns, mixing and segregation in bladed mixers have been studied in detail by several researchers [87, 88, 95]. Zhou et al. [87], in a DEM-based framework, showed that a cylindrical mixer with two flat and opposite blades, de-mixing is observed when there exists a difference between the particle size and density of the granular ingredients. The larger/lighter particles drift to the top of the powder bed, while smaller/heavier particles settle to the bottom. In a more rigorous study on the nature of granular dynamics in a bladed mixer, Radl and coworkers [95] experimentally studied the flow and segregation of granular material in a cylindrical mixer geometry agitated by four 45° pitched blades. Their observations for a high shear system were in accordance with the findings of Zhou et al., where they observed that the larger particles surged to the surface of the powder bed, while the smaller particles trickled to the bottom. The observation is attributed to a commonly known phenomenon called percolation or sieving segregation, where small

particles enter inter-particle spaces created in shear zones, forcing less mobile large particles to rise.

The observations from Figure 5-7 are in accord with the aforementioned phenomenon. The top layer of the powder bed has substantially less API than the theoretical mean. The APAP particles, being 6 times smaller than the MCC particles, seep through the spaces created between the MCC particles. Thus, a drop of water which falls on the powder bed will disproportionately be surrounded by more MCC than APAP, giving the MCC a higher chance of being incorporated in the nucleus.

Another observation that can be made from Figure 5-7 is a slight increase in the potency of the top layer of the powder bed with increasing impeller speed. The APAP content of the samples from batch C (300 rpm) is greater than batch A (225 rpm) for 3% API. Similarly, APAP concentration in the top layer of batch G (300 rpm) is greater than batch E (225 rpm) for 7% API. The extent of demixing thus decreases with increasing impeller speeds, as percolation of the minor ingredients is alleviated with increasing rotation rates. This effect is reflected in the demixing potential of each batch. As can be seen in Figure 5-6, the de-mixing potential reduces from 20.2% to 11.5% with increasing impeller speeds at 3% drug load, while it reduces from 11.2% to 6.9% for 7% drug load. A fraction of the reduction in variance can be attributed to improvement in the state of mixedness with increasing impeller speeds, which lends itself to improvements in the overall homogeneity of the granules.

5.7.1.2 Contribution of powder wettability

The de-mixing potential, however, worsens with increasing wet massing times for both 3% and 7% drug loads, as can be observed from Figure 5-6. The observation can be

explained by comparing the wettabilities of the granulation ingredients. Based on the method described in Section 5.3.1, the contact angles of APAP and MCC with respect to water were calculated as 89.0 ± 0.03° and 36.0 ± 5.6°, respectively. The wettability of MCC with water is thus substantially higher than that of APAP. A large difference in the wettability of the granular ingredients is known to cause selective nucleation and consequently growth of the superior wetting ingredient [91, 92]. Thus, when a droplet comes in contact with the powder bed, it preferentially wets MCC particles due to its superior wetting properties. As the massing continues, granules continue to selectively grow with the MCC, thereby worsening the homogeneity with increasing wet massing times.

From the above results, it appears that the non-uniform distribution of the active ingredient occurs due to a combination of effects. Post the dry mixing stage of the granulation, the top layer of the powder bed in the granulator is sub-potent with respect to the active ingredient. De-mixing in the bladed mixer occurs as the smaller APAP particles seep to the bottom of the powder bed by finding spaces between the larger MCC particles. The binder drop that lands on the bed thus finds itself disproportionately surrounded by MCC. It consequently forms a nucleus with primarily MCC particles and begins to grow. The APAP is thus already handicapped in its race to being incorporated in the granule. As massing progresses, the APAP continues to compete with the MCC. However, being a poorer wetting material compared to MCC, it struggles to grow with the wet mass. A fraction of APAP thus remains ungranulated. The subsequent granules are deficient in the active ingredient, thereby creating a wide disparity of concentrations across size classes.

5.8 Conclusions

A two component high shear wet granulation system comprising of micronized acetaminophen and microcrystalline cellulose was studied for distribution of the active ingredient across size classes. It was observed that the fine granules were super-potent with respect to the active ingredient, while the coarse granules were sub-potent. A dual cause was attributed to the findings. Poor mixing of the active ingredient and the excipient before binder addition caused the fluid drop to be disproportionately surrounded by excipient particles. The excipient was thus hypothesized to preferentially nucleate. This was coupled with the superior wettability of the excipient, which led to preferential growth of the excipient on the granule. A fraction of the active ingredient was thus found to be ungranulated and manifested itself in the fines. This chapter highlights the role of mixing and preferential wetting in high shear wet granulation.

If granule size segregation occurs between the granulation and the tabletting or capsule filling steps, then the composition non-uniformity of granules would translate into content non-uniformity of the final dosage form, which is clearly undesirable. However, if the blending step that typically occurs before tabletting (i.e., the addition of glidants and lubricants such as magnesium stearate) avoids size segregation of granules, then one might argue that composition non-uniformity of the granules does not matter.

The next chapter investigates relationships between granule content uniformity and the final granule properties, such as the rate of release of the active ingredient from the granules. This is because even if segregation of granules before tabletting is avoided, non-trivial dependence of granule quality attributes on processing conditions will make attributes, such as release kinetics, difficult to predict and control. Relationships between

process parameters and granule micro-structure and granule micro-structure on granule quality attributes such as release kinetics are thus investigated. Relationships between the granule content uniformity and the release kinetics of the granules are also investigated.

5.9 Figures for Chapter 5

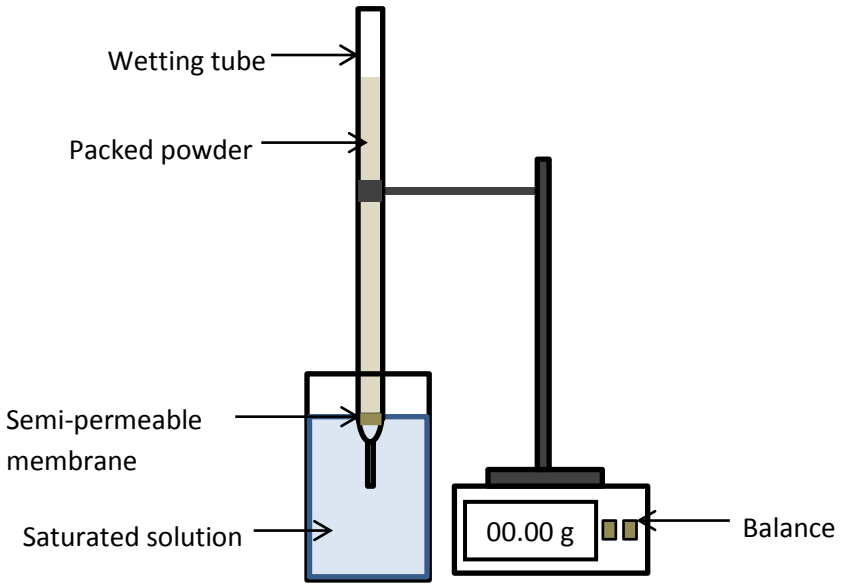

Figure 5-1: Experimental setup of the Washburn capillary rise method. The rate of liquid rise through a powder bed due to capillary action is measured and is quantified as the hydrophobicity of the material. The contact angle of the material with the fluid of interest can be computed by first performing the experiment with a fully wetting liquid followed by the fluid of interest.

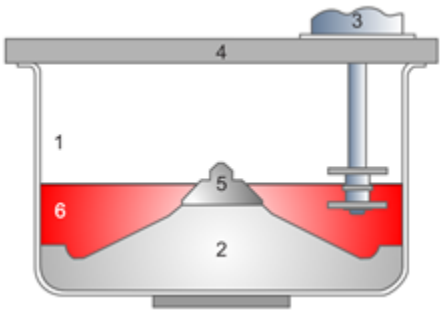

Figure 5-2: Schematic of the batch granulator

1 – stainless steel bowl (volume 3.9 L), 2 – three-blade impeller, 3 – chopper, 4 – impact resistant cover, 5 – safety screw, 6 - batch

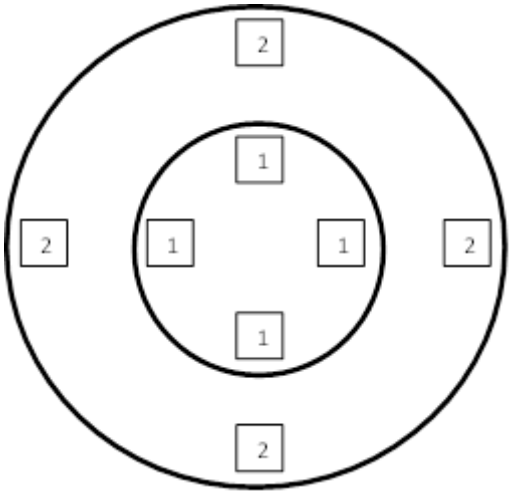

Figure 5-3: Top view of the sampling locations post dry mixing. The sampling area is divided into two regions - one near the center of the vessel and the other on the outer edge.

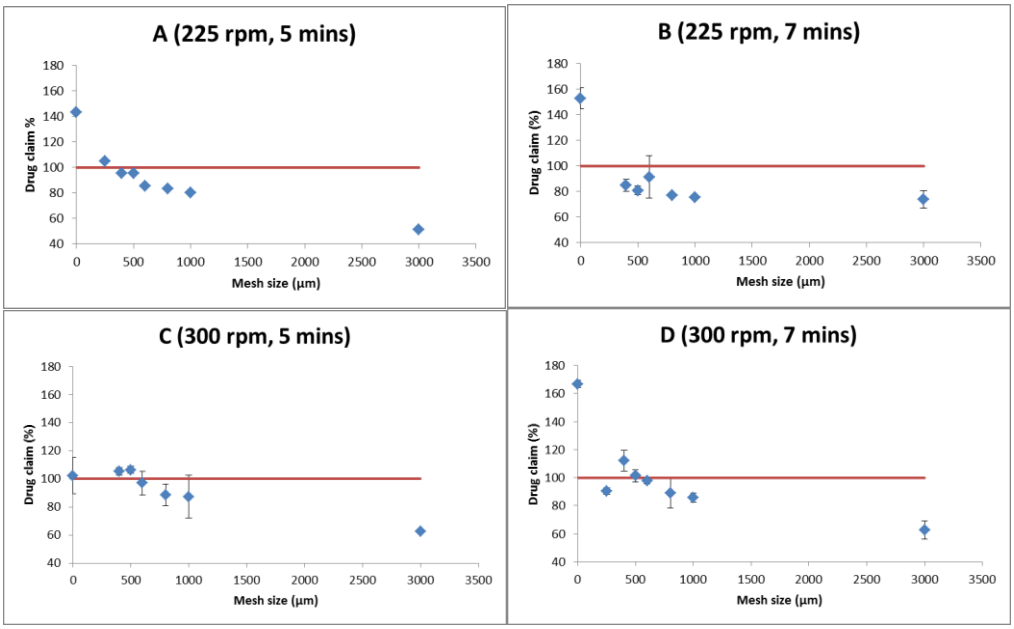

Figure 5-4: Distribution of the active ingredient across granule size classes for 3% drug load

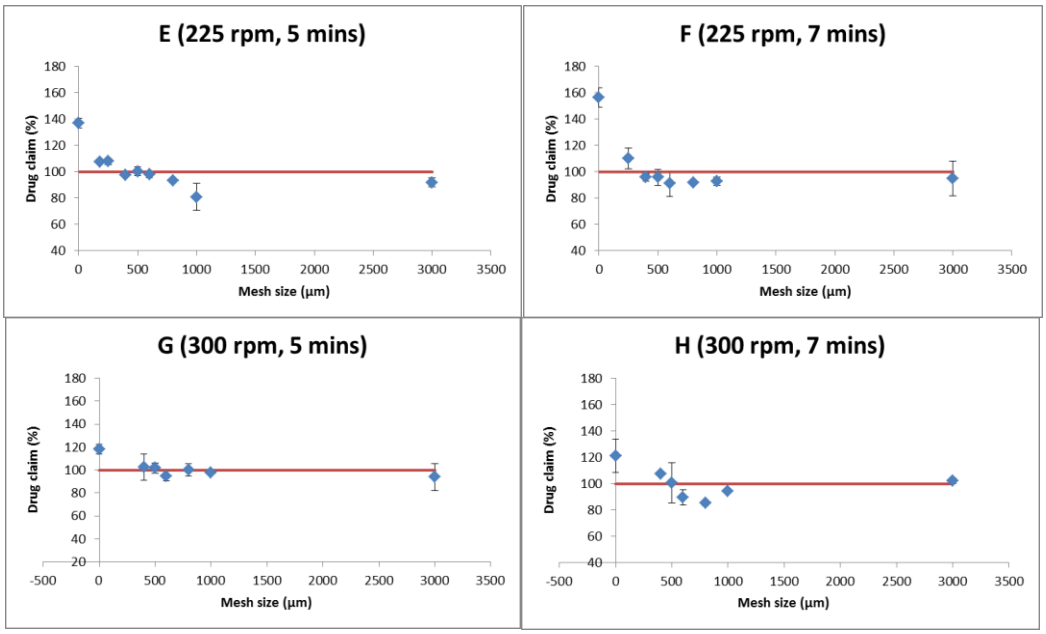

Figure 5-5: Distribution of the active ingredient across granule size classes for 7% drug load

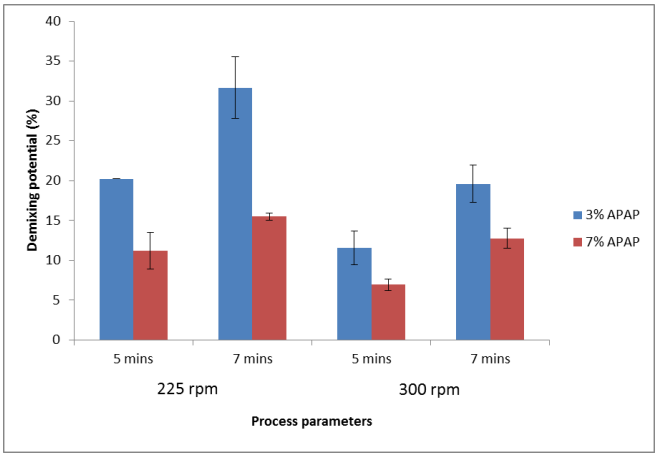

Figure 5-6: Demixing potential and its relationship with process parameters

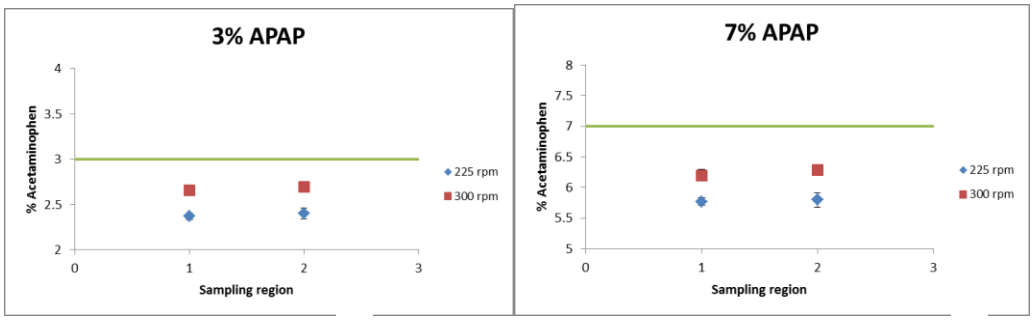

Figure 5-7: Percentage of acetaminophen in the top layer of the powder post dry mixing. The top layer of powder bed is starved of the active ingredient. Increase in the rotation speed of the impeller increases the state of mixedness of the powder bed

5.10 Tables for Chapter 5

Table 5-1: Experimental design space to investigate the effect impeller speed and wet massing time on the content uniformity of the final granules for two drug loads

Parameter	Drug Load (w/w) %	Impeller Speed (rpm)	Wet Massing Time (minutes)
Low	3	225	5
High	7	300	7

Table 5-2: Nomenclature of batches; batches A to D contain 3% (w/w) APAP while E to H have 7% (w/w) APAP

Batch name	Drug Load (%)	Impeller Speed (rpm)	Wet Massing Time (min)
A	3	225	5
B	3	225	7
C	3	300	5
D	3	300	7
E	7	225	5
F	7	225	7
G	7	300	5
H	7	300	7

Table 5-3: Primary particle size distribution parameters of the starting material

PSD parameter (μm)	d10	d50	d90
μ- Acetaminophen	2.9	10.9	31.6
Microcrystalline Cellulose PH101	16.5	57.6	132.4

Table 5-4: Relative standard deviation between samples from different locations - low RSD values are indicative of low between-location variance

Sample	% RSD
A	1.97
C	1.69
E	1.52
G	1.37

Chapter 6 : Process-Structure and Structure-Property Relationships in Granules Made by High Shear Wet Granulation

6.1Introduction

A thorough comprehension of the relationships between process parameters and critical quality attributes is a key enabler of the FDA recommended Quality by Design (ObD) paradigm. There are several definitions of QbD available in regulatory guidelines such as ICHQ8(R2). One is that quality should be built into a product by a thorough understanding of the product and the process by which it is manufactured along with knowledge of the risks involved and how best to mitigate those risks [96]. To improve quality, it must be built into the product and to enable this requires an understanding of how formulation and manufacturing process variables affect product quality. In case of high shear wet granulation, a thorough comprehension of the granulation rate processes and its underlying mechanisms is thus critical.

A number of rate processes, occurring simultaneously contribute to the evolution of the final product attributes in high shear wet granulation. The rate processes can be divided into three classes, namely, nucleation and wetting, growth and consolidation, and attrition and breakage [97]. The final product attributes are dictated by the nature of the dominant rate process or processes, which in turn are dependent on the material properties of the formulation and the process parameters. Often, there is little leeway for a formulator to modify material properties of the formulation and thus mapping of the design space of the process parameters remains the key to achieving granules with desired properties.

Given the large number of process variables that can affect product performance in a high shear wet granulation process, it is critical to identify the ones that have the most significant impact on product performance. This is synonymous to identifying factors that maximize risk (ICH Q9). The guidance document states that in order to minimize risk, it is necessary to identify critical process variables that have the most impact on product performance.

Researchers [98, 99] have shown that the wet massing time, the binder amount and the impeller speed have the most significant impact on the granule CQAs, namely their size distribution, content uniformity, morphology and porosity. Woyna-Orlewicz and Jachowicz [98] used a Plackett-Burman type design to show that the wet massing time, L/S ratio and the impeller speed were the most critical from a total of 7 factors. Recently Pandey et al. [99] reported that the wet massing time, binder amount and impeller speed were statistically significant in terms of their effect on particle growth ratios, the amount of fines, bulk density and granule porosity for a 2:1 ratio of microcrystalline cellulose (MCC), lactose system. Badawy and coworkers [100] reported a similar finding for three weak bases which were used as model compounds and showed that the water amount, impeller speed and wet massing time have a significant effect on granule particle size, growth ratio, density and the amount of fines.

For a rational Quality by Design, not only is it important to establish a relationship between process parameters and bulk granule properties but it is equally important to understand the quantitative relationship between process parameters and the resulting product microstructure and product microstructure and performance attributes such as dissolution characteristics. While classical dissolution tests provide information about

the kinetics of API release into the bulk solution, they do not enable direct observation of sub-particle-level phenomena that govern the dissolution/release process. The dissolution mechanism and the rate-limiting step have to be inferred indirectly from the shape of the release curve [101].

The progress of advanced imaging methods in recent years has made it possible to combine classical dissolution tests with information about the internal distribution of formulation components within the dosage form. For example, two-dimensional (2D) chemical imaging based on FTIR-ATR (Fourier Transform Infrared spectroscopy with Attenuated Total Reflection) [102] or Raman microscopy [103] as well as three-dimensional (3D) visualization methods such as Magnetic Resonance Imaging (MRI) [104-106], Terahertz Pulse Imaging (TPI) [107], Current Density Imaging (CDI) [108], confocal Raman spectroscopy [109] or X-ray micro-tomography (micro-CT) enable direct observation of porosity and API distribution in granules or tablets. When combined with appropriate image processing algorithms and physics-based mathematical models of dissolution [101], a more complete picture of the underlying mechanisms and their parametric sensitivity can be obtained.

The focus of the chapter is two-fold. Relationships between process parameters and granule quality attributes have been developed for a high shear wet granulation process. Specifically, the effect of impeller speed, liquid to solid ratio (L/S) and wet massing time on the granule size distribution, content uniformity, granule porosity, and morphology has been investigated for a two component formulation. Using micro computed tomography in combination with suitable image processing techniques, the effect of process parameters on the internal structure, namely the porosity of the granules has been

examined. Relationship between the internal microstructure and the release kinetics of the API has been examined. Lastly, the effect of the granule microstructure on the release kinetics of the API has been examined for the granule system discussed in Chapter 5. To distinguish between the two granule systems, the granule system discussed in Chapter 5 has been referred to as granule system I while the granule system characterized in this chapter has been labelled as granule system II.

The materials used to study granule system II have presented in Section 6.2. The granulation method is discussed in Section 6.5, granule characterization techniques along with tomography methods discussed in Section 6.6 followed by results in Section 6.7.

6.2 Materials

As previously mentioned, a separate granule system, in addition to the described in Chapter 5, was investigated in order to examine relationships between process parameters and granule properties and between granule properties and granule performance.

Semi-fine acetaminophen (Mallinckrodt Inc, Raleigh, NC) was used for this granule system in combination with microcrystalline cellulose (Avicel PH-102, FMC BioPolymer, Philadelphia, PA). The API load in all cases was 30% (w/w). Similar to the granule system in Chapter 5, water was used as the binder. Ethyl alcohol for UV/VIS spectroscopy (>99.8%) was purchased from Lachner. Water needed for the same was purified by a demineralized water generator (Aqual 25) to a conductivity of ~ 1 $\mu S.cm^{-1}$. All experiments were performed at room temperature.

6.3 Primary Material Characterization

The primary particle size of the starting ingredients was measured by a laser diffraction method described in Section 2.2.1. The bulk density was measured by a method which is described in Section 2.3. Each measurement was repeated thrice and the average value of the particle size distribution parameters and bulk density is reported in Table 6-1.

6.4Experimental Design

Previous experience and a thorough literature review revealed that the impeller speed, L/S ratio and the wet massing time have the most significant impact on granule properties. These parameters were thus decided to be used as variables in the study.

The design space was chosen based on several experimental trials to obtain granules of reasonable quality in terms of size and strength. For L/S ratios less than 60%, granules were found to be flaky while for L/S ratios of more than 80%, the batch was found to be over granulated. The impeller speed was decided with an objective to achieve good mixing keeping in mind that a high impeller speed will lead to vortex like formation of the powder mass which could compromise mixing efficiency and granulation behavior. The wet massing time was selected with an aim to achieve granule properties with a significant variability between those at low wet massing time and high wet massing time. The design of experiment was a full factorial 3x3x3 with details of design parameters specified in Table 6-2 and Table 6-3. The design resulted in 27 batches and the batches are labeled using a batch code, the nomenclature of which is defined in Table 6-4. Data generated from the design of experiments were analyzed using Minitab 16 (*Minitab Inc*, State College, PA).

6.5 High Shear Wet Granulation Process

The high shear wet granulation process was similar to the one described in Section 5.5 of Chapter 5. Granulation was performed in the same laboratory high shear granulator (KG 5 - KEY International Inc., New Jersey) fitted with a 3.9L stainless steel bowl equipped with a blade chopper for the disintegration of larger agglomerates. The batch size was 300 g in all cases resulting in a ~50% fill volume. The API was layered on top of the excipient following which the components were premixed for 2 minutes. The impeller speed during premixing was equal to the impeller speed to be used for the design point. Water was added using a previously calibrated peristaltic pump (Masterflex LS, Model 7518-12) in drip fashion through a tube (Masterflex Silicone #16, ID: 3.1 mm). The chopper speed was kept constant at 6500 rpm. After water addition, the system was run for pre-specified amount of wet massing time based on the design end point. The material was discharged from the granulator bowl and dried in a hot-air convection oven at 60 C to a target loss on drying (LOD) value of 2%.

6.6 Granule Characterization

Granules in granule system II were thoroughly characterized by measuring their granule size distribution, content uniformity and morphology. Moreover, their internal structure was characterized by μ-CT and their internal porosity was computed. Release of the active ingredient in both water and ethanol was studied. The internal structure and porosity was of granules system I was also examined by the same technique along with the release of the API in ethanol.

The particle size distribution of the granules was characterized by sieve analysis (see Section 2.2.2).U.S. Standard sieve numbers of 40, 30, 20, 18, 16, 14 and 12 were used,

corresponding to mesh sizes 425, 600, 850, 1000, 1180, 1400 and 1700 microns, respectively. A total of 100 g of material was used for each measurement.

The content uniformity of the granules of the granules was measured by a UV-VIS spectroscopy method similar to that described in Section 2.4. The release kinetics of the granules was measured in both, ethanol and water. The extinction coefficients for acetaminophen in ethanol and water were determined by calibration measurements and have values of $\lambda_{250,EOH}$ = 12896 $mol.L^{-1}.cm^{-1}$ and $\lambda_{244,H2O}$ = 5800 $mol.L.^{-1}cm^{-1}$, respectively.

6.6.1 Granule Morphology and Inner Structure

The morphology of granules was examined by scanning electron microscopy (SEM Jeol JCM-5700). Before measurement, the samples were sputter-coated by 5 nm gold layer (Emitech K550X). The measurements were performed using a secondary electron imaging detector with acceleration voltage of 20 kV and high vacuum mode. The morphology of the granules was characterized only for granule system II.

A micro-CT attachment for SEM (SkyScan) hosted by a Jeol JCM-5700 SEM was used for the determination of porosity of the granules in granule system II. The SEM-hosted micro-CT attachment uses the electron beam of the host SEM to produce X-ray radiation necessary for the CT measurement by hitting a brass target. The X-ray beam penetrates through the sample placed on the top of a rotation stage, and a transmission image is then acquired by a sensitive X-ray camera. The parameters of the CT scan for all measurements were as follows: 180 degrees scan, number of averages 4, scan step 0.8 degree, FOV 2 mm x 2 mm. Slices in the XY plane were created by the NRecon software (SkyScan) with the following settings: misalignment compensation, object larger then

FOV, accurate ring-artifacts reduction correction and number of smoothing passes 1. The spatial resolution achieved during the CT scan was 3.84 µm/pixel. Granule fractions in the range 1.4 to 1.7 mm were used for CT scans.

Porosity measurements were performed for three different granules of samples mentioned in. The selection of batches to be evaluated was such that extremes and the midpoint of the design space were incorporated. In addition, the effect of single parameter change, keeping the other two constant could also be evaluated.

The porosity of granules obtained from granule system I was evaluated using a similar procedure. The parameters of the CT scan for all measurements for granule system I were as follows: SEM - high vacuum mode, acceleration voltage 20 kV, spot size 100, magnification 300 000x, working distance 8 mm; micro-CT - 180° scan, number of averages 5, scan step 0.8°, field of view (FOV) 1.04 mm. Slices in the XY plane were created by the NRecon software (SkyScan, Bruker) with the following settings: misalignment compensation, object larger than FOV, accurate ring-artefacts reduction correction and number of smoothing passes 1. The spatial resolution achieved during the CT scan was 2.0 µm/pixel.

A step by step method for evaluating the porosity of granules from the raw CT images has been described in brief below.

A raw image stack is rarely suitable for direct binarization due to high noise accompanying raw CT data and insufficient brightness/contrast balance of solids and background. The ImageJ software was used for all following image adjustments and modifications. Initial adjustment of brightness/contrast balance was followed by noise

reduction via the *Despeckle* function. The Otsu algorithm was used for binarization of the image stack. Artefacts of solid phase involved in pores were removed by the *Close* function and a *Mask* of particles smaller than 20 px^2. 3D object plug-in (3D-OC) was applied on the control volume (cube of side 300 μm) inscribed inside the granule to remove "flat" pores (zero volume) and very fine pores (< 20 px^3) and to find connections between all real pores in the control volume. The step by step process is illustrated in Figure 6-1. A unique color and label was assigned to every cluster in the control volume (Figure 6-2) including pores on edges of the control cube. The approach allows one to study in detail every single cluster and determine its unique parameters (volume or surface area).

Porosity was measured by analyzing the area fraction of every slice contained in the control volume for four different granules for every sample. The 3D-OC plug-in was applied to determine the number and volume of clusters in the control volume. This was followed by using CT-Analyser (SkyScan, Bruker) to generate a 3D model (.stl) from the modified binary stack (marching cubes algorithm). Lastly, CT-Volume (SkyScan, Bruker) was used for final rendering and visualization of cluster.

6.7 Results and Discussion

6.7.1 Effect of process parameters on granule properties

6.7.1.1 Particle size distribution

Analysis of variance methods were employed to evaluate the effect of process parameters, namely, the L/S ratio, impeller speed and the wet massing time on the particle size distribution parameters of the granules. It was observed that the L/S ratio ($p = 0.000$), impeller speed ($p = 0.002$) and wet massing time ($p = 0.046$) all have

significant effect on the median particle size of the granules. The interaction between the impeller speed and the wet massing time and between the impeller speed and the L/S ratio was also found to be statistically significant for their effect on d50. The L/S ratio has the most dominant effect on the d50 and exhibits a clear trend (Figure 6-3a). Increasing the binder amount leads to an increase in the median particle size. Increasing water amount increases the pore saturation of the granules. More liquid being available at the surface, the granules becomes deformable increasing the chances of coalescence upon collision. There is no clear trend observed in the median diameter of the granules as a function of impeller speed (Figure 6-3b).

The wet massing time *(p = 0.001)*, the L/S ratio *(p = 0)*, and the two-way interaction between L/S ratio and impeller speed *(p = 0.003)* were found to be statistically significant in terms of their effect on d10. The d10 can be considered to be representative of the amount of fines in the system. Figure 6-4a, Figure 6-4b and Figure 6-4c show that the amount of fines decrease with increasing L/S ratios, increasing wet massing time and increasing impeller speed. As previously mentioned, increasing the binder amount increases the pore saturation of the granules promoting growth by coalescence and layering. Growth of the nuclei by layering of fines becomes particularly important. An increase in the wet massing time and the impeller speed results in an increase number of collisions and the collision frequency, respectively. Both these factors result in the incorporation of fines in the granules, decreasing the total number of ungranulated fines.

The wet massing time *(p = 0.008)*, the impeller speed *(p = 0.01)* and its interaction with the L/S ratio *(p = 0.014)* were found to be statistically significant in terms of their effect on d90.

The wet massing time shows a distinct relationship with the d90 (Figure 6-5c). Increasing wet massing times can increase coalescence and growth but at the same time can lead to enhanced breakage until a steady state distribution is reached [100]. The latter seems to be transpiring. From Figure 6-3c and Figure 6-4c, it can be seen that the d10 and the d50 of the system increase with increasing wet massing time, and thus the particle size distribution of the system gets narrower with increasing wet massing times. The effect of L/S ratio does not exhibit a clear trend (Figure 6-5a) on the d90.

The impeller speed is found to be significant in terms of its effect on d10 and d90. Impeller speed can have contrasting effect on granulation behavior. Increasing impeller speeds can increase collision frequency thus enhancing coalescence and agglomeration. On the other hand, increasing speeds can also lead to increased breakage, thus leading to a decrease in particle size with increasing speeds. The former effect is found to be dominant in this case (Figure 6-4b and Figure 6-5b).

6.7.1.2 API Content

Illustrated in Figure 6-6 is the distribution of the active across granule size classes, for batch 14:MMM. It is observed that there is no preference for the API to adhere to a particle size class. The distribution of the API amongst granules of different sizes is found be uniform, unlike granule system I. Good mixing, a higher drug load and a comparatively high level of total granulation time [99, 100] could explain the degree of content uniformity. The phenomenon is observed in case of all batches (see Table 6-5); the API content being within *two* percentage point around the mean. There is no systematic increase or decrease of API content between the size classes. In case of all batches, the API content is found to be below the expected value of 30%. This could be

explained by differences in measured API weights due to weighing scales differences between the one that was used to weigh the API for the batch and the one that was used to measure the API when building the calibration model for the UV spectrometer.

6.7.1.3 Granule Morphology

The SEM images of granules from granule system II are shown in Figure 6-7. Based on visual analysis of the SEM images of a number of granules from each batch, it was concluded that there are no significant differences in the external characteristics of the granules. Morphological characteristics such as shape and surface roughness were found to be similar and thus independent of the process parameters. There is an absence of any agglomerates. This could be an indicator of a well-mixed system with relatively large shear forces. The granules also exhibit a fair degree of sphericity and growth of the granules may be attributed to layering and consolidation of the material over a primary nucleus.

There were no differences in the API content of the granules, from different batches. Moreover, there were, also, no differences in the external structure and morphology of the granules. Thus, any differences in the quality attributes of the granules between batches can be attributed to differences in their inner structure, in particular, their porosity in conjunction with their particle size. This is discussed in next section.

6.7.1.4 Granule Porosity

Porosity of the granules evaluated for six batches of granule system II is shown in Table 6-6. It can be observed that an increase in the wet massing time or the L/S ratio results in a decrease in the granule porosity. There is almost a 50% change in the porosity of the

granules between the extremities of the design point. It was observed that the wet massing time and the L/S ratio have a significant effect on granule porosity. An increase in both parameters results in a decrease in granule porosity. This is further highlights by Figure 6-8a and Figure 6-8c. Water acts as lubricant which reduces inter-particulate friction within the granule, facilitating particle movement within the granules in response to densifying forces in the high shear granulator [110]. Densification continues to occur with increasing wet massing times and thus the two-fold impact of increasing wet massing time and L/S ratio can result in a significant change in the granule porosity. The impeller speed does not have a large effect and does not exhibit a clear trend (Figure 6-8b).

6.7.2 Effect of granule structure on release kinetics of the active ingredient for granule system II

The dissolution of the active ingredient from the granules can be dictated by two kinetic processes, namely, the diffusion of the API from the granule pore structure and the intrinsic dissolution of the API in the solvent. If the latter is the rate limiting step, then the dissolution profiles of all granules in a batch are similar, independent of their size and internal structure. However, if the rate limiting is the diffusion of the API from the granules, then the release profiles would be dependent on the granule size and the internal structure.

The release profile acetaminophen in pure water for batch 14, the design midpoint, of granule system II, is shown in Figure 6-9. It can be observed that there are no discernible differences between the release profiles between size classes. This suggests that the intrinsic rate of dissolution of acetaminophen in water is the rate limiting step in this scenario. This is expected since it is known that microcrystalline cellulose, the excipient

in this case, swells, resulting in the disintegration of the granule. The porous structure of the granule collapses resulting in no internal diffusion resistance. A similar result was expected from all the other batches. Further investigation into the release of the API in water was not pursued.

Figure 6-10 shows the release profiles of acetaminophen for different size fractions of batch 27:HHH in ethanol. Microcrystalline cellulose is insoluble in ethanol and does not disintegrate in ethanol. The granule structure is preserved and the active ingredient first has to diffuse out of the porous structure before being dissolving in the fluid. It can be observed that there is distinct difference in the dissolution profiles of the three differently sized granules. The time taken to release 90% of the active ingredient, t_{90} is approximately 2.0, 4.8 and 9.0 h for the size classes 0.6 mm – 0.84 mm, 1.00 mm – 1.18 mm and 1.40 – 1.70 mm, respectively. Taking the 0.72 mm size fraction (average particle of the first size class) as a basis, the theoretical t_{90} values for the 1.09 mm and 1.55 mm granules based on quadratic scaling should be 4.58 h and 9.27 h, respectively, which is reasonably close (<5%) to the experimental values. This suggests that the diffusion of the active ingredient through the granule matrix dictates the rate of release of the active ingredient. Longer is the diameter of the granule, the longer it takes for the active ingredient to diffuse out of the granules. The presence of a distinct quadratic relationship also suggests that dissolution relationships established using a single size fraction can be used to predict behavior of the entire batch, if the particle size distribution of the batch is known.

Figure 6-11 compares the release profiles between granules from batches 1:LLL, 14:MMM and 27:HHH, belonging to size class 1.4 – 1.7 mm. It can be clearly observed

that there are distinct differences in the dissolution profiles of the three batches. In the case of sample L, which represents batch 1:LLL, more than 85% of the active ingredient has been liberated into the dissolution medium within 1 h, while in the case of sample H, which represents batch 27:HHH, more than 7 h are needed for dissolving a comparable amount of the API. Since the granules have the same composition, size and shape, the release process of the active ingredient must depend on the internal pore network of the granule. The internal porosity is the only attribute that distinguishes the three granules. From Table 6-6, batch 1:LLL is highly porous compared to batch 27:HHH. A higher internal porosity is thus indicative of a lower diffusion resistance since the batch 1:LLL has a much faster rate of dissolution than batch 27:HHH. The presence of a percolating pore network leading to the granule surface plays an important in the release of the active ingredient.

Thus, not only is the rate of dissolution controlled by the size of the granule but is also dependent on the internal porosity of the granules. The rate of release increases with increase in granule porosity and is proportional to the square of the granule diameter. A small change in particle size distribution or porosity of the granules between batches can thus result in significant changes in their dissolution profiles.

6.7.3 Effect of granule structure on release kinetics of the active ingredient for granule system I

The release profile of the active ingredient from granulation batches, discussed in Chapter 5 was also investigated. This granule system, as previously mentioned, is referred to as granule system I. The release profiles are shown in Figure 6-12.

The drug release was monitored for a period of 24 hours. It was observed that at least 90 % of the drug was released within the first 4 hours. Thus, for the sake of resolution, the 24 hour time point has been omitted from the corresponding figures.

To capture the release of the active ingredient in terms of parameters that could lend physical meaning, the release curves were regressed by a first-order kinetic model of the form:

$$c(t) = c_{burst} + (c_{max} - \quad _{burst}) * (1 - e^{-kt})$$

Where $c(t)$ is the quantity released at time t, c_{max} is the asymptotic quantity released, while c_{burst} and k are fitted parameters. The presence of ungranulated drug particles manifests itself by the so-called "burst effect" (i.e., a sharp increase in the released fraction at the beginning of the dissolution process), which is notable on the release curves in Figure 6-12, and can be as high as 40% of the total drug release in some cases. c_{burst} captures this burst effect. k is a rate constant and quantifies overall the rate of release. Its value depends on the granule microstructure among several other factors. Discrete points on the graphs in Figure 6-12 represent the actual data while the smooth lines represent the above model.

Time taken for 90% of the drug (t_{90}) to be released from the batch is calculated based on the fitted equation and is shown in Figure 6-13(a). Shown in Figure 6-13(b) is the effect of process parameters on the rate constant. By comparing Figure 6-13(a) and Figure 6-13(b) it can be observed that, an increase in the value of the rate constant results in a subsequent decrease in the t_{90} value, further supporting the hypothesis that the fitted constant 'k' allows one to quantify the overall rate of release.

As previously discussed in Section 6.7.2, the process of release of acetaminophen from MCC granules in ethanol depends on the pore structure of the granule and as well the size of the granule. From Figure 6-13(a), it can be observed that an increase in the impeller speed is associated with a decrease in the rate of release. An increase in the impeller speed results in a decrease in the demixing potential (Section 5.7.1), which indicative of fewer ungranulated fines in the system. Ungranulated fines do not encounter any diffusion resistance and thus the rate of release of the active ingredient is the intrinsic dissolution rate of the active ingredient in the medium. A decrease in the ungranulated fine fraction with increasing impeller speeds thus results in slower overall dissolution. Moreover, an increase in the impeller speed also results in increase in granule growth resulting in larger granules (Figure 6-14(a), in the 7% case). This contributes to further decrease in the rate of release. Lastly, increase in impeller speeds also results in decrease in granule porosity (Figure 6-14(b), for 5 mins of wet massing) which as previously discussed increases diffusion resistance, thereby hindering release of the active ingredient from the granules. The three-fold effect of decreasing porosity, increasing particle size and reduction in fines, with increasing impeller speeds explains the generally slower dissolution from batches made at high impeller speeds.

The relationship between decreasing porosity, increasing granule size and consequently decrease in the release rate is not always preserved. However, the relationship between decreasing dissolution rates and increasing speeds is consistent. This indicates that the reduction in fines at higher impeller speeds compensates for any increased dissolution due to unexpected decrease in porosity or granule size.

The effect of wet massing time is similar. Increasing wet massing time results in an increase in demixing potential but also a decrease porosity and increase in granule size , albeit not consistently. Despite the presence of counter-acting effects, the rate of dissolution is always found to be decrease with increasing wet massing time. This indicates that effect of decreased porosity and increasing size over compensates any enhancement in dissolution due to additional fines in the system.

Since clear relationships between complete granule systems, their properties and rate of dissolution were not established, a single granulation batch, batch H, of granule system I was studied in depth to shed light on mechanisms driving dissolution behavior.

Shown in Figure 6-15(a) are the release profiles of selected size fractions for batch H and corresponding model fits. Figure 6-15(b) shows the t_{90} values for all size classes for batch H. It can be observed that the amount of time taken for 90% of the drug to be released from the granule decreases with increasing granule diameter. However, this decrease is not proportional to the square of the granule diameter as observed for granule system II, despite omitting ungranulated fines from the computation. Moreover, the t_{90} value of largest granule fraction is found to be lower than expected.

A plausible explanation of the observed phenomenon is a difference in the solubility of ingredients in the binder fluid coupled with migration of the active ingredient during drying. The solubility of acetaminophen in water is 12.78 g/l while microcrystalline cellulose is completely insoluble in water. It can thus be hypothesized that a part of the acetaminophen dissolves in the binder fluid during the granulation process and this dissolved APAP remains trapped within the granule at the end of the process. When the

granules are dried, the APAP-laden binder migrates out of granule. However, as the binder evaporates the APAP recrystallizes and gets deposited towards the outer boundary and on the crust (the falling off of APAP from the crust contributes to a portion of the super-potent fines). The effective diffusion length for APAP is thus, a fraction of the granule diameter, which explains the lack of dependence of the release rate on granule diameter.

This phenomenon assumes importance in granule system I and not in granule system II. Granule system I has much lower drug loads to compared to granule system II (30% w/w). Dissolution of the acetaminophen in the binder resulting in complete saturation would lead to 1.5% (w/w) of the active ingredient being in solution form. This value is comparable to the drug loads in granule system I, unlike in granule system II where the active ingredient dissolved in the fluid is small compared to the total quantity of the active ingredient in the system.

The presence of a hollow cavity within the large granules, which accounts for approximately 80% of the total porosity, hints at this phenomenon. A similar observation was also made by Ojile et al. and Selkirk et al. [83, 84] . The micro-CT images of the hollow granules for the 800 μm size cut are shown in Figure 6-16. The images are characterized by a distinct central cavity which suggests the presence of a trapped fluid droplet. The fluid evaporates during drying leaving a behind a hollow cavity. The volume fraction of the central cavity was computed and averaged over four granules. The averages and the corresponding standard deviations are reported in Figure 6-17. It can be observed that the central cavity accounts for anywhere from 60 % to 95% of the total granule porosity.

The 1000 μm granules have a distinctly lower t_{90} value. The 1000 μm size fraction contains a lower amount of active ingredient than smaller granules. Thus the total quantity of APAP that must diffuse out is much lower. Consequently, this is transpires faster, than in granules where a larger quantity of APAP must diffuse out, albeit out of smaller diameters.

The above theory of drug migration must be expanded upon by further experimentation and validation to provide further insight.

What is, however, pronounced, is that content non-uniformity can have implications on the release profile of the active ingredients. The ability to predict the dissolution behavior like in the case of granule system II, which exhibited API uniformity across size classes, is not preserved in the case of granule system I. Content non-uniformity distorts the predictive capability of the quality attributes undermining quality by design. Uniform distribution of the active ingredient across granule size classes in conjunction with thorough characterization is paramount to enable predictive capability of product performance.

6.8 Conclusions

Understanding relationships between process parameters and granule properties is paramount, in order to enable quality to be built into the product by design. A full factorial design of experiments was performed to investigate the effect of wet massing time, L/S ratio and impeller speed on the granule size distribution, content uniformity, porosity and morphology of granules produced by a high shear granulation process for a two component system. An ANOVA exercise showed that the effect of all three process parameters on the median granule size was found to be significant with the L/S ratio

being the most significant parameter, exhibiting a clear trend (increasing L/S ratios led to increase in the mean granule size). The granules exhibited robust content uniformity and similar morphologies.

However, relatively minor changes to the process parameters resulted in a significant change to the inner structure of the granules, mainly, their porosity. A 50% change in the granule porosity was observed between the end points of the design space. Change in the inner structure of the granules, in turn, resulted in changes to granule performance, specifically, the rate of release of the active ingredient (acetaminophen) in the dissolution medium (ethanol). The t_{90} value was found to be 1 h at the lower extremity of the design space and 7 h at the highest extremity of the design space.

The influence of content uniformity across granule size classes on the granule performance was investigated by performing dissolution studies on the granule system discussed in Chapter 5. It was found that the lack of uniformity in the distribution of the active ingredient across granule size classes undermines the ability to model and predict dissolution behavior.

6.9Figures for Chapter 6

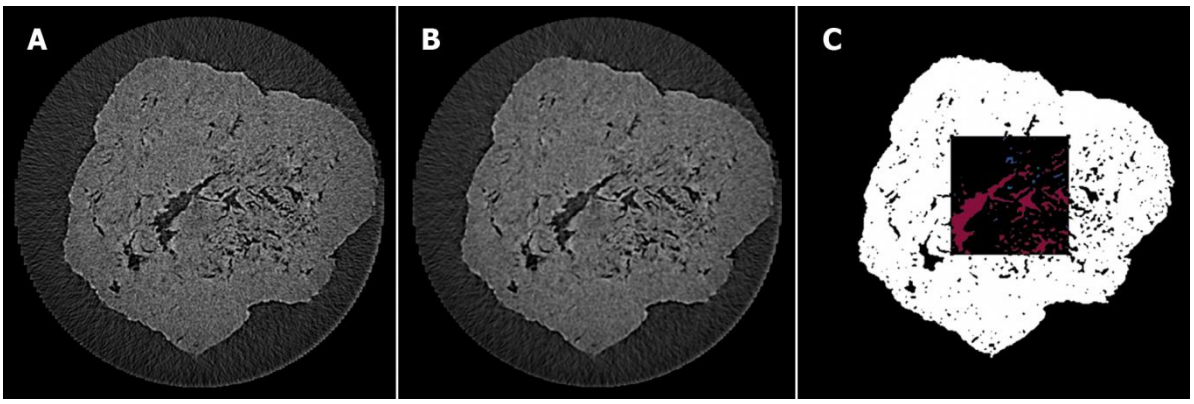

Figure 6-1: Step-by-step preparation of a binary image for the measurement of porosity and cluster size distribution. A) Original micro-CT image B) Image after application of Despeckle function C) center square representing the region of interest chosen for porosity evaluation after application of 3D-OC

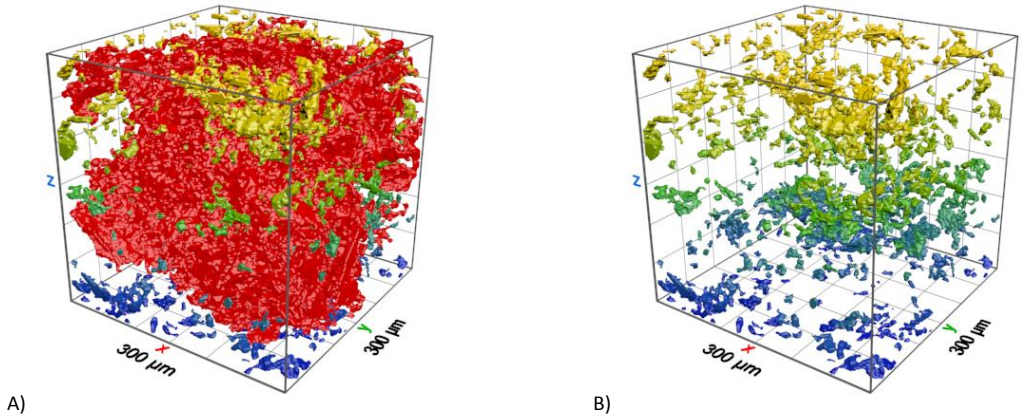

A) B)

Figure 6-2: A) Visualization of pores in control volume - sample C (fraction 0.8 - 1.0 mm) and B) Large central cluster (red color) removed for better overall visibility.

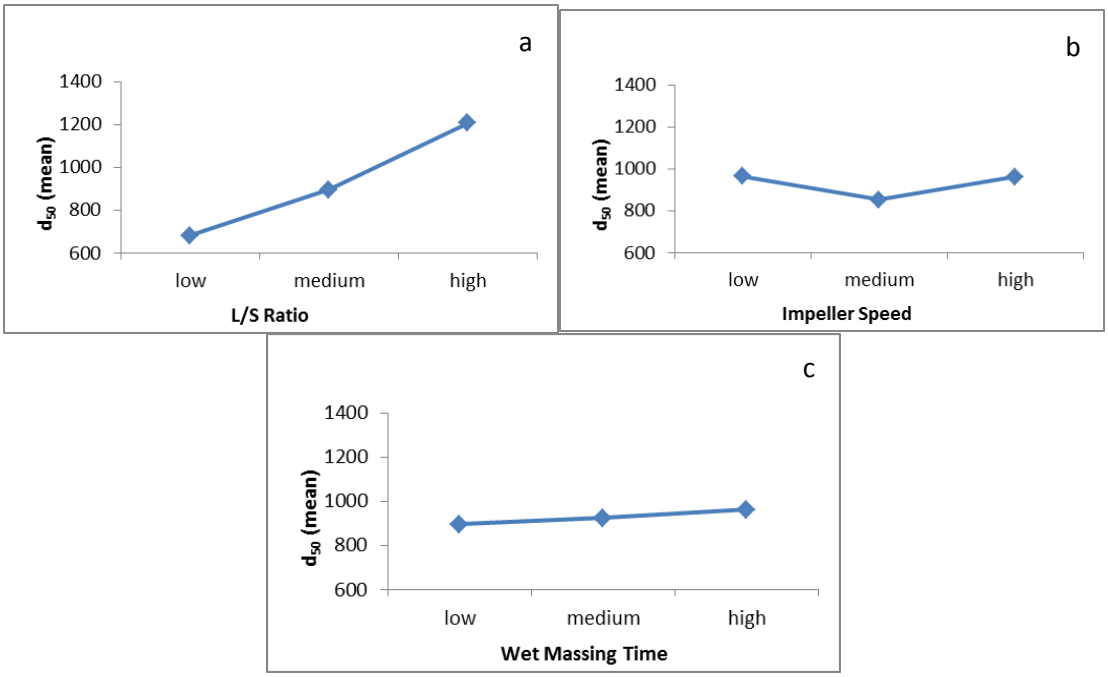

Figure 6-3: Main effects plot for the effect of a) L/S ratio b) Impeller speed and c) Wet massing time on d50

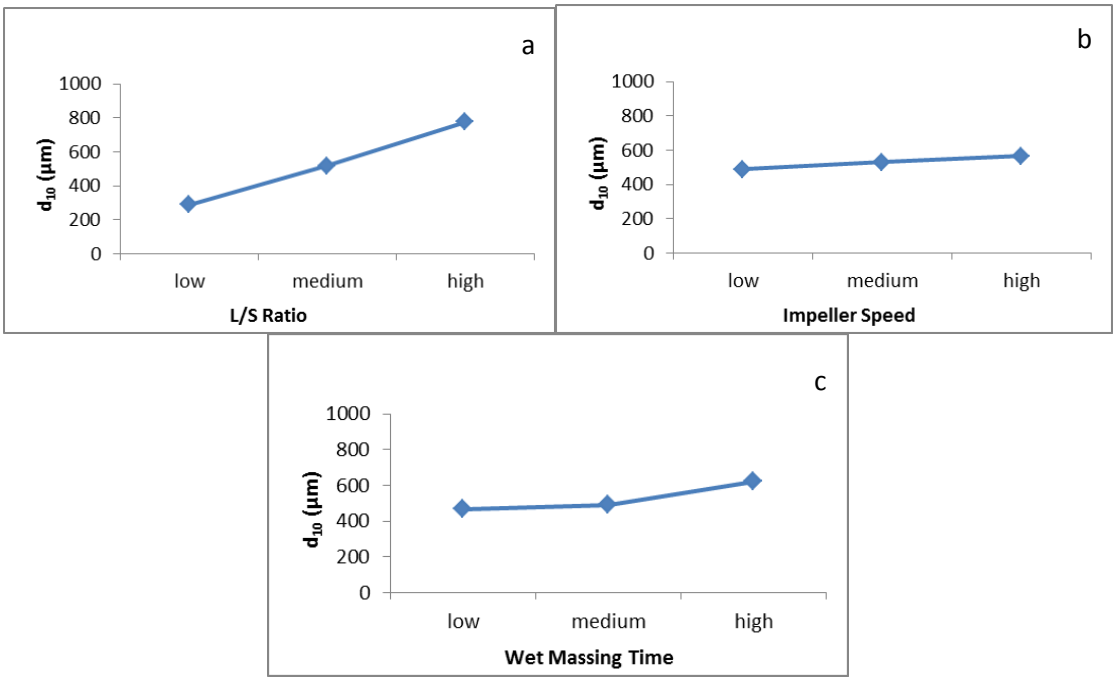

Figure 6-4: Main effects plot for the effect of a) L/S ratio b) Impeller speed and c) Wet massing time on d10

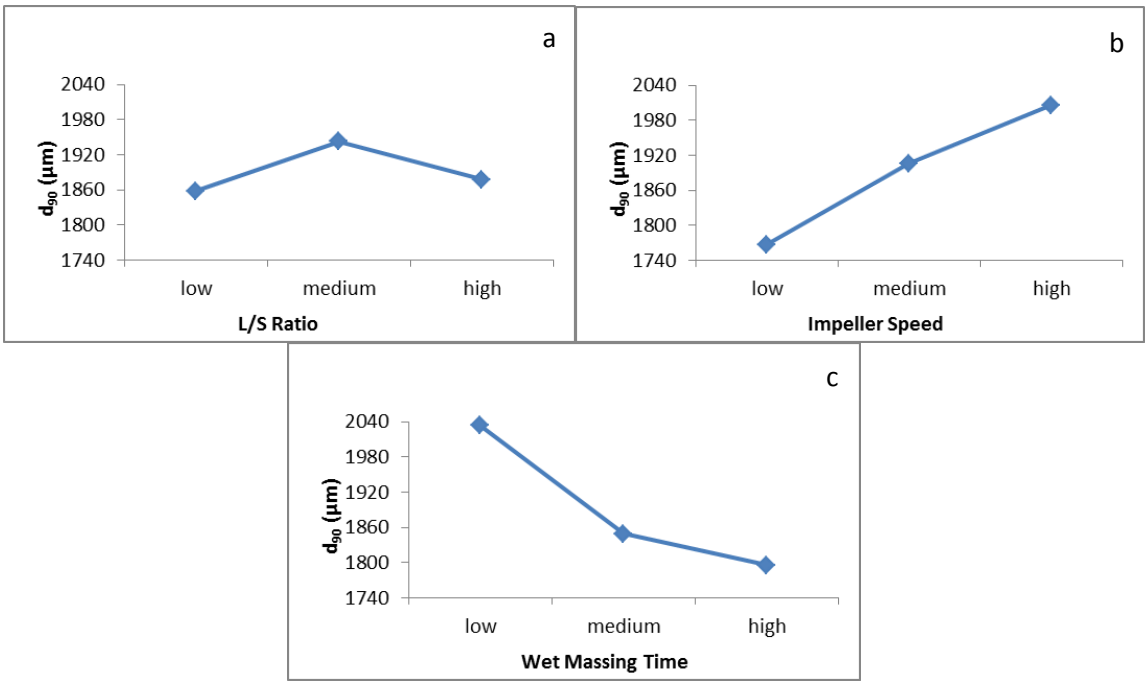

Figure 6-5: Main effects plot for the effect of a) L/S ratio b) Impeller speed and c) Wet massing time on d90

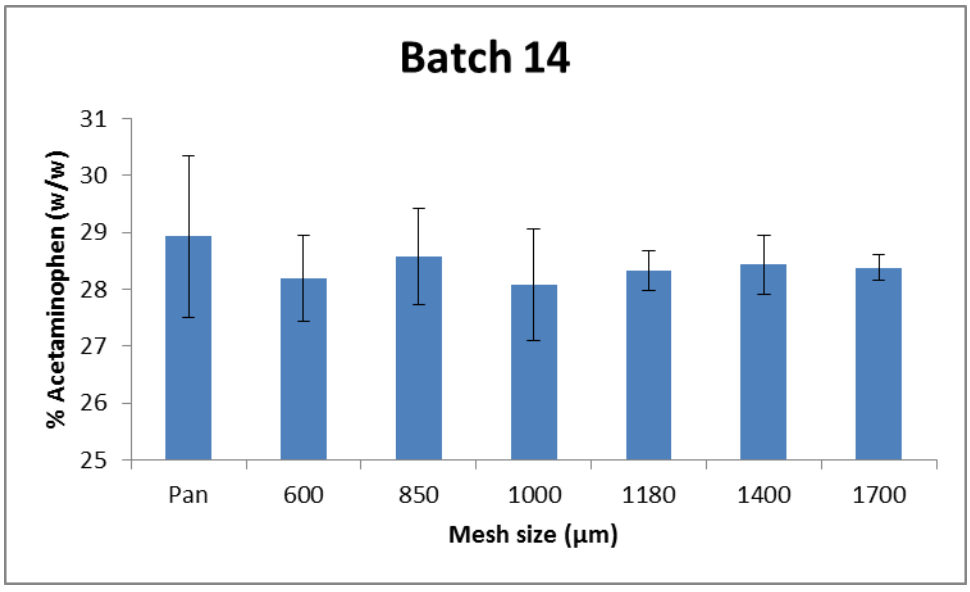

Figure 6-6: Distribution of the active ingredient across granule size class for Batch 14:MMM

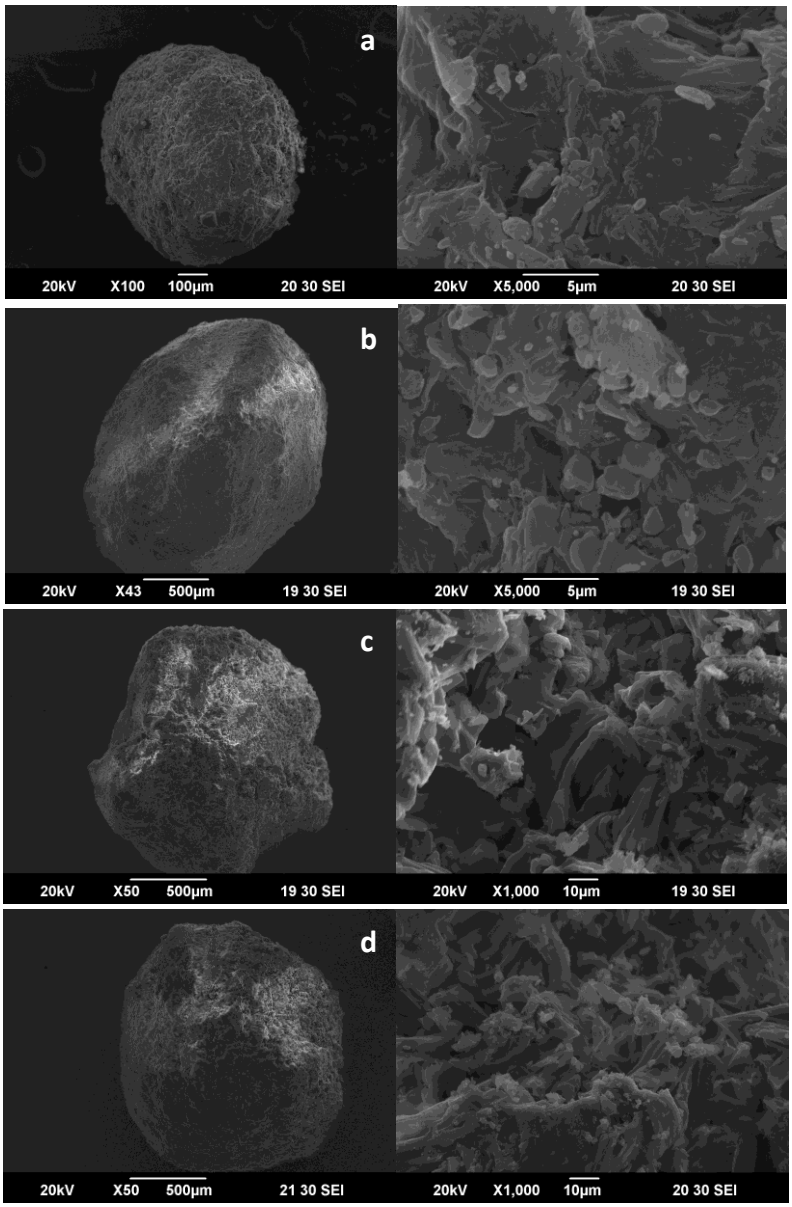

Figure 6-7: SEM of granules from batch a) batch 14:MMM, 600 µm mesh b) batch 14:MMM, 1400 µm mesh c) batch 4:LLL, 1400 µm mesh d) batch 27:HHH, 1400 µm mesh

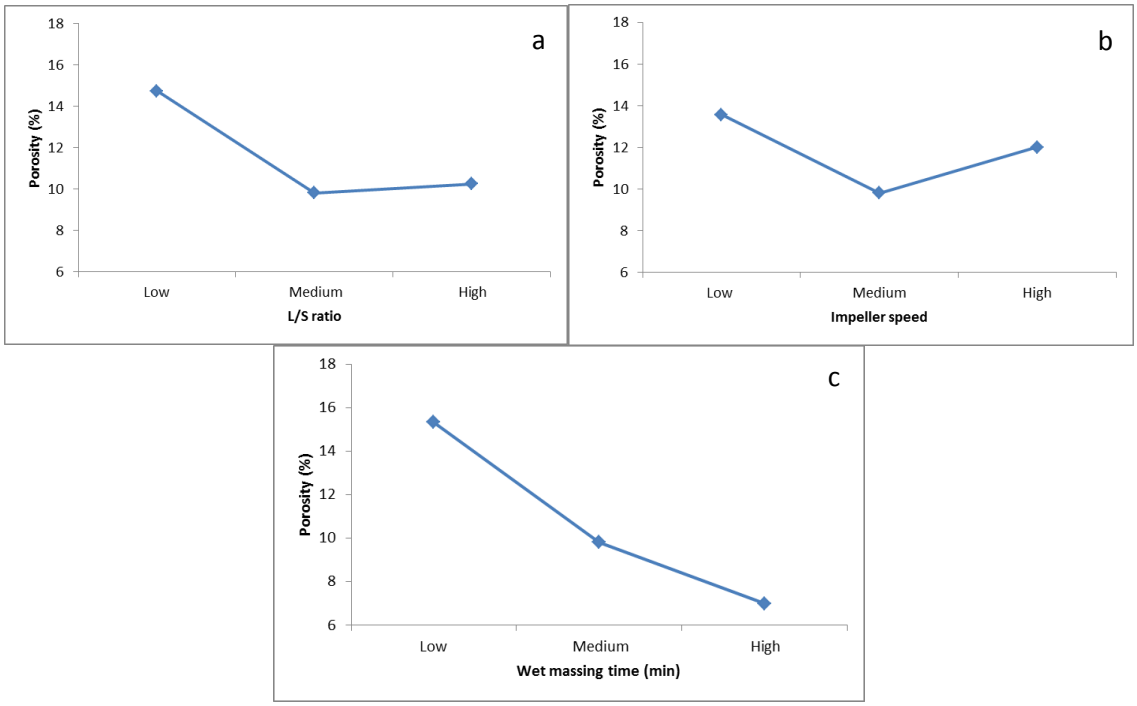

Figure 6-8: Main effects plot for the effect of a) L/S ratio b) Impeller speed and c) Wet massing time on granule porosity

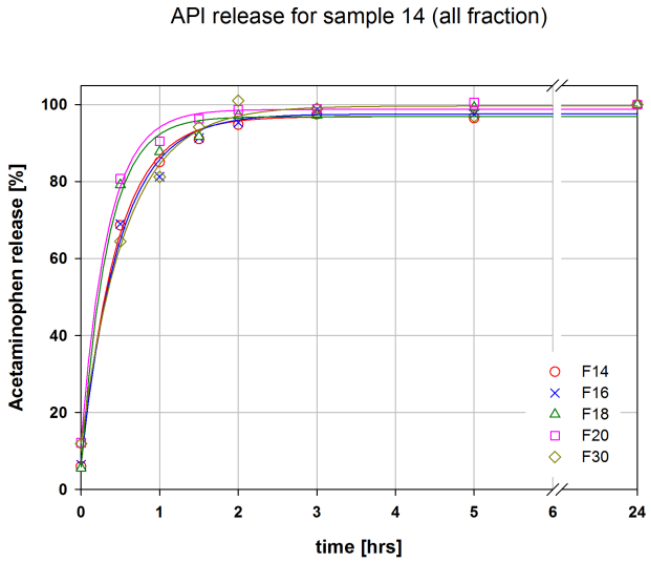

Figure 6-9: Dissolution profile of all granule size classes in batch 14:MMM, of granule system II, in water. The granule disintegrates and the rate of release is controlled by the intrinsic rate of dissolution of aceteminophen in water

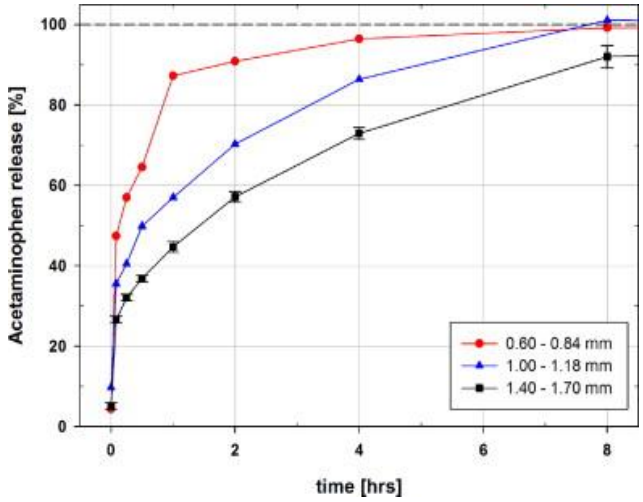

Figure 6-10: Release profiles of three size classes of granules from batch 27:HHH, of granule system II. The dissolution profiles are disticnt and dependent on the size of the granules

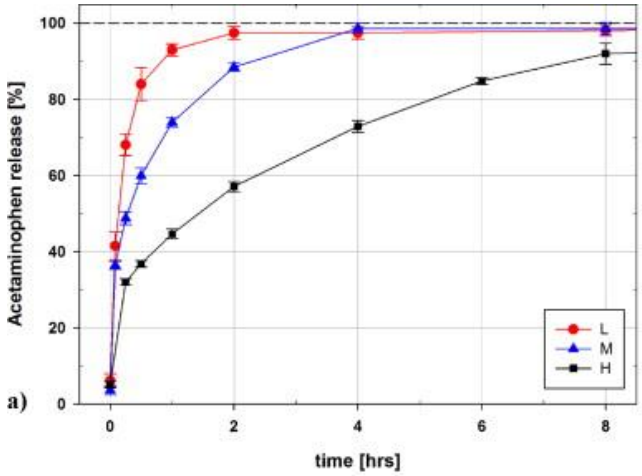

Figure 6-11: Dissolution profiles of batch 1:LLL, 14:MMM and 27:HHH, labelled as L, M and H, respectively. Distinct differences are observed between dissolution profiles

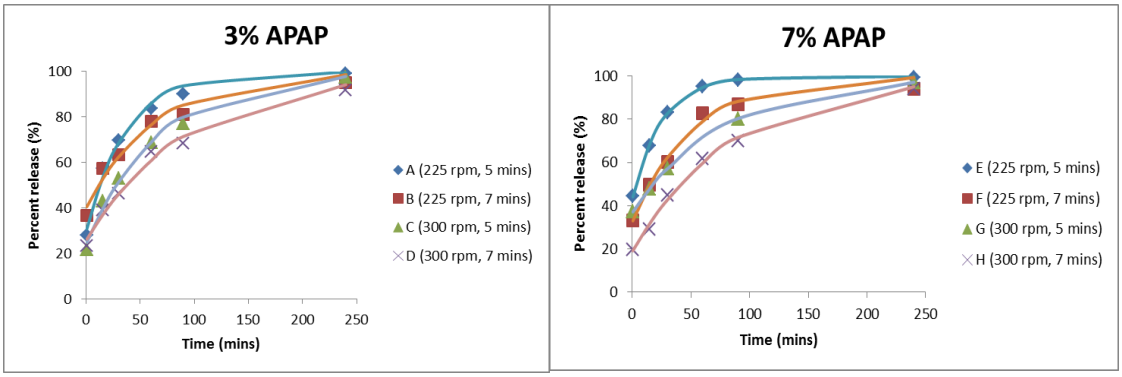

Figure 6-12: Release profiles of acetaminophen from granules for all batches in granule system I. Discrete points on the graphs represent the actual data while the smooth lines represent the model fit.

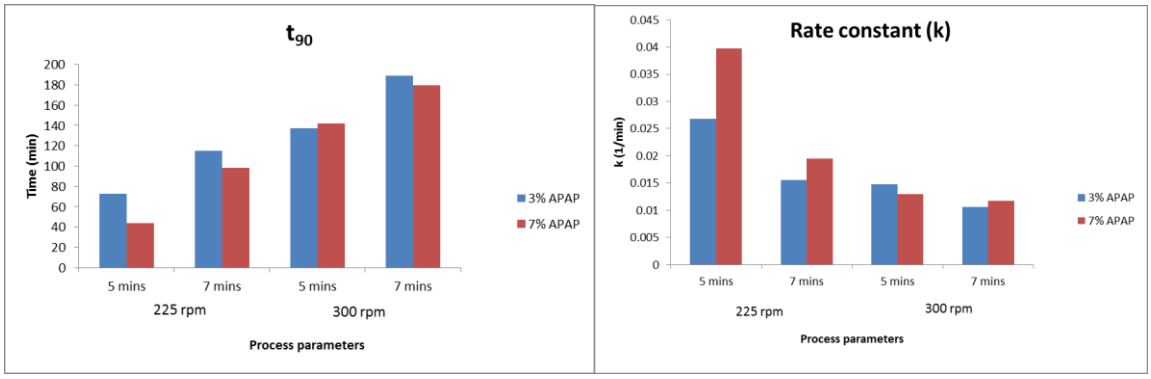

Figure 6-13(a): Time required for 90% of the active ingredient to be released from the granules at different processing condition (b) Rate constant of the release profile at different processing conditions.

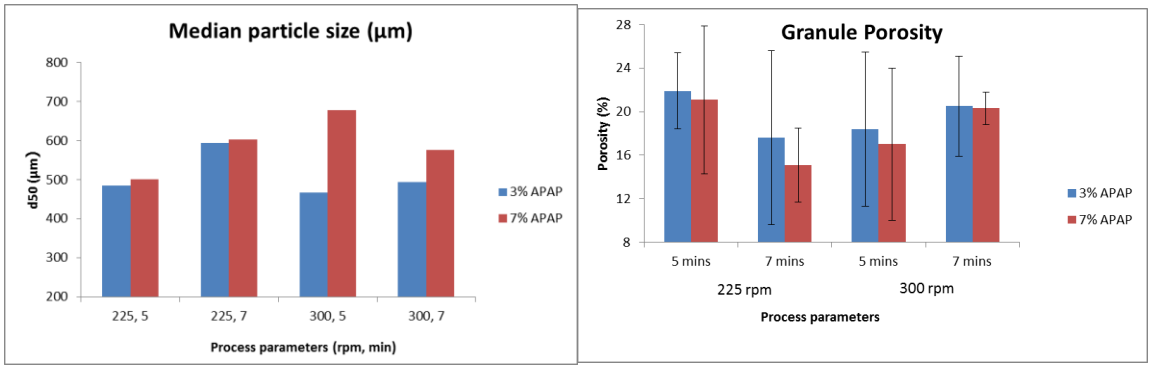

Figure 6-14(a): Median particle size and (b) porosity of granules made at different process parameters

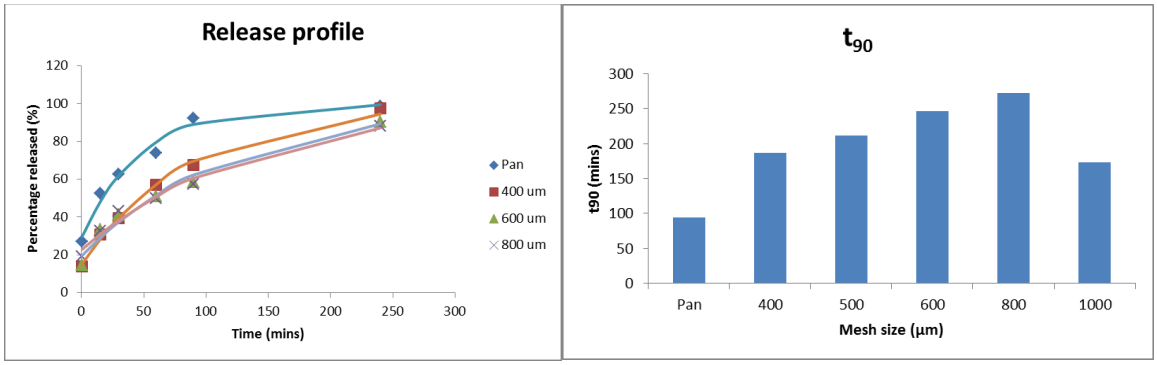

Figure 6-15(a): Release profile of acetaminophen from granule of different size classes for batch H. (b) Corresponding t_{90} values of the release profile

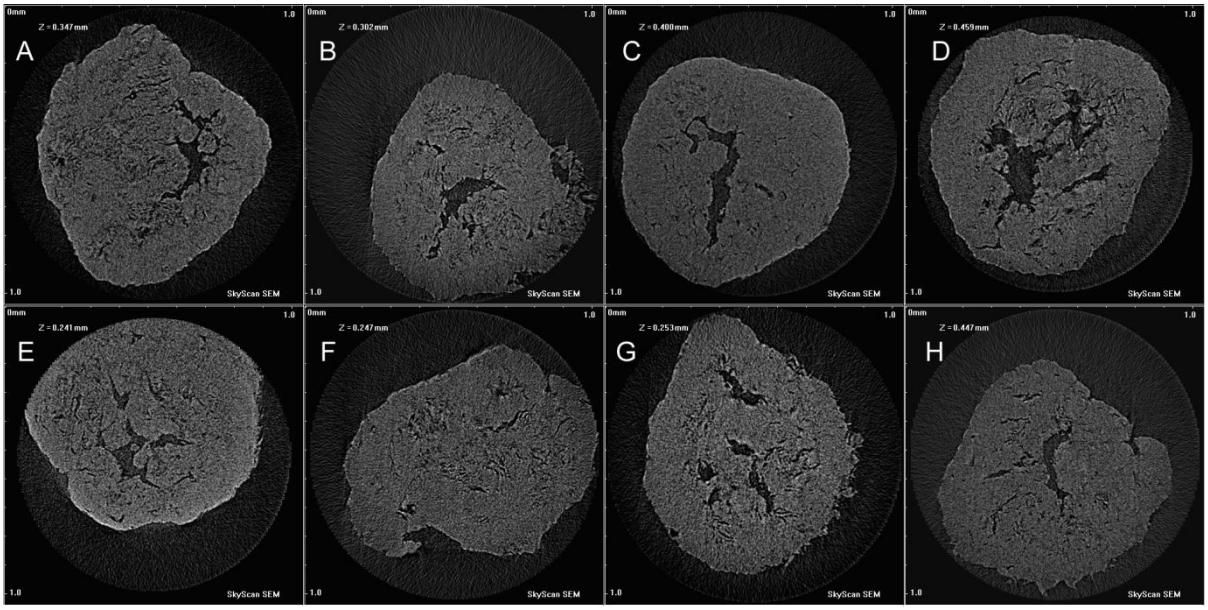

Figure 6-16: Micro-CT images exhibiting the presence of central cavity in the granules. The central cavity is hypothesized to be occupied to be occupied by a binder drop before drying. Surrounding active is hypothesized to partially dissolve in this drop.

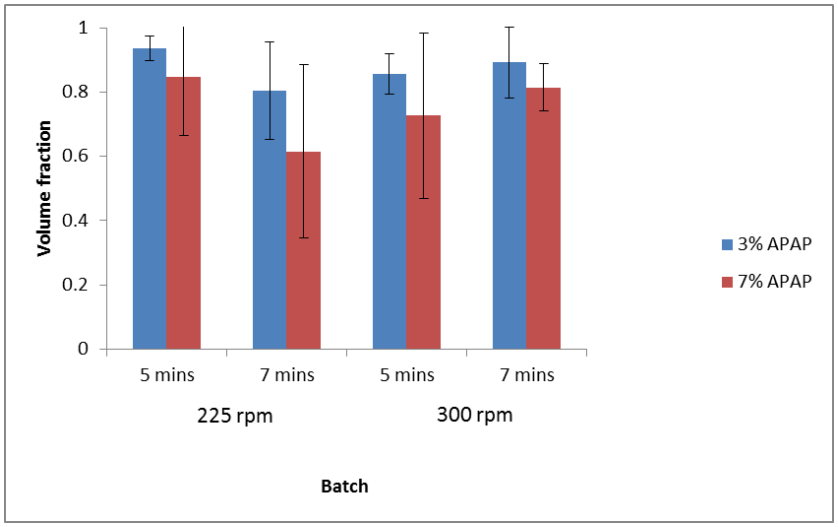

Figure 6-17: Fraction of the total porosity occupied by the central cavity of the granule. In almost all the central cavity account for majority of the pore volume

6.10 Tables for Chapter 6

Table 6-1: Particle size distribution parameters and bulk density of the starting materials used to make granules in granule system II.

Material	D10 (µm)	D50 (µm)	D90 (µm)	Bulk density (g/cc)
Avicel PH-102	19	59	134	0.47
Semi-fine Acetaminophen	5	25	72	0.38

Table 6-2: Design space of process parameters varied in this study. Among a multitude of parameters that can be varied, the impeller speed, wet massing time and the L/S ration were found to be the most significant parameters that affect granule properties.

Parameter	L/S ratio	Impeller speed (rpm)	Wet massing time (min)
Low	0.70	225	3
Medium	0.73	275	5
High	0.77	325	7

Table 6-3: All process and formulation parameters for granule system II

Batch (g)	300
Acetaminophen (g) (API)	90
Avicel (g) (Excipient)	210
Water (g)	210, 220, 230
Chopper speed (rpm)	6500
Impeller speed (rpm)	225, 275, 325
Premixing time (min)	2
Water addition time (min)	3
Wet massing time (min)	3, 5, 7

Table 6-4: Particle size distribution parameters of granules made for granules system II. The granulation batches follow a specific nomenclature. Alphabets L, M and H stand for low, medium and high respectively and they are used to indicate the level of the parameter for L/S ratio, impeller speed and wet massing time, in that order. For example, a batch defined as 9:MHL indicates the 9th experiment of the design point with medium (0.73) L/S ratio, high (325 rpm) impeller speed and low (3 minutes) wet massing time respectively.

Batch number	Batch Code	d10 (µm)	d50 (µm)	d90 (µm)
1	LLM	238	727	1684
2	LMM	394	784	1828
3	LHM	152	683	2127
4	LLL	189	805	1798
5	LML	95	473	1795
6	LHL	175	551	2213
7	MLL	367	925	1922
8	MML	446	731	2571
9	MHL	633	985	2098
10	HLL	799	1267	1937
11	HML	716	1101	2044
12	HHL	794	1212	1925
13	MLM	229	792	1531
14	MMM	523	831	1913
15	MHM	656	962	1962
16	HLM	806	1177	1889
17	HMM	732	1129	1849
18	HHM	700	1235	1859
19	LLH	438	777	1472
20	LMH	436	594	1661
21	LHH	484	735	2145
22	MLH	458	941	1778
23	MMH	613	837	1817
24	MHH	726	1047	1895
25	HLH	869	1276	1890
26	HMH	804	1202	1675
27	HHH	776	1253	1829

Table 6-5: Mean concentration of API in granule size for 27 batches of granule system II. The number adjacent to the mean value is the standard deviation of the measurement

	Mesh size (μm)															
Batch number	PAN		400		600		850		1000		1180		1400		1700	
1	28.96	0.64	28.51	1.40	29.16	0.50	29.57	1.29	28.86	0.88	28.95	0.69	29.63	1.37	29.87	1.64
2	28.47	0.64	28.18	0.79	28.73	1.15	28.19	0.76	28.85	1.33	28.49	0.69	27.97	1.15	27.72	1.50
3	28.51	0.70	0.00	0.00	28.52	0.68	28.78	0.68	28.23	1.22	30.12	2.26	29.17	1.35	28.80	0.73
4	27.70	0.83	27.31	1.45	27.30	1.46	28.70	1.70	28.64	1.64	28.42	1.38	28.41	1.36	27.97	0.51
5	27.36	1.67	0.00	0.00	28.62	1.29	28.38	0.92	28.50	1.11	28.36	0.88	27.81	1.09	28.81	1.53
6	27.17	0.33	26.79	1.13	27.29	0.76	27.78	1.54	28.04	1.83	27.93	1.71	27.41	1.01	27.35	0.89
7	29.21	2.23	27.22	1.48	27.88	0.46	27.53	1.03	27.86	0.34	27.71	0.62	27.43	1.19	27.80	0.25
8	28.28	1.42	27.82	0.60	27.73	0.21	27.52	0.85	28.83	2.01	27.18	1.39	27.46	0.96	27.24	1.32
9	31.23	3.14	29.00	1.41	27.96	1.28	27.82	1.46	28.84	1.20	27.95	1.30	28.55	0.64	29.06	1.49
10	33.63	4.30	28.60	0.87	29.07	1.55	29.70	2.15	28.28	0.62	28.14	0.93	28.84	1.27	27.16	2.08
11	28.58	1.62	0.00	0.00	29.52	2.45	28.90	1.94	24.64	3.39	29.18	2.19	28.67	1.72	27.74	0.60
12	29.07	2.21	0.00	0.00	28.13	1.23	27.93	0.88	27.79	0.55	27.87	0.76	27.63	0.55	26.98	1.62
13	28.07	0.76	0.00	0.00	27.88	1.12	28.97	1.61	28.01	0.88	28.52	1.00	28.85	1.47	28.66	1.23
14	28.93	1.42	0.00	0.00	28.20	0.75	28.57	0.85	28.09	0.98	28.33	0.34	28.44	0.52	28.38	0.22
15	28.55	0.76	0.00	0.00	29.27	1.39	28.36	1.10	28.49	0.87	28.00	1.57	28.45	0.95	29.09	1.16
16	32.01	3.39	27.14	2.35	29.03	1.04	28.79	0.48	29.17	1.25	28.74	0.25	27.90	1.69	28.47	0.93
17	32.34	3.14	0.00	0.00	28.93	1.32	30.10	1.49	28.67	1.62	30.22	1.63	28.87	1.39	29.29	0.72
18	29.41	1.99	0.00	0.00	28.19	0.57	27.87	1.21	28.42	0.69	28.40	0.64	28.41	0.65	27.94	1.11
19	28.38	1.21	29.13	1.06	28.67	0.68	29.44	1.49	28.41	1.17	28.73	0.51	28.95	0.71	28.00	1.67
20	27.71	2.02	28.00	1.76	30.22	2.15	31.32	2.90	29.45	1.40	29.21	1.06	28.79	0.58	28.69	0.83
21	29.45	2.13	28.13	0.33	27.87	1.02	29.33	2.04	28.72	1.40	29.98	2.54	28.79	1.49	27.89	0.98
22	29.12	1.19	0.00	0.00	28.67	0.39	28.31	1.19	28.65	0.49	28.79	0.52	28.93	0.86	28.70	0.26
23	37.22	5.57	27.97	1.22	28.09	1.04	28.19	0.85	28.99	1.44	28.42	0.31	28.69	1.03	28.46	0.47
24	27.92	1.97	0.00	0.00	28.39	1.49	31.03	2.61	28.55	1.30	28.79	0.94	26.27	3.09	28.48	1.39
25	29.12	1.27	0.00	0.00	28.77	0.63	28.86	0.85	28.45	0.85	28.45	0.84	27.93	1.59	29.52	1.73
26	30.39	2.42	27.53	2.02	28.44	0.96	28.47	0.91	28.85	0.70	28.64	0.49	29.05	1.10	28.88	0.78
27	27.83	1.54	0.00	0.00	29.02	1.35	27.92	1.43	28.76	0.96	29.04	1.37	28.13	1.15	28.00	1.32

Table 6-6: Porosity of granules from six selected batches is shown. Granule fractions in the range 1.4 to 1.7 mm were used for CT scans.

Batch	L/S ratio	Impeller speed	Wet massing time	Porosity (%)
4:LLL	*Low*	*low*	*low*	15.5 ± 4.8
6:LHL	*Low*	**high**	*low*	17.0 ± 5.7
10:HLL	**High**	*low*	*low*	13.5 ± 5.2
14:MMM	medium	medium	medium	9.8 ± 0.6
19:LLH	*Low*	*low*	**high**	11.7 ± 2.9
27:HHH	**High**	**high**	**high**	7.0 ± 2.4

6.11 Appendix

Table 6-7: Summary of ANOVA to study the effect of process parameters on D50 of the granule size distribution

Source	DF	Seq SS	AdjSS	Adj MS	F	P
L/S ratio	2	1253884	1253884	626942	279.06	0
Impeller speed	2	72943	72943	36471	16.23	0.002
Wet massing time	2	20832	20832	10416	4.64	0.046
L/S ratio*Impeller speed	4	40933	40933	10233	4.55	0.033
Impeller speed*Wet massing time	4	47537	47537	11884	5.29	0.022
L/S ratio*Wet massing time	4	20446	20446	5111	2.28	0.15
Error	8	17973	17973	2247		
Total	26	1474549				
S = 47.3985	R-Sq = 98.78%		R-Sq(adj) = 96.04%			

Table 6-8: Summary of ANOVA to study the effect of process parameters on D10 of the granule size distribution

Source	DF	Seq SS	AdjSS	Adj MS	F	P
L/S ratio	2	1075010	1075010	537505	154.14	0
Impeller speed	2	27396	27396	13698	3.93	0.065
Wet massing time	2	124374	124374	62187	17.83	0.001
L/S ratio*Impeller speed	4	139209	139209	34802	9.98	0.003
Impeller speed*Wet massing time	4	25811	25811	6453	1.85	0.213
L/S ratio*Wet massing time	4	52225	52225	13056	3.74	0.053
Error	8	27897	27897	3487		
Total	26	1471923				
S = 59.0522	R-Sq = 98.10%		R-Sq(adj) = 93.84%			

Table 6-9: Summary of ANOVA to study the effect of process parameters on D90 of the granule size distribution

Source	DF	SeqSS	Adj SS	Adj MS	F	P
L/S ratio	2	35589	35589	17794	1.17	0.358
Impeller speed	2	259820	259820	129910	8.54	0.01
Wet massing time	2	280702	280702	140351	9.22	0.008
L/S ratio*Impeller speed	4	375926	375926	93981	6.18	0.014
Impeller speed*Wet massing time	4	79865	79865	19966	1.31	0.344
L/S ratio*Wet massing time	4	103630	103630	25907	1.7	0.242
Error	8	121720	121720	15215		
Total	26	1257251				
S = 123.349	R-Sq = 90.32%		R-Sq(adj) = 68.54%			

Chapter 7 : Conclusions and Future Directions

The concluding comments in each technical Chapter suggest that there are some intuitive future undertakings which could provide further the undertaking.

7.1 Mechanistic scale-up equations for dispersive mixing of cohesive powder

Chapter 4 concluded that the scaling up of granular dispersion of poorly flowing powders is a non-trivial exercise. The dispersion behavior is dependent on the properties of the material, the scale and regime of operation. Axial dispersion increases with increasing powder cohesion as the material travels in aggregates, exhibiting a higher effective particle size. Breaking of the aggregates results in enhanced dispersion. The dispersion behavior also increases with increasing scale of the system. At higher scales, the powder experiences higher normal consolidation stresses resulting in larger aggregates, again leading to higher dispersion. An empirical relationship was proposed correlating the axial dispersion coefficient to the Bond number and the Froude number of the system. In order to develop the purely mechanistic correlations, dispersion behavior in a single operating regime should be studied. The effect of operating regimes cannot be captured in the existing correlations. Examination in a single regime will allow for in depth examination of relations between size of the aggregates, and system scale and the material. This is currently lacking.

7.2 Dense granular flow in vertical pipes

Chapter 4 found that continuous mixing processes are superior compared to batch mixing processes in their ability to blend highly segregating ingredients. The finding opens the door to manufacture highly segregating formulations by direct compaction – currently, they are either reformulated to closely match ingredient properties, or granulated. However, to fully validate this hypothesis, a continuously blended segregating mixture

must be tableted. The RSD on the content uniformity of the resultant tablets should be less 6%, the FDA recommended threshold. However, since these mixtures easily demix, care should be taken while transporting the homogenized mixture from the blender to the tablet press. The blended mixture must not be provided with any space or time where its particles could rearrange and segregate.

Material exiting the blender is typically transported to the tablet press via a transfer pipe, also called a transition. Transitions are connections that transport material from unit operation to another, generally by gravity. They are typically vertical and transport the powder in a dense state. An alternative to transporting them in a dense state is vertical free fall, which is known to cause demixing [57]. Understanding granular transport of powder in vertical transitions is thus critical.

A vertical transition is illustrated in Figure 7-1. Material is being constantly added to the top and is withdrawn from the bottom. At the steady state, the rate of input is equal to the rate of output and the mass holdup inside the bed is constant. Under unsteady conditions, if the rate at which material is being added exceeds the rate of output, the level of the bed and consequently the mass holdup inside the bed rises. Conversely, if the rate at which material is being withdrawn from the bed exceeds the rate at which new material is added to the bed, the level of the bed and mass holdup inside the bed will drop.

Rearrangement of the material while it traverses the pipes can occur in two directions – radial and axial. Radial rearrangement can have serious consequences on content uniformity of the tableted product if the amount of material (weight) in a radial cross-section is greater than the weight of the tablet. It can also have consequences on sensing.

Most probes only sense a small fraction of the radial cross-section. For accurate sensing and consequently appropriate control, it is important that probe is presented with a representative sample or a sample in which the radial arrangement is known a priori and thus accounted for in the sensing model. In addition to radial rearrangement, the axial rearrangement and segregation of the material is equally important. Axial segregation can lead to the formation of bands, like those in Figure 7-2. These bands, if not re-homogenized can manifest in the final leading to content non-uniformity.

Examination of the dense vertical transport of granular material in a pipe is thus advocated. Discrete element modeling (DEM) based simulations are being proposed, since it is challenging to examine the system experimentally. A screen shot of the simulation is shown in Figure 7-3.

Equally important is the starting position of the particles in pipe. Material is introduced to the transition via a hopper and lands on the material forming heaps. It is well known that granular material added to a heap is prone to sifting segregation. The formation of powder heaps must therefore be studied. Heap formation is affected by nature of emptying. Typically, materials enter the transfer pipes from hoppers and studying emptying of hoppers along with the consequent packing of the heaping powder is also of interest. Screen shots from sample simulations are shown in Figure 7-4.

7.3 Identifying dominant mechanisms causing content non-uniformity in high shear wet granulation

Chapter 5 concluded that there are several reasons for content non-uniformity in high shear wet granulation. Content non-uniformity in granules manifests as the preferential presence of the active ingredient in the coarse or the fine granules. The chapter identified

three main causes of content non-uniformity. It was found that the disparity between the wettabilities of the excipient and the active ingredient can lead to preferential nucleation and growth of the superior wetting ingredient leading to non-uniform distribution of the ingredients across size classes. Content non-uniformity can also occur due insufficient homogenization of the dry powder mixture prior to binder addition, leading to preferential wetting of one class of ingredient over the other. Lastly, solubility of the active ingredient in the binder fluid was identified as a cause of content non-uniformity. The active ingredient may dissolve in the binder fluid and granulate. However, the API may recrystallize during drying and appear as fines.

Future work focuses on identifying which mechanism for content non-uniformity will dominate in a given situation.

The effect of drug solubilization and consequent migration during drying has not been explicitly studied. A study is underway that adds the active ingredient to the system in the solubilized form. The distribution of the drug in this case depends on the liquid distribution. For uniform liquid distribution, the active ingredient must be uniformly distributed across the size classes. The presence of super potent fines in such a case must hint at drug migration during drying.

In order to test the contribution of the state of initial mixedness of the powder to the content uniformity of the granules, it is proposed to perform the granulation experiments with variable states of initial powder mixedness. A correlation between the states of initial homogeneity of the powder to the uniformity in the distribution of the ingredients

will enable quantification of this effect. This work has been performed and a manuscript is in preparation.

During testing, it was observed that the contact angle of the acetaminophen with water tested using the Washburn method was found to be unusually high, compared to literature sources [111, 112]. The contact angle of acetaminophen found in literature is higher than the contact angle of Avicel PH-101 and the hypothesis on which this study is based is thus preserved. However, a new robust and a direct method for determining preferential wetting, one that does not depend on variable measurements, must be developed.

One alternative is to perform the traditional drop penetration test, followed by extracting the subsequent nucleus, drying it and then analyzing it for its content. Mixtures of several grades of acetaminophen were prepared with Avicel PH-101 to test the potential of this method. It was observed that the resultant nucleus contains APAP and Avicel PH-101 in the same ratio as the bulk mixture (Figure 7-5). Water, thus, did not preferentially nucleate either ingredient.

7.4 Examination of granule and tablet microstructure by Raman imaging

Chapter 6 highlighted the importance of granule microstructure on performance attributes of the granules. It was observed that the granule microstructure, specifically, the porosity of the granule has an impact on the rate of release of the active ingredient from the granule. The active ingredient has to diffuse through the porous structure before being incorporated in the bulk solvent. The presence of a well-connected porous structure facilitates this diffusion. The rate of release thus increases with increasing porosity of the granules. The time required for the active ingredient to diffuse out of the granule is also a quadratic function of the granule diameter. Thus, thorough characterization of the particle

size distribution and porosity of the granules enables one to model and predict the rate of release of the active ingredient from a batch of granules. It was also observed that the ability to model and predict this rate of release is undermined if there is non-uniform distribution of the active ingredient across size classes.

To visually examine the distribution of the active ingredients in a granule or a tablet, raman based spectroscopic imaging is being proposed. A sample image is shown in Figure 7-6. The imaging helps to highlight the nature of the distribution of the active ingredient within the granule/tablet. This can be correlated to product performance, facilitating Quality by Design.

Powder mixing is complex phenomenon, primarily due to inability to mechanistically model powder behavior. Scaling up of dispersive mixing of poorly flowing materials is a challenge. Poorly flowing materials exhibit multiple states of density and form aggregates, both of which are difficult to model and predict. Powder segregation has been the subject of intense examination for the past several decades and major progress in the design of strategies to mitigate segregation has been made. However, there are more than one mechanisms of segregation, which can occur simultaneously. A magic bullet that addresses demixing remains elusive. Most new drugs are hydrophobic, are poorly soluble and flow very poorly. Powder mixing and wetting in granulation, to ensure uniform distribution of the active ingredient across granule size classes thus continues to attract attention. Despite the challenges, there has been remarkable progress in characterizing powder mixing mechanisms. This has enabled the design and development of processes which are robust, efficient and deliver high quality product.

7.5 Figures for Chapter 7

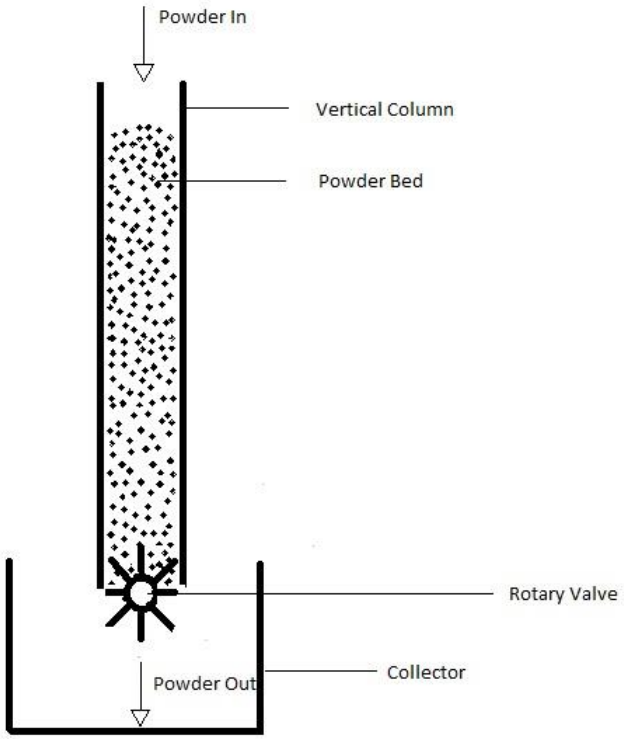

Figure 7-1: Dense granular transport in a vertical bed. Material can segregate axially and radially in the bed.

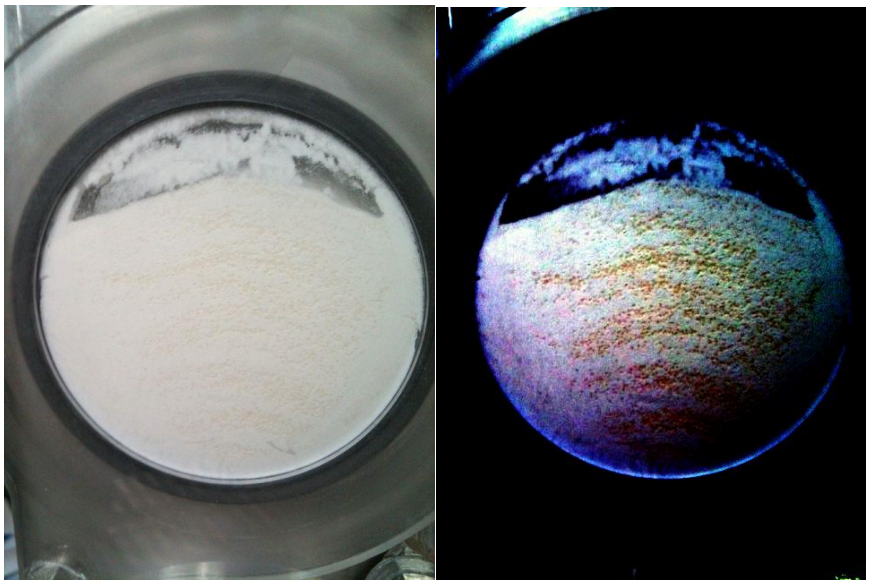

Figure 7-2: Formation of axial bands in during transport of material in a vertical packed bed. The axial bands can manifest in the final product leading to content non-uniformity.

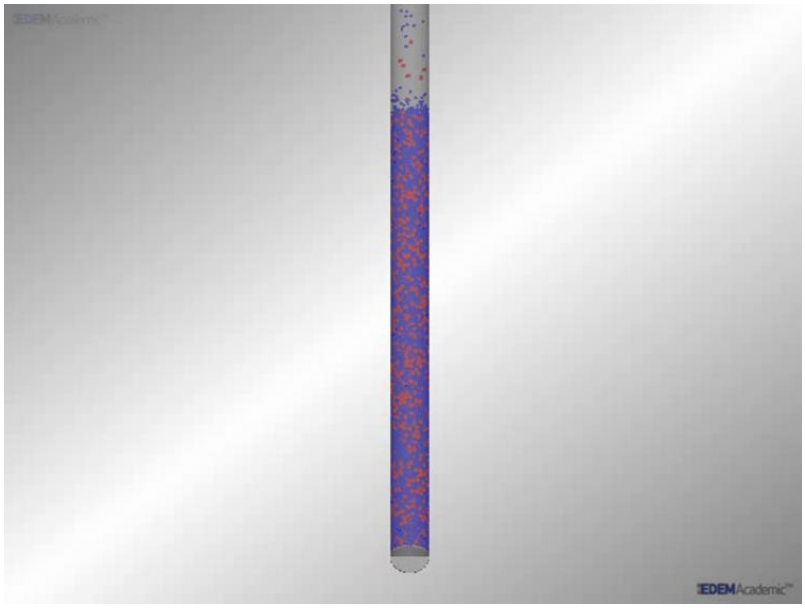

Figure 7-3: A screen shot of a simulation modeling dense granular transport in a vertical bed. The rotation speed of the valve is tuned to match the rate of material addition to the simulation

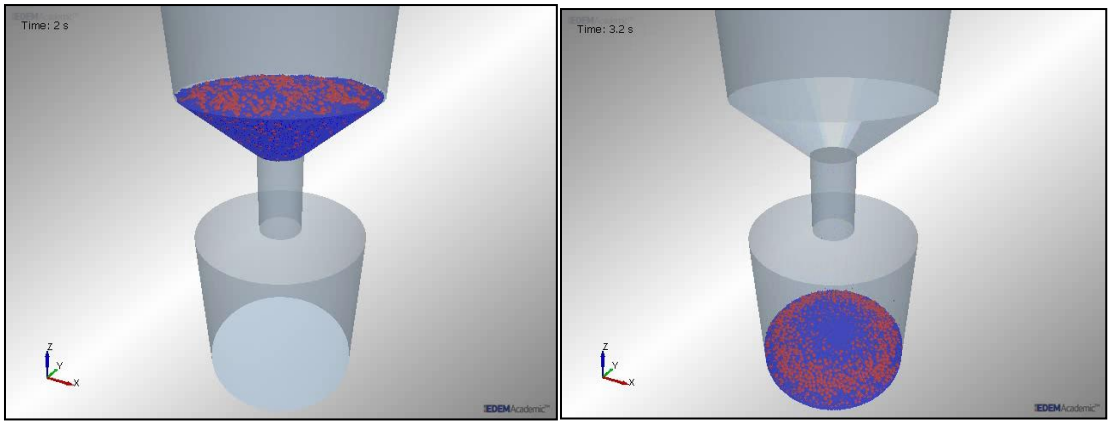

Figure 7-4: Simulation showing emptying of a hopper in a vessel. The figure shows a distinct arrangement of particles. The outermost layer is occupied by smaller particles due to their ability to pack in smaller spaces. This is followed by a ring of larger particles. Larger particle posses greater interia and thus roll to further along the heap.

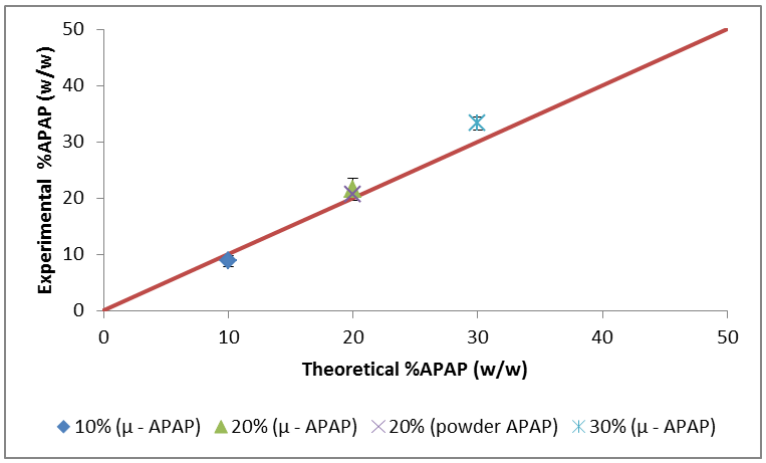

Figure 7-5: Content of the nucleus formed after a drop penetration experiment. The content of the nucleus is same as the content of the bulk mixture indicative of impartial wetting

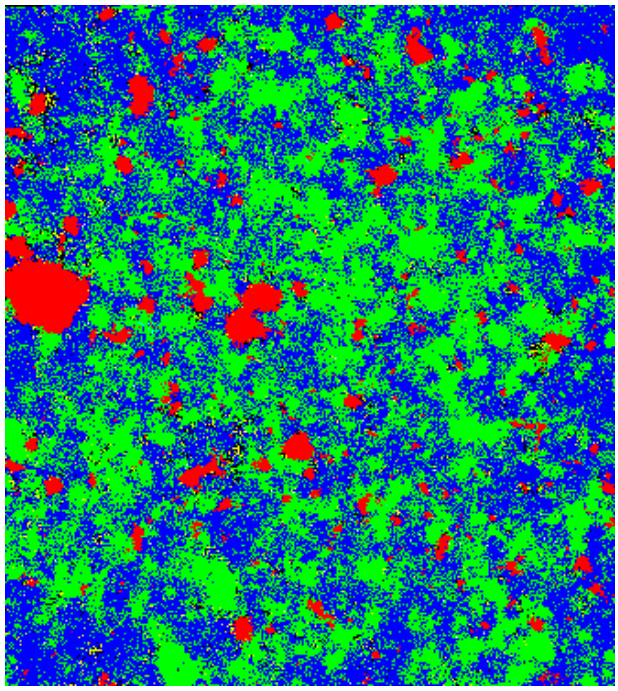

Figure 7-6: Raman image of the top layer of a tablet containing acetaminophen (red), microcrystalline cellulose (green), lactose (blue) and polyvinyl pyrolidone (yellow). The method enables the characterization of the distribution of the ingredients within the tablet or granule

Acknowledgement of Previous Publications

Portion of this thesis is based on previously published work of the student. Specifically, Chapter 5 is based on Oka *et.* al [113]. Chapter 6 is a combination of Oka *et.* al [59, 113] and Kaspar *et.* al [29]. The student is a contributing author of Kaspar *et.* al [29]. Only those results where the student has had a direct contribution in the work Kaspar *et.* al [29] have been presented in this thesis. Publications in support of this thesis and other collaborative publications of the student along with conference proceedings have been summarized below.

Publications in support of this thesis

1. **Oka S**., Emady H., Kašpar O., Tokárová V., Štěpánek F., Muzzio F. and Ramachandran R., *The effects of improper mixing and preferential wetting of active and excipient ingredients on content uniformity in high shear wet granulation.* Powder Technology, 2015, 278:266-277.

2. **Oka, S**., Kašpar O., Tokárová V., Sowrirajan K., Wu H., Khan M., Muzzio F., Štěpánek F. and Ramachandran R., *A Quantitative Study on the Effect of Process Parameters on Key Granule Characteristics in a High Shear Wet Granulation Process Involving a Two Component Pharmaceutical Blend. Advanced Powder Technology,* 2015, 26:315-322.

3. Kašpar O., Tokárová V., **Oka S**., Sowrirajan K., Ramachandran R., and Štěpánek F., *Combined UV/vis and micro-tomography investigation of acetaminophen dissolution from granules*. International Journal of Pharmaceutics, 2013, 458:272-281.

Other collaborative publications

1. Adepu M., Hate S., Betard A., **Oka S**., Schongut M., Sen M., Sood Y., Wolf D., Wieland S., Stepanek F., Muzzio F., Glasser B., and Ramachandran R. *Quantitative validation and analysis of the regime map approach for the wet granulation of industrially relevant zirconium hydroxide powders*. Powder Technology, 2016, 294:177-184

2. Vanarase A., Aslam R., **Oka S**., and Muzzio F., *Effects of mill design and process parameters in milling dry extrudates*. Powder Technology, 2015, 278:84-93.

Barrasso D., **Oka S**., Muliadi A., Litster J., Wassgren C., and Ramachandran R., *Population Balance Model Validation and Prediction of CQAs for Continuous Milling*

Processes: toward QbD in Pharmaceutical Drug Product Manufacturing. Journal of Pharmaceutical Innovation, 2013, 8:147-162

Conference Proceedings

1. **Oka S**., Emady H., Kašpar O., Tokárová V., Štěpánek F., Ramachandran R. and Muzzio F., "Understanding content non-homogeneity in high shear wet granulation: effects of powder segregation, preferential wetting and solubility" 7th Granulation Workshop, Sheffield, UK,2015.
2. **Oka S.**, Sahay A., and Muzzio F., "Experimental and Modeling Study of Powder Segregation in the Feeding Tube of a Tablet Press", IFPAC Annual Meeting, Arlington, 2015.
3. **Oka S**., Koynov S., and Muzzio F., "Axial Dispersion Coefficient of Mixing in Dilute Systems", AIChE Annual Meeting, Atlanta, 2014.
4. **Oka S**., Sahay A., and Muzzio F., "Parametric Study of Powder Flow (quasi-static bed) Down a Vertical Pipe", AIChE Annual Meeting, Atlanta, 2014.
5. Kaspar O., Tokarova V., **Oka S.**, Ramachandra R., and Stepanek F., "Determination of Structure, Porosity and API Distribution in Granules By the Computed Micro-Tomography", AIChE Annual Meeting, San Francisco, 2013.
6. **Oka S.**, Sowrirajan K., Kaspar O., Tokarova V., Barrasso B., Chaudhury A., Stepanek F., and Ramachandran R., "A Combined Experimental and Computational Analysis of the Effect of Powder and Granule Properties on Tablet Compaction Characteristics", 6th Granulation workshop, Sheffield, UK, 2013.
7. **Oka S**., Pawar P., Boukouvala F., and Muzzio F., "Effect of Lubricant Mixing Time and Concentration, Compaction Speed and Compression Force On the Dissolution Profile of a Control Release Formulation", AIChE Annual Meeting, Pittsburg, 2012.
8. **Oka S**., Tuncer A., Cuitinio A., and Muzzio F., "Effect of Water and Magnesium Stearate on the Strength of Ceramic Compacts", AIChE Annual Meeting, Pittsburg, 2012.

References

1. Muzzio, F.J., T. Shinbrot, and B.J. Glasser, *Powder technology in the pharmaceutical industry: the need to catch up fast.* Powder Technology, 2002. **124**(1–2): p. 1-7.
2. Muzzio, F.J., et al., *Sampling and characterization of pharmaceutical powders and granular blends.* International Journal of Pharmaceutics, 2003. **250**(1): p. 51-64.
3. Muzzio, F.J., et al., *Sampling practices in powder blending.* International Journal of Pharmaceutics, 1997. **155**(2): p. 153-178.
4. Bridgwater, J., *Fundamental powder mixing mechanisms.* Powder Technology, 1976. **15**(2): p. 215-236.
5. Fan, L.T., Y.-m. Chen, and F.S. Lai, *Recent developments in solids mixing.* Powder Technology, 1990. **61**(3): p. 255-287.
6. Nienow, A.W., M.F. EDWARDS, and N. Harnby, *Mixing in the process industries*. 1997: Butterworth-Heinemann.
7. Brone, D., A. Alexander, and F. Muzzio, *Quantitative characterization of mixing of dry powders in V-blenders.* American Institute of Chemical Engineers. AIChE Journal, 1998. **44**(2): p. 271.
8. Lemieux, M., et al., *Comparative study of the mixing of free-flowing particles in a V-blender and a bin-blender.* Chemical Engineering Science, 2007. **62**(6): p. 1783-1802.
9. Moakher, M., T. Shinbrot, and F.J. Muzzio, *Experimentally validated computations of flow, mixing and segregation of non-cohesive grains in 3D tumbling blenders.* Powder Technology, 2000. **109**(1–3): p. 58-71.
10. Alexander, A.W., et al., *Avalanching flow of cohesive powders.* Powder Technology, 2006. **164**(1): p. 13-21.
11. Faqih, A., et al., *Flow - induced dilation of cohesive granular materials.* AIChE Journal, 2006. **52**(12): p. 4124-4132.
12. Faqih, A., et al., *An experimental/computational approach for examining unconfined cohesive powder flow.* International Journal of Pharmaceutics, 2006. **324**(2): p. 116-127.
13. Shi, W., E. Galella, and O. Sprockel, *Macro- and micro-mixing of a cohesive pharmaceutical powder during scale up.* Powder Technology, 2015. **274**: p. 319-323.
14. Sudah, O.S., et al., *Mixing of cohesive pharmaceutical formulations in tote (bin) blenders.* Drug development and industrial pharmacy, 2002. **28**(8): p. 905-918.
15. Sudah, O.S., D. Coffin-Beach, and F.J. Muzzio, *Effects of blender rotational speed and discharge on the homogeneity of cohesive and free-flowing mixtures.* International Journal of Pharmaceutics, 2002. **247**(1–2): p. 57-68.
16. Alexander, A., et al., *Characterization of the performance of bin blenders: Part 3 of 3: Cohesive powders.* Pharmaceutical technology, 2004. **28**(9): p. 54-74.
17. Van der Watt, J.G. and M.M. de Villiers, *The effect of V-mixer scale-up on the mixing of magnesium stearate with direct compression microcrystalline cellulose.* European Journal of Pharmaceutics and Biopharmaceutics, 1997. **43**(1): p. 91-94.
18. Duong, N.-H., et al., *A Homogeneity Study Using NIR Spectroscopy: Tracking Magnesium Stearate in Bohle Bin-Blender.* Drug Development and Industrial Pharmacy, 2003. **29**(6): p. 679-687.
19. Mehrotra, A., et al., *Influence of shear intensity and total shear on properties of blends and tablets of lactose and cellulose lubricated with magnesium stearate.* International Journal of Pharmaceutics, 2007. **336**(2): p. 284-291.
20. Alexander, A., F.J. Muzzio, and T. Shinbrot, *Segregation patterns in V-blenders.* Chemical Engineering Science, 2003. **58**(2): p. 487-496.
21. Alexander, A., et al., *V-blender segregation patterns for free-flowing materials: effects of blender capacity and fill level.* International Journal of Pharmaceutics, 2004. **269**(1): p. 19-28.

22. Alexander, A.W., T. Shinbrot, and F.J. Muzzio, *Granular segregation in the double-cone blender: Transitions and mechanisms.* Physics of Fluids, 2001. **13**(3): p. 578-587.
23. Pernenkil, L. and C.L. Cooney, *A review on the continuous blending of powders.* Chemical Engineering Science, 2006. **61**(2): p. 720-742.
24. Schaber, S.D., et al., *Economic Analysis of Integrated Continuous and Batch Pharmaceutical Manufacturing: A Case Study.* Industrial & Engineering Chemistry Research, 2011. **50**(17): p. 10083-10092.
25. Chatterjee, S. *FDA perspective on continuous manufacturing*. in *IFPAC Annual Meeting, Baltimore, MD*. 2012.
26. Escotet-Espinoza, S., et al., *Flowsheet Models Modernize Pharmaceutical Manufacturing Design and Risk Assessment*, in *Pharmaceutical Technology*. 2015. p. 34-42.
27. van den Dries, K. and H. Vromans, *Relationship between inhomogeneity phenomena and granule growth mechanisms in a high-shear mixer.* International Journal of Pharmaceutics, 2002. **247**(1–2): p. 167-177.
28. Vromans, H., H. Poels-Janssen, and H. Egermann, *Effects of High-Shear Granulation on Granulate Homogeneity.* Pharmaceutical Development & Technology, 1999. **4**(3): p. 297.
29. Kašpar, O., et al., *Combined UV/vis and micro-tomography investigation of acetaminophen dissolution from granules.* International Journal of Pharmaceutics, 2013. **458**(2): p. 272-281.
30. Emady, H.N., et al., *A simple color concentration measurement technique for powders.* Powder Technology, 2015. **286**: p. 392-400.
31. Lacey, P.M.C., *Developments in the theory of particle mixing.* Journal of Applied Chemistry, 1954. **4**(5): p. 257-268.
32. Sherritt, R.G., et al., *Axial dispersion in the three-dimensional mixing of particles in a rotating drum reactor.* Chemical Engineering Science, 2003. **58**(2): p. 401-415.
33. Rao, S.J., S.K. Bhatia, and D.V. Khakhar, *Axial transport of granular solids in rotating cylinders. Part 2: Experiments in a non-flow system.* Powder Technology, 1991. **67**(2): p. 153-162.
34. Ingram, A., et al., *Axial and radial dispersion in rolling mode rotating drums.* Powder technology, 2005. **158**(1): p. 76-91.
35. Kohav, T., J.T. Richardson, and D. Luss, *Axial dispersion of solid particles in a continuous rotary kiln.* AIChE Journal, 1995. **41**(11): p. 2465-2475.
36. Hogg, R., et al., *Diffusional mixing in an ideal system.* Chemical Engineering Science, 1966. **21**(11): p. 1025-1038.
37. Parker, D.J., et al., *Positron emission particle tracking studies of spherical particle motion in rotating drums.* Chemical Engineering Science, 1997. **52**(13): p. 2011-2022.
38. McLaren, C., J. Third, and C. Müller, *Experimental investigation of axial dispersion in a horizontal rotating cylinder.* Granular Matter, 2015. **17**(1): p. 43-48.
39. Third, J.R., D.M. Scott, and S.A. Scott, *Axial dispersion of granular material in horizontal rotating cylinders.* Powder Technology, 2010. **203**(3): p. 510-517.
40. Third, J.R. and C.R. Müller, *Is axial dispersion within rotating cylinders governed by the Froude number?* Physical Review E, 2012. **86**(6): p. 061314.
41. Ding, Y., et al., *Scaling relationships for rotating drums.* Chemical engineering science, 2001. **56**(12): p. 3737-3750.
42. Vasilenko, A., et al., *Role of consolidation state in the measurement of bulk density and cohesion.* Powder technology, 2013. **239**: p. 366-373.
43. Faqih, A.N., et al., *A method for predicting hopper flow characteristics of pharmaceutical powders.* Chemical Engineering Science, 2007. **62**(5): p. 1536-1542.
44. Debacq, M., et al., *A hydrodynamic model for flighted rotary kilns used for the conversion of cohesive uranium powders.* Chemical Engineering Science, 2013. **104**: p. 586-595.

45. Debacq, M., et al., *Transverse motion of cohesive powders in flighted rotary kilns: experimental study of unloading at ambient and high temperatures.* Powder Technology, 2013. **245**: p. 56-63.
46. Koynov, S., et al., *Measurement of the axial dispersion coefficient of powders in a rotating cylinder: Dependence on bulk flow properties.* Powder Technology.
47. Rumpf, H., *Grundlagen und methoden des granulierens.* Chemie Ingenieur Technik, 1958. **30**(3): p. 144-158.
48. Quintanilla, M., A. Castellanos, and J. Valverde, *Correlation between bulk stresses and interparticle contact forces in fine powders.* Physical Review E, 2001. **64**(3): p. 031301.
49. Sudah, O.S., et al., *Simulation and experiments of mixing and segregation in a tote blender.* AIChE Journal, 2005. **51**(3): p. 836-844.
50. Arratia, P.E., et al., *A study of the mixing and segregation mechanisms in the Bohle Tote blender via DEM simulations.* Powder Technology, 2006. **164**(1): p. 50-57.
51. Khakhar, D.V., J.J. McCarthy, and J.M. Ottino, *Radial segregation of granular mixtures in rotating cylinders.* Physics of Fluids, 1997. **9**(12): p. 3600-3614.
52. Khakhar, D.V., A.V. Orpe, and S.K. Hajra, *Segregation of granular materials in rotating cylinders.* Physica A: Statistical Mechanics and its Applications, 2003. **318**(1–2): p. 129-136.
53. Savage, S. and C. Lun, *Particle size segregation in inclined chute flow of dry cohesionless granular solids.* Journal of Fluid Mechanics, 1988. **189**: p. 311-335.
54. Bhattacharya, T. and J.J. McCarthy, *Chute flow as a means of segregation characterization.* Powder Technology, 2014. **256**: p. 126-139.
55. Baxter, J., et al., *Stratification in poured granular heaps.* Nature, 1998. **391**(6663): p. 136-136.
56. Grasselli, Y. and H. Herrmann, *Experimental study of granular stratification.* Granular Matter, 1998. **1**(1): p. 43-47.
57. Liss, E.D., et al., *Segregation of Powders during Gravity Flow through Vertical Pipes.* Pharmaceutical Technology, 2004. **28**(2): p. 78-96.
58. Olivieri, G., A. Marzocchella, and P. Salatino, *Segregation of fluidized binary mixtures of granular solids.* AIChE journal, 2004. **50**(12): p. 3095-3106.
59. Oka, S., et al., *A Quality-by-Design Case Study: Effect of Process and Formulation Parameters on Granule Characteristics in a High Shear Wet Granulation Process.* European Journal of Pharmaceutical Sciences 2013.
60. Emady, H., K. Hapgood, and R. Smith, *Granulation and Tabletting*, in *Production, Handling and Characterization of Particulate Materials*, H.G. Merkus and G.M.H. Meesters, Editors. 2016, Springer International Publishing. p. 107-136.
61. Kristensen, H.G. and T. Schaefer, *Granulation: A review on pharmaceutical wet-granulation.* Drug Development and Industrial Pharmacy, 1987. **13**(4-5): p. 803-872.
62. Harwood, C.F., et al., *The performance of continuous mixers for dry powders.* Powder Technology, 1975. **11**(3): p. 289-296.
63. Weinekötter, R. and L. Reh, *Continuous mixing of fine particles.* Particle & particle systems characterization, 1995. **12**(1): p. 46-53.
64. Laurent, B. and J. Bridgwater, *Continuous mixing of solids.* Chemical engineering & technology, 2000. **23**(1): p. 16-18.
65. Ziegler, G.R. and C.A. Aguilar, *Residence time distribution in a co-rotating, twin-screw continuous mixer by the step change method.* Journal of Food Engineering, 2003. **59**(2–3): p. 161-167.
66. Portillo, P.M., M.G. Ierapetritou, and F.J. Muzzio, *Characterization of continuous convective powder mixing processes.* Powder Technology, 2008. **182**(3): p. 368-378.
67. Portillo, P.M., M.G. Ierapetritou, and F.J. Muzzio, *Effects of rotation rate, mixing angle, and cohesion in two continuous powder mixers—A statistical approach.* Powder Technology, 2009. **194**(3): p. 217-227.

68. Vanarase, A.U. and F.J. Muzzio, *Effect of operating conditions and design parameters in a continuous powder mixer.* Powder Technology, 2011. **208**(1): p. 26-36.
69. Vanarase, A.U., et al., *Real-time monitoring of drug concentration in a continuous powder mixing process using NIR spectroscopy.* Chemical Engineering Science, 2010. **65**(21): p. 5728-5733.
70. Vanarase, A.U., J.G. Osorio, and F.J. Muzzio, *Effects of powder flow properties and shear environment on the performance of continuous mixing of pharmaceutical powders.* Powder Technology, 2013. **246**(0): p. 63-72.
71. Gao, Y., et al., *Characterizing continuous powder mixing using residence time distribution.* Chemical Engineering Science, 2011. **66**(3): p. 417-425.
72. Dubey, A., et al., *Computational approaches for studying the granular dynamics of continuous blending processes, 1–DEM based methods.* Macromolecular Materials and Engineering, 2011. **296**(3-4): p. 290-307.
73. Sarkar, A. and C. Wassgren, *Continuous blending of cohesive granular material.* Chemical Engineering Science, 2010. **65**(21): p. 5687-5698.
74. Sarkar, A. and C.R. Wassgren, *Effect of particle size on flow and mixing in a bladed granular mixer.* AIChE Journal, 2015. **61**(1): p. 46-57.
75. Sarkar, A. and C.R. Wassgren, *Simulation of a continuous granular mixer: Effect of operating conditions on flow and mixing.* Chemical Engineering Science, 2009. **64**(11): p. 2672-2682.
76. Alexander, A., et al., *A method to quantitatively describe powder segregation during discharge from vessels.* Pharmaceutical Technology Yearbook, 2000: p. 6-21.
77. Paul, E.L., V.A. Atiemo-Obeng, and S.M. Kresta, *Handbook of industrial mixing: science and practice*. 2004: John Wiley & Sons.
78. Kristensen, H.G. and T. Schaefer, *GRANULATION - A REVIEW OF PHARMACEUTICAL WET-GRANULATION.* Drug Development and Industrial Pharmacy, 1987. **13**(4-5): p. 803-872.
79. Kristensen, H.G., *AGGLOMERATION OF POWDERS.* Acta Pharmaceutica Suecica, 1988. **25**(4-5): p. 187-204.
80. McCormick, D., *Evolutions in Direct Compression*, in *Pharmaceutical Technology*. 2005.
81. Ansari, M.A. and F. Stepanek, *The effect of granule microstructure on dissolution rate.* Powder Technology, 2008. **181**(2): p. 104-114.
82. Egermann, H. and R. W, *Effect of particle size of drug and diluent on drug distribution in granule size fractions.* Acta Pharmaceutica Suecica, 1988. **34**.
83. Ojile, J.E., C.B. Macfarlane, and A.B. Selkirk, *Drug distribution during massing and its effect on dose uniformity in granules.* International Journal of Pharmaceutics, 1982. **10**(2): p. 99-107.
84. Selkirk, A.B., *The effect of solute migration on the distribution of borax throughout a batch of granules.* Journal of Pharmacy and Pharmacology, 1976. **28**(6): p. 512-514.
85. Warren, J.W., Jr. and J.C. Price, *Drug migration during drying of tablet granulations II: effect of binder solution viscosity and drying temperature.* J Pharm Sci, 1977. **66**(10): p. 1409-12.
86. Ottino, J.M. and D.V. Khakhar, *Mixing and Segregation of Granular Materials.* Annual Review of Fluid Mechanics, 2000. **32**(1): p. 55.
87. Zhou, Y.C., A.B. Yu, and J. Bridgwater, *Segregation of binary mixture of particles in a bladed mixer.* Journal of Chemical Technology & Biotechnology, 2003. **78**(2-3): p. 187-193.
88. Conway, S.L., et al., *Granular flow and segregation in a four-bladed mixer.* Chemical Engineering Science, 2005. **60**(24): p. 7091-7107.
89. Lerk, C.F., A.J.M. Schoonen, and J.T. Fell, *Contact angles and wetting of pharmaceutical powders.* Journal of Pharmaceutical Sciences, 1976. **65**(6): p. 843-847.

90. Aulton, M.E., M. Banks, and D.K. Smith, *THE WETTABILITY OF POWDERS DURING FLUIDIZED BED GRANULATION.* Journal of Pharmacy and Pharmacology, 1977. **29**(S1): p. 59P-59P.
91. Nguyen, T.H., W. Shen, and K. Hapgood, *Effect of formulation hydrophobicity on drug distribution in wet granulation.* Chemical Engineering Journal, 2010. **164**(2–3): p. 330-339.
92. Cavinato, M., et al., *Combining formulation and process aspects for optimizing the high-shear wet granulation of common drugs.* International Journal of Pharmaceutics, 2011. **416**(1): p. 229-241.
93. Thiel, W.J. and L.T. Nguyen, *Fluidized bed granulation of an ordered powder mixture.* Journal of Pharmacy and Pharmacology, 1982. **34**(11): p. 692-699.
94. Granberg, R.A. and A.C. Rasmuson, *Solubility of paracetamol in pure solvents.* Journal of Chemical and Engineering Data, 1999. **44**(6): p. 1391-1395.
95. Radl, S., et al., *Mixing characteristics of wet granular matter in a bladed mixer.* Powder Technology, 2010. **200**(3): p. 171-189.
96. Yu, L.X., *Pharmaceutical quality by design: product and process development, understanding, and control.* Pharmaceutical Research, 2008. **25**(4): p. 781-791.
97. Iveson, S.M., et al., *Nucleation, growth and breakage phenomena in agitated wet granulation processes: a review.* Powder Technology, 2001. **117**(1–2): p. 3-39.
98. Woyna-Orlewicz, K. and R. Jachowicz, *Analysis of wet granulation process with Plackett-Burman design--case study.* Acta Pol Pharm, 2011. **68**(5): p. 725-33.
99. Pandey, P., et al., *A combined experimental and modeling approach to study the effects of high-shear wet granulation process parameters on granule characteristics.* Pharmaceutical Development and Technology, 2013. **18**(1): p. 210-224.
100. Badawy, S.I.F., et al., *Mechanistic basis for the effects of process parameters on quality attributes in high shear wet granulation.* International Journal of Pharmaceutics, 2012. **439**(1-2): p. 324-333.
101. Kimber, J.A., S.G. Kazarian, and F. Štěpánek, *Formulation design space analysis for drug release from swelling polymer tablets.* Powder Technology, 2013. **236**: p. 179-187.
102. Wray, P., et al., *Compaction of pharmaceutical tablets with different polymer matrices studied by FTIR imaging and X-ray microtomography.* Journal of Pharmaceutical Sciences, 2008. **97**(10): p. 4269-4277.
103. Crean, B., et al., *Elucidation of the internal physical and chemical microstructure of pharmaceutical granules using X-ray micro-computed tomography, Raman microscopy and infrared spectroscopy.* European Journal of Pharmaceutics and Biopharmaceutics, 2010. **76**(3): p. 498-506.
104. Nott, K.P., *Magnetic resonance imaging of tablet dissolution.* European Journal of Pharmaceutics and Biopharmaceutics, 2010. **74**(1): p. 78-83.
105. Richardson, J.C., et al., *Pharmaceutical applications of magnetic resonance imaging (MRI).* Advanced Drug Delivery Reviews, 2005. **57**(8): p. 1191-1209.
106. Wang, Y., F. Ravenelle, and X. Zhu, *NMR imaging study of cross-linked high-amylose starch tablets-The effect of drug loading.* Canadian Journal of Chemistry, 2010. **88**(3): p. 202-207.
107. Ho, L., et al., *Terahertz pulsed imaging as an analytical tool for sustained-release tablet film coating.* European Journal of Pharmaceutics and Biopharmaceutics, 2009. **71**(1): p. 117-123.
108. Mikac, U., et al., *A study of tablet dissolution by magnetic resonance electric current density imaging.* Journal of magnetic resonance, 2007. **185**(1): p. 103-109.
109. Poutiainen, S., et al., *Evolution of granule structure and drug content during fluidized bed granulation by X-ray microtomography and confocal Raman spectroscopy.* J Pharm Sci, 2011. **100**(12): p. 5254-69.
110. Iveson, S.M., J.D. Litster, and B.J. Ennis, *Fundamental studies of granule consolidation part 1: Effects of binder content and binder viscosity.* Powder Technology, 1996. **88**(1): p. 15-20.

111. Granberg, R.A., et al., *Primary nucleation of paracetamol in acetone–water mixtures.* Chemical Engineering Science, 2001. **56**(7): p. 2305-2313.
112. Kawaguchi, T., et al., *Granulation of acetaminophen by a rotating fluidized-bed granulator.* Pharmaceutical development and technology, 2000. **5**(2): p. 141-151.
113. Oka, S., et al., *The effects of improper mixing and preferential wetting of active and excipient ingredients on content uniformity in high shear wet granulation.* Powder Technology, 2015. **278**: p. 266-277.